

DEUTSCHES ELEKTRONEN-SYNCHROTRON
Ein Forschungszentrum der Helmholtz-Gemeinschaft



DESY 19-149
ADP-19-19/T1099
Liverpool LTH 1211
arXiv:1909.02521
September 2019

**Patterns of Flavour Symmetry Breaking in
Hadron Matrix Elements Involving u, d and s Quarks**

QCDSF-UKQCD-CSSM Collaboration

ISSN 0418-9833

NOTKESTRASSE 85 - 22607 HAMBURG

DESY behält sich alle Rechte für den Fall der Schutzrechtserteilung und für die wirtschaftliche Verwertung der in diesem Bericht enthaltenen Informationen vor.

DESY reserves all rights for commercial use of information included in this report, especially in case of filing application for or grant of patents.

To be sure that your reports and preprints are promptly included in the
HEP literature database
send them to (if possible by air mail):

DESY Zentralbibliothek Notkestraße 85 22607 Hamburg Germany	DESY Bibliothek Platanenallee 6 15738 Zeuthen Germany
---	---

Patterns of flavour symmetry breaking in hadron matrix elements involving u, d and s quarks

J. M. Bickerton^a, R. Horsley^b, Y. Nakamura^c,
H. Perlt^d, D. Pleiter^e, P. E. L. Rakow^f, G. Schierholz^g,
H. Stüben^h, R. D. Young^a and J. M. Zanotti^a

– QCDSF-UKQCD-CSSM Collaboration –

^a CSSM, Department of Physics, University of Adelaide,
Adelaide SA 5005, Australia

^b School of Physics and Astronomy, University of Edinburgh,
Edinburgh EH9 3FD, UK

^c RIKEN Center for Computational Science,
Kobe, Hyogo 650-0047, Japan

^d Institut für Theoretische Physik, Universität Leipzig,
04103 Leipzig, Germany

^e Jülich Supercomputer Centre, Forschungszentrum Jülich,
52425 Jülich, Germany
Institut für Theoretische Physik, Universität Regensburg,
93040 Regensburg, Germany

^f Theoretical Physics Division, Department of Mathematical Sciences,
University of Liverpool, Liverpool L69 3BX, UK

^g Deutsches Elektronen-Synchrotron DESY,
22603 Hamburg, Germany

^h Universität Hamburg, Regionales Rechenzentrum,
20146 Hamburg, Germany

Abstract

By considering a flavour expansion about the $SU(3)$ -flavour symmetric point, we investigate how flavour-blindness constrains octet baryon matrix elements after $SU(3)$ is broken by the mass difference between quarks. Similarly to hadron masses we find the expansions to be constrained along a mass trajectory where the singlet quark mass is held constant, which provides invaluable insight into the mechanism of flavour symmetry breaking and proves beneficial for extrapolations to the physical point. Expansions are given up to third order in the expansion parameters. Considering higher orders would give no further constraints on the expansion parameters. The relation of the expansion coefficients to the quark-line-connected and quark-line-disconnected terms in the three-point correlation functions is also given. As we consider Wilson clover-like fermions, the addition of improvement coefficients is also discussed and shown to be included in the formalism developed here. As an example of the method we investigate this numerically via a lattice calculation of the flavour-conserving matrix elements of the vector first class form factors.

Contents

1	Introduction	5
2	Baryon matrix elements and generalised currents	7
3	Quark mass expansions	11
3.1	Choice of quark masses	11
3.2	Matrix elements	12
3.3	Simple cases I: Decay constants f_π and f_K	13
4	Method for matrix elements	13
4.1	Sign conventions: Octet operators and octet hadrons	14
4.2	$SU(2)$ relations	15
5	Mass dependence of amplitudes	18
5.1	Simple cases II: Flavour-singlet operators	18
5.2	Group theory classification: Flavour-octet operators	19
5.3	The $SU(3)$ symmetry-breaking expansions	20
5.3.1	Basis	20
5.3.2	Transformations	22
6	Coefficient tables	26
6.1	Leading-order coefficient tables	26
6.2	Higher-order coefficient tables	27
7	Amplitudes at the symmetric point	29
8	Mass dependence: ‘fan’ plots	31
8.1	The d -fan	31
8.2	The f -fan	32
9	Quark-line-connected and -disconnected diagrams	33
10	Mass dependence: flavour-diagonal matrix elements	35
10.1	Connected terms	35
10.2	The electromagnetic current	37
11	Renormalisation and $O(a)$ improvement for the vector current	37
11.1	General comments	37
11.1.1	$V_\mu^{\pi^0 R}$	39
11.1.2	$V_\mu^{\eta R}$	39
11.1.3	$V_\mu^{\eta' R}$	39
11.1.4	Concluding remarks	39

11.2	Determination of \hat{Z}_V and $\hat{b}_V, \hat{f}_V^{\text{con}}$	40
11.2.1	$V_4^{\pi^0\text{R}}$	40
11.2.2	$V_4^{\eta\text{R}}$	41
11.2.3	The Ademollo–Gatto theorem	41
12	Lattice computations of form factors	41
12.1	General discussion	41
12.2	Lattice details	43
13	Results	45
13.1	X plots	45
13.2	Fan plots	48
13.3	Estimating \hat{Z}_V and $\hat{b}_V, \hat{f}_V^{\text{con}}$	53
13.4	Electromagnetic form factor results	53
14	Conclusions and outlook	56
A	Non-zero tensor elements	59
B	Alternative fan plots	59
B.1	The doubly represented – singly represented fan, the P -fan	59
B.2	The V -fan	64
C	LO flavour diagonal matrix elements	64
D	LO disconnected flavour diagonal matrix elements	65

1 Introduction

Understanding the pattern of flavour symmetry breaking and mixing, and the origin of CP violation, remains one of the outstanding problems in particle physics. The big questions to be answered are (i) What determines the observed pattern of quark and lepton mass matrices and (ii) Are there other sources of flavour symmetry breaking? In [1, 2] we have outlined a programme to systematically investigate the pattern of flavour symmetry breaking. The program has been successfully applied to meson and baryon masses involving up, down and strange quarks. In this article we will extend the investigation to include matrix elements.

The QCD interaction is flavour-blind. Neglecting electromagnetic and weak interactions, the only difference between flavours comes from the quark mass matrix. We have our best theoretical understanding when all three quark flavours have the same masses, because we can use the full power of flavour $SU(3)$. The strategy is to keep the average bare quark mass $\bar{m} = (m_u + m_d + m_s)/3$ constant and expand the matrix elements about the flavour symmetric point $m_u = m_d = m_s$. Thus all the quark mass dependence will be expressed as polynomials in $\delta m_q = m_q - \bar{m}$, $q = u, d, s$. It should be mentioned that this is a completely different approach for studying the manifestations of low-energy QCD than chiral perturbation theory. It is a complementary method and based on group theory rather than effective field theory.

The programme has been successfully applied to meson and baryon masses in [1, 2] including an extension to incorporate QED effects [3, 4, 5]. Besides constraining the quark mass dependence of hadron masses, which helps in extrapolations to the physical point, it provides valuable information on the physics of flavour symmetry breaking. For example, the order of the polynomial can be associated with the order of $1/N_c$ corrections, [6]. Furthermore, similar to the analysis of Gell-Mann and Okubo [7, 8], the order of the polynomial classifies the order of $SU(3)$ breaking, [1, 2]. As opposed to the conventional method of keeping the strange quark mass fixed, our method has the further advantage that flavour singlet quantities which are difficult to compute can now be disentangled in the extrapolation, and are largely constant on the \bar{m} constant line.

In this article we shall concentrate on matrix elements for the baryon octet as sketched in the $Y - I_3$ plane in the left hand panel of Fig. 1. It is easy to translate the results to octet mesons sketched in the right hand panel of Fig. 1. Furthermore we restrict ourselves to the case of $n_f = 2 + 1$, i.e. the case of degenerate u and d quark masses, $m_u = m_d \equiv m_l$. (Initial results were given in [9].) However our method is also applicable to isospin breaking effects arising from non-degenerate u and d quark masses. We postpone this analysis to a separate paper, including electromagnetic effects, [10]. The formalism is general. In our application we consider for definiteness just local currents, but covering

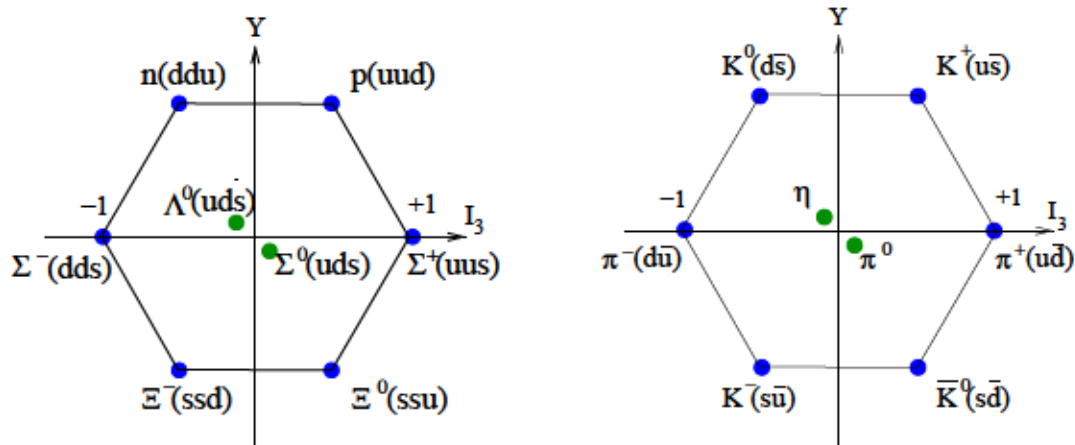


Figure 1: Left panel: The baryon octet. Right panel: The meson octet.

all possible Dirac gamma matrix structure¹.

While of intrinsic interest in itself, an obvious application of this formalism is the determination of semileptonic decay form factors and the associated CKM matrix element, $|V_{us}|$. In general disentangling quark mass and momentum dependencies is helpful for determining generalised form factors of baryons, as described for example in the forthcoming Electron Ion Collider (EIC) programme, [11].

The structure of this article is as follows. In section 2, we discuss all possible currents (which we call ‘generalised currents’ here) and also their splitting into ‘first’ class and ‘second’ class currents. Then in sections 3, 4, 5 we discuss the group theory. In section 3 we define our expansion parameter, δm_l and the general structure of our expansions. Also discussed there (and at the beginning of section 5.1) are simple cases which have previously been determined. In particular the singlet case will be used later in this article. The next section, section 4 gives our sign conventions (commonly employed in chiral perturbation theory). As we have mass degenerate u and d quarks then there is an $SU(2)$ isospin symmetry. We then use the Wigner-Eckart theorem to give the reduced matrix elements, contrasting the difference here to the usual conventions. Then in section 5, after discussing the group theory classification of $SU(3)$ tensors, we determine those relevant to our study (with complete tables being given in Appendix A), and then in section 6.1 give the LO expansions. Higher-order terms are given in section 6.2. These sections giving the expansion coefficients form the heart of this report. This is followed by section 7 where we briefly restrict ourselves to a discussion of the amplitudes at the symmetric point.

Continuing with the main thread, in section 8 linear combinations of the matrix elements are constructed for the various baryons, leading to functions

¹It can also easily be extended to currents including covariant derivatives.

that all have the same value at the $SU(3)$ flavour symmetric point. Four different ‘fan’ plots are constructed, two detailed in section 8 and a further two given in Appendix B.

Lattice QCD determinations of matrix elements involve the computation of 3-point correlation functions, which fall into two classes – quark-line connected diagrams and quark line disconnected diagrams. In section 9, we discuss the implications of this splitting for the $SU(3)$ symmetry flavour breaking expansions at LO. In particular for the connected terms, there are further constraints on the expansion coefficients. In section 10 this is applied to the baryon-diagonal matrix elements (and as a special case to the electromagnetic current). The quark-line connected expansions are given there with the general expressions described in Appendix C while the quark-line disconnected expansions are given in Appendix D.

In section 11 we discuss improvement coefficients for the currents, see e.g. [12], and show that they lead to (small) modifications of the $SU(3)$ flavour symmetric breaking expansion coefficients. Using the vector current as an example, we show how we can determine two improvement coefficients (and the renormalisation constant). Section 12.1 briefly describes how matrix elements (i.e. form factors) are computed from the ratios of 3-point to 2-point correlation functions. In section 12.2, we describe our $n_f = 2 + 1$ flavour Wilson clover action used and provide some numerical details. In section 13, specialising to the vector current again we give some flavour singlet ‘ X ’-plots, showing their constancy for the F_1 and F_2 form factors. This is followed by some fan plots revealing $SU(3)$ -breaking effects. The momentum transfer (Q^2) dependence of the expansion coefficients is also investigated. The numerical values of two improvement coefficients are also determined. Finally in section 14 we give our conclusions.

2 Baryon matrix elements and generalised currents

We take here ‘generalised currents’ to be

$$J^{\mathbb{F}(\mathcal{M})} = \bar{q} F \gamma^{(\mathcal{M})} q \equiv \sum_{f_1, f_2=1}^3 F_{f_1 f_2} \bar{q}_{f_1} \gamma^{(\mathcal{M})} q_{f_2}, \quad (1)$$

where q is a flavour vector, $q = (u, d, s)^T$, F is a flavour matrix and $\gamma^{(\mathcal{M})}$ is some Dirac gamma matrix. In particular we have $\gamma^{(\mathcal{M})} = \gamma^{(\mathcal{M})\mu}$, $\gamma^{(\mathcal{M})\mu} \gamma_5^{(\mathcal{M})}$, I , $i\gamma_5^{(\mathcal{M})}$ and $\sigma^{(\mathcal{M})\mu\nu}$ for the vector $V^{(\mathcal{M})\mu}$, axial $A^{(\mathcal{M})\mu}$, scalar $S^{(\mathcal{M})}$, pseudoscalar $P^{(\mathcal{M})}$ and tensor $T^{(\mathcal{M})\mu\nu}$ generalised currents respectively. The further generalisation to operators including covariant derivatives is straightforward. With our gamma matrix conventions, we obviously have

$$J^{\mathbb{F}(\mathcal{M})\dagger} = \bar{q} F^T \gamma^{(\mathcal{M})} q, \quad (2)$$

and so are Hermitian if the flavour matrix, F , is symmetric and anti-Hermitian if F is antisymmetric.

We use Minkowski space², and to emphasise this we use the superscript: (\mathcal{M}) . The expansion described later will be valid whether we are working in Minkowski or Euclidean space (when we will drop the superscript). We wish to compute matrix elements for $B \rightarrow B'$

$$A(B \rightarrow B') = \langle B', \vec{p}', \vec{s}' | J^{F(\mathcal{M})}(q) | B, \vec{p}, \vec{s} \rangle \equiv A_{B'B}, \quad (3)$$

where B and B' belong to the baryon octet, the members of which are shown in Fig. 1 (the quark content of each baryon is also depicted there). This can thus include scattering processes for example $Be \rightarrow Be$ or semi-leptonic (or β -decays) $B \rightarrow B'e\bar{\nu}_e$ from a parent baryon, B , to a daughter baryon B' . For semi-leptonic decays in the standard model, neutral currents are flavour diagonal, and hence there is an absence of flavour-changing neutral currents (FCNCs), i.e. $s \rightarrow d$ transitions. In addition $\Delta S = \Delta Q$ violating modes are not seen. From Fig. 1 we see that this means that transitions from right to the left in the picture are suppressed or absent. For example twelve allowed non-hyperon and hyperon β -decays, are listed in Table 1 of [13]. Of course the present formalism does not incorporate these constraints, but this can motivate our choice of independent matrix elements, which are transitions from the left to the right in Fig. 1.

Momentum transfer $p^{(\mathcal{M})} - p^{(\mathcal{M})'}$ is more natural to take for semi-leptonic decays, as this is the momentum carried by the lepton and neutrino. However for scattering processes $p^{(\mathcal{M})'} - p^{(\mathcal{M})}$ is more natural. We wish to adopt a unified notation here, so we define the momentum transfer as

$$q^{(\mathcal{M})} = p^{(\mathcal{M})'} - p^{(\mathcal{M})} = (E_{B'}(\vec{p}') - E_B(\vec{p}), \vec{p}' - \vec{p}). \quad (4)$$

The decompositions of the matrix elements in eq. (3) are standard, and we write

$$\langle B', \vec{p}', \vec{s}' | J^{F(\mathcal{M})}(q) | B, \vec{p}, \vec{s} \rangle = \bar{u}_{B'}(\vec{p}', \vec{s}') \mathcal{J}^{(\mathcal{M})}(q) u_B(\vec{p}, \vec{s}), \quad (5)$$

with for $\mathcal{J}^{(\mathcal{M})}$

$$\begin{aligned} \mathcal{V}^{(\mathcal{M})\mu} &= \gamma^{(\mathcal{M})\mu} F_1 + i\sigma^{(\mathcal{M})\mu\nu} q_\nu^{(\mathcal{M})} \frac{F_2}{M_B + M_{B'}} + q^{(\mathcal{M})\mu} \frac{F_3}{M_B + M_{B'}}, \\ \mathcal{A}^{(\mathcal{M})\mu} &= \left(\gamma^{(\mathcal{M})\mu} G_1 + i\sigma^{(\mathcal{M})\mu\nu} q_\nu^{(\mathcal{M})} \frac{G_2}{M_B + M_{B'}} + q^{(\mathcal{M})\mu} \frac{G_3}{M_B + M_{B'}} \right) \gamma_5^{(\mathcal{M})}, \\ \mathcal{S}^{(\mathcal{M})} &= g_S, \\ \mathcal{P}^{(\mathcal{M})} &= i\gamma_5^{(\mathcal{M})} g_P, \\ \mathcal{T}^{(\mathcal{M})\mu\nu} &= \sigma^{(\mathcal{M})\mu\nu} h_1 + i(q^{(\mathcal{M})\mu} \gamma^{(\mathcal{M})\nu} - q^{(\mathcal{M})\nu} \gamma^{(\mathcal{M})\mu}) \frac{h_2}{M_B + M_{B'}} \end{aligned} \quad (6)$$

²The conventions used include $\eta^{\mu\nu} = \text{diag}(1, -1, -1, -1)$, $\gamma^{(\mathcal{M})\mu\dagger} = \gamma^{(\mathcal{M})0} \gamma^{(\mathcal{M})\mu} \gamma^{(\mathcal{M})0}$, $\gamma_5^{(\mathcal{M})} = i\gamma^{(\mathcal{M})0} \gamma^{(\mathcal{M})1} \gamma^{(\mathcal{M})2} \gamma^{(\mathcal{M})3}$ and $\sigma^{(\mathcal{M})\mu\nu} = i/2[\gamma^{(\mathcal{M})\mu}, \gamma^{(\mathcal{M})\nu}]$.

$$\begin{aligned}
& +i(q^{(\mathcal{M})\mu}P^{(\mathcal{M})\nu} - q^{(\mathcal{M})\nu}P^{(\mathcal{M})\mu})\frac{h_3}{(M_B + M_{B'})^2} \\
& +i(\gamma^{(\mathcal{M})\mu}\not{q}^{(\mathcal{M})}\gamma^{(\mathcal{M})\nu} - \gamma^{(\mathcal{M})\nu}\not{q}^{(\mathcal{M})}\gamma^{(\mathcal{M})\mu})\frac{h_4}{M_B + M_{B'}} ,
\end{aligned}$$

where $P^{(\mathcal{M})} = p^{(\mathcal{M})} + p^{(\mathcal{M})'}$. $F_i \equiv F_i^{\mathcal{B}'\mathcal{F}\mathcal{B}}$, $G_i \equiv G_i^{\mathcal{B}'\mathcal{F}\mathcal{B}}$, $g_S \equiv g_S^{\mathcal{B}'\mathcal{F}\mathcal{B}}$, $g_P \equiv g_P^{\mathcal{B}'\mathcal{F}\mathcal{B}}$ and $h_i \equiv h_i^{\mathcal{B}'\mathcal{F}\mathcal{B}}$ are the form factors and are functions of $q^{(\mathcal{M})2}$ and the masses of the baryons (or alternatively the quark masses). Each combination in eqs. (5, 6) represents a current times a form factor (i.e. the coefficient). For example the first term for the vector current reads $\bar{u}_{B'}(\vec{p}', \vec{s}')\gamma^{(\mathcal{M})\mu}u_B(\vec{p}, \vec{s}) \times F_1^{\mathcal{B}'\mathcal{F}\mathcal{B}}(q^{(\mathcal{M})2})$. The goal of this article is to establish ways in which these form factors depend on the transition taking place and on the quark masses.

From eqs. (2, 3) we have

$$A_{\mathcal{B}\mathcal{F}\mathcal{T}\mathcal{B}'}^* = A_{\mathcal{B}'\mathcal{F}\mathcal{B}} , \quad (7)$$

and we now apply this to eq. (5) with individual terms defined by eq. (6). Consider first the current pieces. For example for the vector currents we find that the first and second terms (i.e. currents) are unaltered, $(\bar{u}_B\gamma^{(\mathcal{M})\mu}u_{B'})^* = \bar{u}_{B'}\gamma^{(\mathcal{M})\mu}u_B$, $(\bar{u}_{B'}i\sigma^{(\mathcal{M})\mu\nu}(-q_\nu^{(\mathcal{M})})u_B)^* = \bar{u}_B i\sigma^{(\mathcal{M})\mu\nu}q_\nu^{(\mathcal{M})}u_{B'}$ while the third current changes sign, $(\bar{u}_B(-q^{(\mathcal{M})\mu})u_{B'})^* = -\bar{u}_{B'}q^{(\mathcal{M})\mu}u_B$. Strong interactions are invariant under T -parity and from this it can be shown that the form factors can be chosen to be all real. Hence from eq. (7) we must have

$$F_1^{\mathcal{B}\mathcal{F}\mathcal{T}\mathcal{B}'} = F_1^{\mathcal{B}'\mathcal{F}\mathcal{B}} , \quad F_2^{\mathcal{B}\mathcal{F}\mathcal{T}\mathcal{B}'} = F_2^{\mathcal{B}'\mathcal{F}\mathcal{B}} , \quad (8)$$

but

$$F_3^{\mathcal{B}\mathcal{F}\mathcal{T}\mathcal{B}'} = -F_3^{\mathcal{B}'\mathcal{F}\mathcal{B}} . \quad (9)$$

F_1 and F_2 are called first class form factors while F_3 is called a second class form factor. This can be applied to all the further currents. These properties of the form factors thus give rise to the notation, [14]

$$\begin{array}{l}
\text{first class } F_1, F_2, G_1, G_3, g_S, g_P, h_1, h_2, h_3 \\
\text{second class } F_3, G_2, h_4
\end{array} , \quad (10)$$

(with the meaning given by eqs. (8, 9)). Note that when $B' = B$, then the second class currents (i.e. form factors) vanish. This occurs, either for a scattering process (i.e. a diagonal current in flavour space, so the matrix F is symmetric and the current is Hermitian) or for semi-leptonic processes at the quark mass symmetric point.

We now consider the flavour structures, i.e. the possible flavour matrices in eq. (1). In Table 1 we give the possible octet states, $i = 1, \dots, 8$ and in addition the singlet state, labelled by $i = 0$. As we are primarily concerned with the

Index	Baryon (B)	Meson (F)	Current (J^F)
1	n	K^0	$\bar{d}\gamma s$
2	p	K^+	$\bar{u}\gamma s$
3	Σ^-	π^-	$\bar{d}\gamma u$
4	Σ^0	π^0	$\frac{1}{\sqrt{2}}(\bar{u}\gamma u - \bar{d}\gamma d)$
5	Λ^0	η	$\frac{1}{\sqrt{6}}(\bar{u}\gamma u + \bar{d}\gamma d - 2\bar{s}\gamma s)$
6	Σ^+	π^+	$\bar{u}\gamma d$
7	Ξ^-	K^-	$\bar{s}\gamma u$
8	Ξ^0	\bar{K}^0	$\bar{s}\gamma d$
0		η'	$\frac{1}{\sqrt{3}}(\bar{u}\gamma u + \bar{d}\gamma d + \bar{s}\gamma s)$

Table 1: Our numbering and conventions for the generalised currents. For example, $B_3 = \Sigma^-$, $F_3 = \pi^-$, $J^{F_3} \equiv J^{\pi^-}$. We use the convention that current (i.e. operator) numbered by i has the same effect as absorbing a meson with the index i . γ represents an arbitrary Dirac matrix.

flavour structure of bilinear operators, we use the corresponding meson name for the flavour structure of the bilinear quark currents. So for example the $i = 5$ current is given by the flavour matrix $F_\eta = \text{diag}(1, 1, -2)/\sqrt{6}$. We shall use the convention that the current i has the same effect as absorbing a meson with the same index. In the operator expressions q is the annihilation operator and \bar{q} the creation operator. As an example, we note that absorbing a π^+ annihilates one d quark and creates a u quark. That is

$$J^{\pi^+}|0\rangle \propto |\pi^+\rangle, \quad (11)$$

while $\langle p|\bar{u}\gamma d|n\rangle = \langle p|J^{\pi^+}|n\rangle$ represents $p = \pi^+n$.

As an example of this (current) notation the quark electromagnetic current can be written by defining an appropriate flavour matrix F or alternatively as

$$\begin{aligned} J_{\text{em}\mu} &= \frac{2}{3}\bar{u}\gamma_\mu u - \frac{1}{3}\bar{d}\gamma_\mu d - \frac{1}{3}\bar{s}\gamma_\mu s \\ &\equiv \frac{1}{\sqrt{2}}V_\mu^{\pi^0} + \frac{1}{\sqrt{6}}V_\mu^\eta. \end{aligned} \quad (12)$$

Furthermore the charged W s currents are a mixture of the charged π and K currents, while the Z current is diagonal and thus a mixture of the π^0 , η and η' currents. The K^0 current is a FCNC, so only contributes to beyond the standard model (BSM) or higher-order processes.

The previous discussion on first and second class currents can now be reformulated in terms of these flavour matrices and isospin rotations³. The diagonal

³This discussion follows [15].

currents, and hence diagonal matrix elements, discussed here are given by $i = 4, 5$ and 0 with F_{π^0}, F_η and $F_{\eta'}$ respectively. As a result F_3, G_2, g_P, h_2 and h_3 all vanish for these currents. For the off-diagonal currents consider the $SU(3)$ -flavour symmetric point. As all the quark masses have the same mass, and in particular the u and d quarks then we first consider isospin, I , invariance. Isospin rotations are d - u rotations and relate off-diagonal currents to diagonal currents. (For example $\langle p|J^{\pi^+}|n\rangle$ is related to $\langle p|J^{\pi^0}|p\rangle$, see section 4.2.) Similarly for U -spin rotations s - d , and V -spin rotations s - u . Hence we expect that for transitions within a given multiplet (whether I, U or V) at the $SU(3)$ -flavour symmetric point then again F_3, G_2, g_P, h_2 and h_3 all vanish. Between isospin multiplets they need not vanish when $SU(3)$ flavour symmetry is broken. We later discuss this in more detail and our coefficient tables, for example Table 6, reflect these results.

3 Quark mass expansions

3.1 Choice of quark masses

As mentioned already, we follow the strategy used in [2] of holding constant the average bare quark mass

$$\bar{m} = \frac{1}{3}(m_u + m_d + m_s). \quad (13)$$

This greatly reduces the number of mass polynomials which can occur in Taylor expansions of physical quantities, and relates the quark-mass dependencies of hadron masses or matrix elements within an $SU(3)$ multiplet. Since we expand about the symmetric point where all three quarks have the same mass, it is useful to introduce the notation

$$\delta m_q \equiv m_q - \bar{m}, \quad q = u, d, s, \quad (14)$$

to describe the ‘distance’ from the $SU(3)$ flavour symmetry point. Note that it follows from the definition that we have the identity

$$\delta m_u + \delta m_d + \delta m_s = 0, \quad (15)$$

so we can always eliminate one of the δm_q . In this article we concentrate on the $n_f = 2 + 1$ case, i.e. we keep

$$m_u = m_d \equiv m_l. \quad (16)$$

All our expansion coefficients are functions of \bar{m} . The methods developed here can be generalised to the case of $n_f = 1 + 1 + 1$ non-degenerate quark-mass flavours. For this case eq. (15) reduces to

$$2\delta m_l + \delta m_s = 0, \quad (17)$$

which we use to eliminate δm_s . Thus, all mass dependences will be expressed as polynomials in the single variable δm_l . At the physical point $m_l \ll \bar{m}$, so δm_l is negative. However on the lattice in principle we are free to choose δm_l positive, and look at matrix elements on both sides of the symmetric point.

3.2 Matrix elements

In the following we want to use group theory in flavour space to calculate the possible quark-mass dependence of baryonic form factors. However for simplicity of notation we shall continue to discuss matrix elements and amplitudes, but it should be noted that for form factors the Lorentz/Dirac structure has been factored out. So we shall consider the quark mass expansion for

$$\langle B_i | J^{F_j} | B_k \rangle \equiv A_{\bar{B}_i F_j B_k}. \quad (18)$$

The indices i and k will run from 1 to 8 for octet hadrons (or 1 to 10 for decuplets). The currents/operators we are interested in are quark bilinears, so the index j will run from 1 to 8 for non-singlets, or 0 for the singlet. In the following the singlet will be considered separately. When $i \neq k$ we get transition matrix elements; when $i = k$ within the same multiplet, we get operator expectation values. This has already been indicated in Table 1.

The allowed quark mass Taylor expansion for a hadronic matrix element must follow the schematic pattern

$$\begin{aligned} \langle B_i | J^{F_j} | B_k \rangle &= \sum (\text{singlet mass polynomial}) \times (\text{singlet tensor})_{ijk} \\ &+ \sum (\text{octet mass polynomial}) \times (\text{octet tensor})_{ijk} \\ &+ \sum (\text{27-plet mass polynomial}) \times (\text{27-plet tensor})_{ijk} \\ &+ \dots \end{aligned} \quad (19)$$

The mass polynomials have been determined and given in Table III of [2]. The relevant part of this table is given in Table 2 where we classify all the polynomials which could occur in a Taylor expansion about the symmetric point, $\delta m_q = 0$, $q = u, d, s$ up to $O(\delta m_q^3)$. The tensors in eq. (19) are 3-dimensional arrays of integers and square-roots of integers; objects somewhat analogous to three-dimensional Gell-Mann matrices. We recover the standard results for unbroken $SU(3)$ by only keeping singlet tensors on the right-hand side of eq. (19). Adding higher dimensional flavour tensors tells us the allowed mass dependences of matrix elements. The dots in eq. (19) represent terms that are cubic or higher in δm_q .

We now need to classify the three-index tensors according to their group transformations, using the same techniques we used for masses [2]. The new cases to look at will be $8 \otimes 8 \otimes 8$ and $10 \otimes 8 \otimes 10$ for octet and decuplet hadrons respectively, $10 \otimes 8 \otimes 8$ for transitions between octet and decuplet baryons, and

Polynomial	$SU(3)$		
1	1		
δm_s	8		
$(\delta m_u - \delta m_d)$	8		
$\delta m_u^2 + \delta m_d^2 + \delta m_s^2$	1	27	
$3\delta m_s^2 - (\delta m_u - \delta m_d)^2$	8	27	
$\delta m_s(\delta m_d - \delta m_u)$	8	27	
$\delta m_u \delta m_d \delta m_s$	1	27	64
$\delta m_s(\delta m_u^2 + \delta m_d^2 + \delta m_s^2)$	8	27	64
$(\delta m_u - \delta m_d)(\delta m_u^2 + \delta m_d^2 + \delta m_s^2)$	8	27	64
$(\delta m_s - \delta m_u)(\delta m_s - \delta m_d)(\delta m_u - \delta m_d)$	10	$\overline{10}$	64

Table 2: All the quark-mass polynomials up to $O(\delta m_q^3)$, classified by symmetry properties.

$3 \otimes 8 \otimes 3$ for quark matrix elements, useful for considering renormalisation and improvement of quark bilinear operators. We shall only consider the octet (and singlet) baryon cases here.

3.3 Simple cases I: Decay constants f_π and f_K

The vacuum is a singlet, so vacuum to meson, M , matrix elements or decay constants $\langle 0 | J^{F_j} | M_k \rangle$, $j = 1, \dots, 8$ are proportional to $1 \otimes 8 \otimes 8$ tensors, i.e. $8 \otimes 8$ matrices. So again the allowed mass dependence of f_π and f_K is similar to the allowed dependence of M_π^2 and M_K^2 , as given in [2]. Results using this approach are given in [16]. For example to LO we have

$$\begin{aligned} f_\pi &= F_0 + 2G\delta m_l, \\ f_K &= F_0 - G\delta m_l. \end{aligned} \quad (20)$$

The same argument applies in principle to hyperon distribution amplitudes qqq , and to baryon decays via $qqqe$ 4-fermi grand unified theory (GUT) interactions, but in this work we shall only consider bilinear operators.

4 Method for matrix elements

Recall from eq. (3) that we have used the notation for the matrix element transition $B \rightarrow B'$ of

$$A_{B'FB} = \langle B' | J^F | B \rangle, \quad (21)$$

where J^F is the appropriate operator from Table 1 and F denotes the flavour structure of the operator. But note that as we are suppressing the Lorentz structure, this includes first and second class form factors as given in eq. (10).

4.1 Sign conventions: Octet operators and octet hadrons

In the case of a $n_f = 2 + 1$ simulation we only need to give the amplitudes for one particle in each isospin multiplet, and can then use isospin symmetry to calculate all other amplitudes in (or between) the same multiplets. So, for example, we can calculate the Σ^- and Σ^0 matrix elements if we are given all the Σ^+ matrix elements. Similarly, given the $\Sigma^+ \rightarrow p$ transition amplitude, we can find all the other $\Sigma \rightarrow N$ transition amplitudes. All the symmetry factors will be listed in section 4.2.

In the next section we will calculate the allowed quark-mass dependencies of the amplitudes between the baryons. Within this set there are 7 diagonal matrix elements, and 5 transition amplitudes making $7 + 5 = 12$ in total. The 7 diagonal elements are

$$A_{N\eta N}, A_{\Sigma\eta\Sigma}, A_{\Lambda\eta\Lambda}, A_{\Xi\eta\Xi} \text{ and } A_{N\pi N}, A_{\Sigma\pi\Sigma}, A_{\Xi\pi\Xi}, \quad (22)$$

because there are four $I = 0$ amplitudes, one for each particle, but only three $I = 1$ amplitudes, because isospin symmetry rules out an $I = 1, \Lambda^0 \leftrightarrow \Lambda^0$ amplitude. There are only 5 transition amplitudes

$$A_{\Sigma\pi\Lambda} \text{ and } A_{\bar{N}K\Sigma}, A_{\bar{N}K\Lambda}, A_{\bar{\Lambda}K\Xi}, A_{\bar{\Sigma}K\Xi}, \quad (23)$$

because no octet operator changes strangeness by ± 2 , so there is no $p \leftrightarrow \Xi^0$ transition amplitude. See the forthcoming Tables 3 and 4 for the explicit results.

To discuss transition matrix elements, we need to specify the hadron states carefully. If we do not, then the phases and signs of transition matrix elements become ambiguous. (This is not a problem with masses, or diagonal matrix elements such as $\langle p|J|p\rangle$.)

We follow a convention commonly used in chiral perturbation theory⁴, e.g. [18, 19] where the mesons transform under $SU(3)$ rotations like the 3×3 matrix

$$M = \begin{pmatrix} \frac{1}{\sqrt{2}}\pi^0 + \frac{1}{\sqrt{6}}\eta & \pi^+ & K^+ \\ \pi^- & -\frac{1}{\sqrt{2}}\pi^0 + \frac{1}{\sqrt{6}}\eta & K^0 \\ K^- & \bar{K}^0 & -\frac{2}{\sqrt{6}}\eta \end{pmatrix}, \quad (24)$$

and octet baryons like the matrix

$$B = \begin{pmatrix} \frac{1}{\sqrt{2}}\Sigma^0 + \frac{1}{\sqrt{6}}\Lambda^0 & \Sigma^+ & p \\ \Sigma^- & -\frac{1}{\sqrt{2}}\Sigma^0 + \frac{1}{\sqrt{6}}\Lambda^0 & n \\ \Xi^- & \Xi^0 & -\frac{2}{\sqrt{6}}\Lambda^0 \end{pmatrix},$$

⁴However some papers use different definitions, e.g. in chapter 18 of [17] the meson matrix M is defined the same way as in eq. (24), but in the baryon matrix B the Ξ^- appears with a minus sign in comparison to eq. (25). Using the Gasiorowicz convention, [17], would give the opposite sign to all transition matrix elements to or from the Ξ^- .

$$\bar{B} = \begin{pmatrix} \frac{1}{\sqrt{2}}\bar{\Sigma}^0 + \frac{1}{\sqrt{6}}\bar{\Lambda}^0 & \bar{\Sigma}^- & \bar{\Xi}^- \\ \bar{\Sigma}^+ & -\frac{1}{\sqrt{2}}\bar{\Sigma}^0 + \frac{1}{\sqrt{6}}\bar{\Lambda}^0 & \bar{\Xi}^0 \\ \bar{p} & \bar{n} & -\frac{2}{\sqrt{6}}\bar{\Lambda}^0 \end{pmatrix}. \quad (25)$$

So for example π^+ , π^0 , π^- are represented by the matrices

$$\begin{pmatrix} 0 & 1 & 0 \\ 0 & 0 & 0 \\ 0 & 0 & 0 \end{pmatrix}, \quad \begin{pmatrix} \frac{1}{\sqrt{2}} & 0 & 0 \\ 0 & -\frac{1}{\sqrt{2}} & 0 \\ 0 & 0 & 0 \end{pmatrix}, \quad \begin{pmatrix} 0 & 0 & 0 \\ 1 & 0 & 0 \\ 0 & 0 & 0 \end{pmatrix}, \quad (26)$$

respectively. Under an $SU(3)$ rotation the M , B and \bar{B} matrices transform as

$$M \rightarrow U M U^\dagger, \quad B \rightarrow U B U^\dagger, \quad \text{and} \quad \bar{B} \rightarrow U \bar{B} U^\dagger. \quad (27)$$

4.2 $SU(2)$ relations

As discussed previously we use the convention that operator number i , representing an appropriate flavour matrix, has the same effect on quantum numbers as the absorption of a meson with the index i . So for example, from Table 1 operator 6 annihilates a d quark and creates a u , and hence changes a neutron into a proton, i.e.

$$\langle p | \bar{u} \gamma d | n \rangle \equiv \langle p | J^{\pi^+} | n \rangle \equiv \langle B_2 | J^{F_6} | B_1 \rangle. \quad (28)$$

In Tables 3 and 4 we list the isospin relationships between all of the allowed matrix elements in the octet, and our standard $7 + 5 = 12$ matrix elements.

Making the choice given in eqs. (24, 25) which is conventional in chiral perturbation theory, the isospin raising and lowering operators do not follow the usual Condon–Shortley sign convention. The Wigner–Eckart theorem applies, but the signs are not always the ones from the standard Clebsch–Gordan coefficients.

To demonstrate this, consider the transformations given in eq. (27) with $U = \exp(i\alpha_i \lambda^i)$. Infinitesimal transformations ($\alpha_i \rightarrow 0$) correspond to commutators of the type $[\lambda^i, B]$ or $[\lambda^i, M]$. The isospin operations are constructed from the first three λ matrices

$$\begin{aligned} I_3 &= \frac{1}{2}\lambda^3, \\ I_+ &= \frac{1}{2}(\lambda^1 + i\lambda^2), \\ I_- &= \frac{1}{2}(\lambda^1 - i\lambda^2). \end{aligned} \quad (29)$$

I_3 has the expected result

$$\hat{I}_3 M = \frac{1}{2}[\lambda^3, M] = \begin{pmatrix} 0 & \pi^+ & \frac{1}{2}K^+ \\ -\pi^- & 0 & -\frac{1}{2}K^0 \\ -\frac{1}{2}K^- & \frac{1}{2}\bar{K}^0 & 0 \end{pmatrix}, \quad (30)$$

I			I		
0	$\langle n J^0 n\rangle$	$A_{\bar{N}\eta N}$	1	$\langle n J^{\pi^0} n\rangle$	$-A_{\bar{N}\pi N}$
0	$\langle p J^0 p\rangle$	$A_{\bar{N}\eta N}$	1	$\langle p J^{\pi^0} p\rangle$	$A_{\bar{N}\pi N}$
0	$\langle \Sigma^- J^0 \Sigma^- \rangle$	$A_{\bar{\Sigma}\eta\Sigma}$	1	$\langle n J^{\pi^-} p\rangle$	$\sqrt{2}A_{\bar{N}\pi N}$
0	$\langle \Sigma^0 J^0 \Sigma^0 \rangle$	$A_{\bar{\Sigma}\eta\Sigma}$	1	$\langle p J^{\pi^+} n\rangle$	$\sqrt{2}A_{\bar{N}\pi N}$
0	$\langle \Sigma^+ J^0 \Sigma^+ \rangle$	$A_{\bar{\Sigma}\eta\Sigma}$	1	$\langle \Sigma^- J^{\pi^0} \Sigma^- \rangle$	$-A_{\bar{\Sigma}\pi\Sigma}$
0	$\langle \Lambda^0 J^0 \Lambda^0 \rangle$	$A_{\bar{\Lambda}\eta\Lambda}$	1	$\langle \Sigma^0 J^{\pi^0} \Sigma^0 \rangle$	0
0	$\langle \Xi^- J^0 \Xi^- \rangle$	$A_{\bar{\Xi}\eta\Xi}$	1	$\langle \Sigma^+ J^{\pi^0} \Sigma^+ \rangle$	$A_{\bar{\Sigma}\pi\Sigma}$
0	$\langle \Xi^0 J^0 \Xi^0 \rangle$	$A_{\bar{\Xi}\eta\Xi}$	1	$\langle \Sigma^- J^{\pi^-} \Sigma^0 \rangle$	$A_{\bar{\Sigma}\pi\Sigma}$
			1	$\langle \Sigma^0 J^{\pi^-} \Sigma^+ \rangle$	$-A_{\bar{\Sigma}\pi\Sigma}$
			1	$\langle \Sigma^0 J^{\pi^+} \Sigma^- \rangle$	$A_{\bar{\Sigma}\pi\Sigma}$
			1	$\langle \Sigma^+ J^{\pi^+} \Sigma^0 \rangle$	$-A_{\bar{\Sigma}\pi\Sigma}$
			1	$\langle \Lambda^0 J^{\pi^0} \Lambda^0 \rangle$	0
			1	$\langle \Xi^- J^{\pi^0} \Xi^- \rangle$	$-A_{\bar{\Xi}\pi\Xi}$
			1	$\langle \Xi^0 J^{\pi^0} \Xi^0 \rangle$	$A_{\bar{\Xi}\pi\Xi}$
			1	$\langle \Xi^- J^{\pi^-} \Xi^0 \rangle$	$-\sqrt{2}A_{\bar{\Xi}\pi\Xi}$
			1	$\langle \Xi^0 J^{\pi^+} \Xi^- \rangle$	$-\sqrt{2}A_{\bar{\Xi}\pi\Xi}$

Table 3: The isospin relations connecting the set of octet matrix elements with our standard subsets $A_{\bar{B}FB}$ (each independent set separated by horizontal lines). Left table: The $I = 0$ diagonal relations; right table: the $I = 1$ transition relations within the same isospin multiplet.

$$\hat{I}_3 B = \frac{1}{2}[\lambda^3, B] = \begin{pmatrix} 0 & \Sigma^+ & \frac{1}{2}p \\ -\Sigma^- & 0 & -\frac{1}{2}n \\ -\frac{1}{2}\Xi^- & \frac{1}{2}\Xi^0 & 0 \end{pmatrix}. \quad (31)$$

For example regarding π^- as the matrix in eq. (26) gives

$$\hat{I}_3 \pi^- = \begin{pmatrix} 0 & 0 & 0 \\ -1 & 0 & 0 \\ 0 & 0 & 0 \end{pmatrix} = -\pi^-, \quad (32)$$

(see Fig. 1). Similarly for the baryons, for example $\hat{I}_3 n = -\frac{1}{2}n$, etc...

However \hat{I}_+ and \hat{I}_- produce results at odds with the Condon-Shortley or CS phase convention, which has positive coefficients for the non-zero matrix elements of the raising and lowering operators.

$$\hat{I}_+ M = \frac{1}{2}[\lambda^1 + i\lambda^2, M] = \begin{pmatrix} \pi^- & -\sqrt{2}\pi^0 & K^0 \\ 0 & -\pi^- & 0 \\ 0 & -K^- & 0 \end{pmatrix}. \quad (33)$$

I			I		
1	$\langle \Sigma^- J^{\pi^-} \Lambda^0 \rangle$	$A_{\Sigma\pi\Lambda}$	1	$\langle \Lambda^0 J^{\pi^+} \Sigma^- \rangle$	$A_{\bar{\Lambda}\pi\Sigma}$
1	$\langle \Sigma^0 J^{\pi^0} \Lambda^0 \rangle$	$A_{\bar{\Sigma}\pi\Lambda}$	1	$\langle \Lambda^0 J^{\pi^0} \Sigma^0 \rangle$	$A_{\bar{\Lambda}\pi\Sigma}$
1	$\langle \Sigma^+ J^{\pi^+} \Lambda^0 \rangle$	$A_{\bar{\Sigma}\pi\Lambda}$	1	$\langle \Lambda^0 J^{\pi^-} \Sigma^+ \rangle$	$A_{\bar{\Lambda}\pi\Sigma}$
$\frac{1}{2}$	$\langle n J^{K^+} \Sigma^- \rangle$	$A_{\bar{N}K\Sigma}$	$\frac{1}{2}$	$\langle \Sigma^- J^{K^-} n \rangle$	$A_{\bar{\Sigma}K N}$
$\frac{1}{2}$	$\langle n J^{K^0} \Sigma^0 \rangle$	$-A_{\bar{N}K\Sigma}/\sqrt{2}$	$\frac{1}{2}$	$\langle \Sigma^0 J^{K^0} n \rangle$	$-A_{\bar{\Sigma}K N}/\sqrt{2}$
$\frac{1}{2}$	$\langle p J^{K^+} \Sigma^0 \rangle$	$A_{\bar{N}K\Sigma}/\sqrt{2}$	$\frac{1}{2}$	$\langle \Sigma^0 J^{K^-} p \rangle$	$A_{\bar{\Sigma}K N}/\sqrt{2}$
$\frac{1}{2}$	$\langle p J^{K^0} \Sigma^+ \rangle$	$A_{\bar{N}K\Sigma}$	$\frac{1}{2}$	$\langle \Sigma^+ J^{K^0} p \rangle$	$A_{\bar{\Sigma}K N}$
$\frac{1}{2}$	$\langle n J^{K^0} \Lambda^0 \rangle$	$A_{\bar{N}K\Lambda}$	$\frac{1}{2}$	$\langle \Lambda^0 J^{K^0} n \rangle$	$A_{\bar{\Lambda}K N}$
$\frac{1}{2}$	$\langle p J^{K^+} \Lambda^0 \rangle$	$A_{\bar{N}K\Lambda}$	$\frac{1}{2}$	$\langle \Lambda^0 J^{K^-} p \rangle$	$A_{\bar{\Lambda}K N}$
$\frac{1}{2}$	$\langle \Lambda^0 J^{K^+} \Xi^- \rangle$	$A_{\bar{\Lambda}K\Xi}$	$\frac{1}{2}$	$\langle \Xi^- J^{K^-} \Lambda^0 \rangle$	$A_{\Xi\bar{K}\Lambda}$
$\frac{1}{2}$	$\langle \Lambda^0 J^{K^0} \Xi^0 \rangle$	$A_{\bar{\Lambda}K\Xi}$	$\frac{1}{2}$	$\langle \Xi^0 J^{K^0} \Lambda^0 \rangle$	$A_{\Xi\bar{K}\Lambda}$
$\frac{1}{2}$	$\langle \Sigma^- J^{K^0} \Xi^- \rangle$	$A_{\bar{\Sigma}K\Xi}$	$\frac{1}{2}$	$\langle \Xi^- J^{K^0} \Sigma^- \rangle$	$A_{\Xi\bar{K}\Sigma}$
$\frac{1}{2}$	$\langle \Sigma^0 J^{K^+} \Xi^- \rangle$	$A_{\bar{\Sigma}K\Xi}/\sqrt{2}$	$\frac{1}{2}$	$\langle \Xi^- J^{K^-} \Sigma^0 \rangle$	$A_{\Xi\bar{K}\Sigma}/\sqrt{2}$
$\frac{1}{2}$	$\langle \Sigma^0 J^{K^0} \Xi^0 \rangle$	$-A_{\bar{\Sigma}K\Xi}/\sqrt{2}$	$\frac{1}{2}$	$\langle \Xi^0 J^{K^0} \Sigma^0 \rangle$	$-A_{\Xi\bar{K}\Sigma}/\sqrt{2}$
$\frac{1}{2}$	$\langle \Sigma^+ J^{K^+} \Xi^0 \rangle$	$A_{\bar{\Sigma}K\Xi}$	$\frac{1}{2}$	$\langle \Xi^0 J^{K^-} \Sigma^+ \rangle$	$A_{\Xi\bar{K}\Sigma}$

Table 4: The isospin relations connecting the transition set of octet matrix elements with our standard subsets $A_{\bar{B}'FB}$ (each independent set separated by horizontal lines). Left table: The ‘forward’ $I = 1$ and $\frac{1}{2}$ relations; right table: the inverse relations.

Again using the π^- as an example and comparing this result with eq. (24) we see that we have

$$\hat{I}_+\pi^- = \begin{pmatrix} 1 & 0 & 0 \\ 0 & -1 & 0 \\ 0 & 0 & 0 \end{pmatrix} = \sqrt{2}\pi^0. \quad (34)$$

Listing all the relations gives

$$\begin{aligned} \hat{I}_+\pi^- &= \sqrt{2}\pi^0, \\ \hat{I}_+\pi^0 &= -\sqrt{2}\pi^+, \\ \hat{I}_+K^0 &= K^+, \\ \hat{I}_+K^- &= -\bar{K}^0. \end{aligned} \quad (35)$$

Similarly

$$\begin{aligned} \hat{I}_+\Sigma^- &= \sqrt{2}\Sigma^0, \\ \hat{I}_+\Sigma^0 &= -\sqrt{2}\Sigma^+, \\ \hat{I}_+n &= p, \\ \hat{I}_+\Xi^- &= -\Xi^0. \end{aligned} \quad (36)$$

The action of \hat{I}_- is similar. Since these relations are not those usually used to calculate the Clebsch-Gordon coefficients, we need to tabulate the isospin relations within each multiplet. The signs of the \hat{I}_+ matrix elements follow directly from the choice of signs in the chiral perturbation theory representation of the meson and baryon octets as 3×3 matrices in eqs. (24, 25). The guiding principle is to make the off-diagonal entries there positive. However this tidy choice of matrix leads to a non-standard phase convention within isospin multiplets.

In the CS convention all the coefficients in eqs. (35, 36) would be positive. Looking at the baryon results, eq. (36), we see that the neutron and proton are consistent with that convention, while, for example, the Ξ^- and Ξ^0 are not. The minus sign tells us that one of the Ξ states must have the opposite phase to the CS convention. Since only relative phases are observable, we could choose the Ξ^0 to have the CS phase, and the Ξ^- to have the flipped phase. (Making the other choice would not change the final result.) Similarly looking at the Σ baryons we could choose the Σ^+ to have the CS phase, and the Σ^- and Σ^0 to have flipped phase (or vice versa).

One choice of phases that would match eqs. (35, 36) would be to choose the n , p , Σ^+ and Ξ^0 as standard, and the Σ^- , Σ^0 and Ξ^- as flipped, and the equivalent choice for the meson currents (i.e. π^- , π^0 , K^- flipped). If we look in Tables 3 and 4 we see that matrix elements involving an even number of hadrons from the flipped group, the Clebsch-Gordon factor is the same as that in the usual tables, if an odd number of flipped hadrons are involved, the sign is the opposite to that in the usual tables.

As an example of the use of Table 3, we show how the unbroken $SU(2)$ symmetry can be used to find the transition amplitude $\langle p|J^{\pi^+}|n\rangle$ from the corresponding diagonal amplitude $\langle p|J^{\pi^0}|p\rangle$. From the table

$$\langle p|J^{\pi^+}|n\rangle = \sqrt{2} A_{\bar{N}\pi N} = \sqrt{2} \langle p|J^{\pi^0}|p\rangle, \quad (37)$$

giving

$$\langle p|\bar{u}\gamma d|n\rangle = \langle p|(\bar{u}\gamma u - \bar{d}\gamma d)|p\rangle, \quad (38)$$

which is again the simple example showing the relation between off-diagonal and diagonal currents briefly discussed in section 2.

5 Mass dependence of amplitudes

We first consider the simple singlet case (operators with the η' flavour structure, $i = 0$, see Table 1) and then consider the octet states.

5.1 Simple cases II: Flavour-singlet operators

For matrix elements involving singlet currents, $\langle B_i|J^{F_0}|B_i\rangle \equiv \langle B_i|J^{\eta'}|B_i\rangle$, we need the $SU(3)$ analysis of $8 \otimes 1 \otimes 8$ tensors. These are just the $8 \otimes 8$ matrices

already analysed in [2]. The conclusion is thus that matrix elements of flavour singlet operators follow the same formulae as the hadron masses. An example of a flavour singlet operator is the quark component to the baryon spin, $\Delta\Sigma$. For example the LO expansion is given by

$$\begin{aligned}
A_{\bar{N}\eta'N} &= a_0 + 3a_1\delta m_l, \\
A_{\bar{\Lambda}\eta'\Lambda} &= a_0 + 3a_2\delta m_l, \\
A_{\bar{\Sigma}\eta'\Sigma} &= a_0 - 3a_2\delta m_l, \\
A_{\Xi\eta'\Xi} &= a_0 - 3(a_1 - a_2)\delta m_l,
\end{aligned}
\tag{39}$$

with higher orders given in [2].

5.2 Group theory classification: Flavour-octet operators

To find the allowed mass dependence of octet matrix elements of octet hadrons we need the $SU(3)$ decomposition of $8 \otimes 8 \otimes 8$. Using the intermediate result

$$8 \otimes 8 = 1 \oplus 8 \oplus 8 \oplus 10 \oplus \bar{10} \oplus 27, \tag{40}$$

we find

$$\begin{aligned}
&8 \otimes 8 \otimes 8 \\
&= 1 \oplus 1 \oplus 8 \oplus 8 \oplus 8 \oplus 8 \oplus 8 \oplus 8 \oplus 8 \oplus 8 \oplus 8 \oplus 8 \oplus 27 \oplus 27 \oplus 27 \oplus 27 \oplus 27 \oplus 27 \oplus 64 \\
&\quad \oplus 10 \oplus 10 \oplus 10 \oplus 10 \oplus \bar{10} \oplus \bar{10} \oplus \bar{10} \oplus \bar{10} \oplus 35 \oplus 35 \oplus \bar{35} \oplus \bar{35}.
\end{aligned}
\tag{41}$$

With three unequal quark masses, the $n_f = 1 + 1 + 1$ case, I_3 and Y are both ‘good’ flavour quantum numbers, so the tensors in eq. (19) will satisfy $I_3 = 0$, $Y = 0$, i.e. they will be the central locations (spots) in each multiplet in Fig. 2. Thus in a full $n_f = 1 + 1 + 1$ flavour calculation (three different quark masses) we would see contributions from all the representations in eq. (41).

Fortunately in the $n_f = 2 + 1$ case the good flavour quantum numbers are I and Y , giving us the stronger constraint that only tensors with $I = 0$, $Y = 0$ enter into eq. (19). The 10, $\bar{10}$, 35 and $\bar{35}$ do not contain any $I = 0$, $Y = 0$ operators, so they no longer contribute in the $2 + 1$ case, which means that we can neglect those representations at present [17, 20]. For example for the $Y = 0$ line for the octet, we have an isospin triplet and singlet of states and similarly for the 27-plet (isospin 5-plet, triplet and singlet) and 64-plet (isospin 7-plet, 5-plet, triplet and singlet). However for the 10-plet we have just an isospin triplet and for the 35-plet a 5-plet and triplet. In both cases there is no $Y = 0$ isospin singlet.

We have already seen this phenomenon in [2] for the case of the 10 and $\bar{10}$. The simplest quark-mass polynomial with 10, $\bar{10}$ symmetry was $(\delta m_s - \delta m_u)(\delta m_s - \delta m_d)(\delta m_u - \delta m_d)$ (see Table 2), which vanishes if any two quark masses are equal. The 10 and $\bar{10}$ only appeared in two quantities we have considered, the violation of the Coleman-Glashow mass relation, and in $\Sigma^0 - \Lambda^0$ mixing [21], both of which are isospin violating.

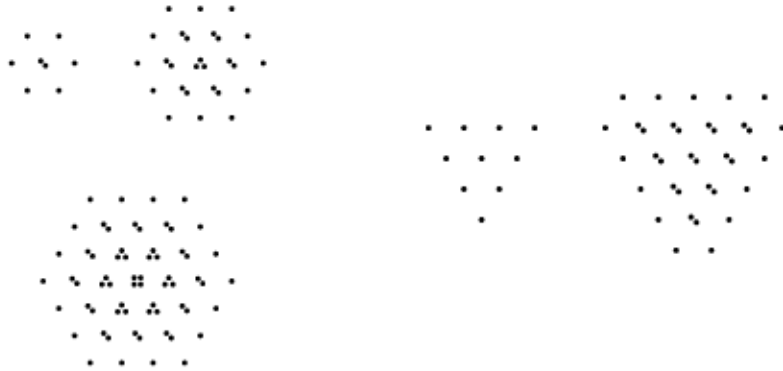


Figure 2: I_3, Y plots for some of the $SU(3)$ multiplets which appear in the decomposition of $8 \otimes 8 \otimes 8$. The left-hand plot illustrates the octet, 27-plet and 64-plet representations (clockwise). The right-hand plot shows the 10 and 35-plets (left to right). The number of spots in the central location gives the number of flavour-conserving operators in each multiplet.

5.3 The $SU(3)$ symmetry-breaking expansions

5.3.1 Basis

Because $8 \times 8 \times 8$ tensors are easier to think about than $3 \times 3 \times 3 \times 3 \times 3 \times 3$ tensors we switch to regarding baryons and mesons as vectors of length 8. We have used the ordering

$$\begin{pmatrix} n \\ p \\ \Sigma^- \\ \Sigma^0 \\ \Lambda^0 \\ \Sigma^+ \\ \Xi^- \\ \Xi^0 \end{pmatrix} \quad \text{and} \quad \begin{pmatrix} K^0 \\ K^+ \\ \pi^- \\ \pi^0 \\ \eta \\ \pi^+ \\ K^- \\ \bar{K}^0 \end{pmatrix}. \quad (42)$$

The 8 generators of $SU(3)$ are now a set of 8×8 matrices, chosen so that λB in the matrix-vector notation has the same effect as $[\lambda, B]$ in the 3×3 matrix-matrix notation. We have

$$\lambda^1 = \begin{pmatrix} 0 & 1 & 0 & 0 & 0 & 0 & 0 & 0 \\ 1 & 0 & 0 & 0 & 0 & 0 & 0 & 0 \\ 0 & 0 & 0 & \sqrt{2} & 0 & 0 & 0 & 0 \\ 0 & 0 & \sqrt{2} & 0 & 0 & -\sqrt{2} & 0 & 0 \\ 0 & 0 & 0 & 0 & 0 & 0 & 0 & 0 \\ 0 & 0 & 0 & -\sqrt{2} & 0 & 0 & 0 & 0 \\ 0 & 0 & 0 & 0 & 0 & 0 & 0 & -1 \\ 0 & 0 & 0 & 0 & 0 & 0 & -1 & 0 \end{pmatrix},$$

$$\lambda^2 = \begin{pmatrix} 0 & i & 0 & 0 & 0 & 0 & 0 & 0 \\ -i & 0 & 0 & 0 & 0 & 0 & 0 & 0 \\ 0 & 0 & 0 & i\sqrt{2} & 0 & 0 & 0 & 0 \\ 0 & 0 & -i\sqrt{2} & 0 & 0 & -i\sqrt{2} & 0 & 0 \\ 0 & 0 & 0 & 0 & 0 & 0 & 0 & 0 \\ 0 & 0 & 0 & i\sqrt{2} & 0 & 0 & 0 & 0 \\ 0 & 0 & 0 & 0 & 0 & 0 & 0 & -i \\ 0 & 0 & 0 & 0 & 0 & 0 & i & 0 \end{pmatrix},$$

$$\lambda^3 = \begin{pmatrix} -1 & 0 & 0 & 0 & 0 & 0 & 0 & 0 \\ 0 & 1 & 0 & 0 & 0 & 0 & 0 & 0 \\ 0 & 0 & -2 & 0 & 0 & 0 & 0 & 0 \\ 0 & 0 & 0 & 0 & 0 & 0 & 0 & 0 \\ 0 & 0 & 0 & 0 & 0 & 0 & 0 & 0 \\ 0 & 0 & 0 & 0 & 0 & 2 & 0 & 0 \\ 0 & 0 & 0 & 0 & 0 & 0 & -1 & 0 \\ 0 & 0 & 0 & 0 & 0 & 0 & 0 & 1 \end{pmatrix},$$

$$\lambda^4 = \frac{1}{\sqrt{2}} \begin{pmatrix} 0 & 0 & -\sqrt{2} & 0 & 0 & 0 & 0 & 0 \\ 0 & 0 & 0 & -1 & -\sqrt{3} & 0 & 0 & 0 \\ -\sqrt{2} & 0 & 0 & 0 & 0 & 0 & 0 & 0 \\ 0 & -1 & 0 & 0 & 0 & 0 & 1 & 0 \\ 0 & -\sqrt{3} & 0 & 0 & 0 & 0 & \sqrt{3} & 0 \\ 0 & 0 & 0 & 0 & 0 & 0 & 0 & \sqrt{2} \\ 0 & 0 & 0 & 1 & \sqrt{3} & 0 & 0 & 0 \\ 0 & 0 & 0 & 0 & 0 & \sqrt{2} & 0 & 0 \end{pmatrix},$$

$$\lambda^5 = \frac{1}{\sqrt{2}} \begin{pmatrix} 0 & 0 & i\sqrt{2} & 0 & 0 & 0 & 0 & 0 \\ 0 & 0 & 0 & i & i\sqrt{3} & 0 & 0 & 0 \\ -i\sqrt{2} & 0 & 0 & 0 & 0 & 0 & 0 & 0 \\ 0 & -i & 0 & 0 & 0 & 0 & -i & 0 \\ 0 & -i\sqrt{3} & 0 & 0 & 0 & 0 & -i\sqrt{3} & 0 \\ 0 & 0 & 0 & 0 & 0 & 0 & 0 & -i\sqrt{2} \\ 0 & 0 & 0 & i & i\sqrt{3} & 0 & 0 & 0 \\ 0 & 0 & 0 & 0 & 0 & i\sqrt{2} & 0 & 0 \end{pmatrix},$$

$$\lambda^6 = \frac{1}{\sqrt{2}} \begin{pmatrix} 0 & 0 & 0 & 1 & -\sqrt{3} & 0 & 0 & 0 \\ 0 & 0 & 0 & 0 & 0 & -\sqrt{2} & 0 & 0 \\ 0 & 0 & 0 & 0 & 0 & 0 & \sqrt{2} & 0 \\ 1 & 0 & 0 & 0 & 0 & 0 & 0 & -1 \\ -\sqrt{3} & 0 & 0 & 0 & 0 & 0 & 0 & \sqrt{3} \\ 0 & -\sqrt{2} & 0 & 0 & 0 & 0 & 0 & 0 \\ 0 & 0 & \sqrt{2} & 0 & 0 & 0 & 0 & 0 \\ 0 & 0 & 0 & -1 & \sqrt{3} & 0 & 0 & 0 \end{pmatrix},$$

$$\begin{aligned}
\lambda^7 &= \frac{1}{\sqrt{2}} \begin{pmatrix} 0 & 0 & 0 & -i & i\sqrt{3} & 0 & 0 & 0 \\ 0 & 0 & 0 & 0 & 0 & i\sqrt{2} & 0 & 0 \\ 0 & 0 & 0 & 0 & 0 & 0 & -i\sqrt{2} & 0 \\ i & 0 & 0 & 0 & 0 & 0 & 0 & i \\ -i\sqrt{3} & 0 & 0 & 0 & 0 & 0 & 0 & -i\sqrt{3} \\ 0 & -i\sqrt{2} & 0 & 0 & 0 & 0 & 0 & 0 \\ 0 & 0 & i\sqrt{2} & 0 & 0 & 0 & 0 & 0 \\ 0 & 0 & 0 & -i & i\sqrt{3} & 0 & 0 & 0 \end{pmatrix}, \\
\lambda^8 &= \sqrt{3} \begin{pmatrix} 1 & 0 & 0 & 0 & 0 & 0 & 0 & 0 \\ 0 & 1 & 0 & 0 & 0 & 0 & 0 & 0 \\ 0 & 0 & 0 & 0 & 0 & 0 & 0 & 0 \\ 0 & 0 & 0 & 0 & 0 & 0 & 0 & 0 \\ 0 & 0 & 0 & 0 & 0 & 0 & 0 & 0 \\ 0 & 0 & 0 & 0 & 0 & 0 & 0 & 0 \\ 0 & 0 & 0 & 0 & 0 & 0 & -1 & 0 \\ 0 & 0 & 0 & 0 & 0 & 0 & 0 & -1 \end{pmatrix}. \tag{43}
\end{aligned}$$

These 8×8 λ matrices follow similar relations to the familiar 3×3 matrices,

$$[\lambda^i, \lambda^j] = 2i f^{ijk} \lambda^k, \quad \text{Tr}(\lambda^i \lambda^j) = 12 \delta^{ij}, \tag{44}$$

and

$$I_3 = \frac{1}{2} \lambda^3, \quad Y = \frac{1}{\sqrt{3}} \lambda^8, \tag{45}$$

with the difference that the 3×3 matrices tell us about I_3 and Y for the individual quarks, but the 8×8 matrices give the quantum numbers of the octet baryons or octet mesons.

5.3.2 Transformations

Under an $SU(3)$ rotation the tensors on the right-hand side of eq. (19) transform according to

$$T'_{ijk} = U_{ia}^\dagger T_{abc} U_{bj} U_{ck}. \tag{46}$$

The change in T under an infinitesimal transformation by the generator λ^α is

$$\hat{O}^\alpha T \equiv -\lambda_{ia}^\alpha T_{ajk} + T_{ibk} \lambda_{bj}^\alpha + T_{ijc} \lambda_{ck}^\alpha. \tag{47}$$

The Casimir operator for the $SU(3)$ representation is

$$\hat{C}T = \frac{1}{4} \sum_{\alpha=1,8} \hat{O}^\alpha \hat{O}^\alpha T, \tag{48}$$

while the Casimir for the $SU(2)$ isospin subgroup is

$$\hat{I}^2 T = \frac{1}{4} \sum_{\alpha=1,3} \hat{O}^\alpha \hat{O}^\alpha T. \tag{49}$$

The $n_f = 2 + 1$ mass matrix commutes with $\lambda^1, \lambda^2, \lambda^3$ (the generators of isospin) and λ^8 (hypercharge). We are looking for tensors which obey these symmetries, so we require

$$\hat{O}^\alpha T = 0, \quad \alpha = 1, 2, 3, 8. \quad (50)$$

The Casimir operator has the following eigenvalues for the representations occurring in $8 \otimes 8 \otimes 8$, see for example chapter 4 of [20] or chapter 7 (exercise 7.12) of [22]

representation	1	8	10	$\overline{10}$	27	35	$\overline{35}$	64	
Casimir eigenvalue	0	3	6	6	8	12	12	15	(51)

We now want to construct tensors which are eigenstates of the Casimir operator, and which satisfy the conditions in eq. (50). This is analogous to constructing an eigenvector if we know the eigenvalues. We have a large number of simultaneous linear equations involving the numbers T_{ijk} . The solutions tend to be sparse with the conditions in eq. (50) forcing many entries to be zero. We calculate the tensors of a given symmetry with the help of Mathematica, [23]. We begin with a completely general tensor T_{ijk} with 8^3 entries, and impose the conditions eq. (50). This forces many entries to be zero, as it eliminates all entries in which the flavour quantum numbers of the ‘outgoing’ particle i is not the sum of the flavours of j and k (for example $\langle \Xi^0 | J^{\pi^+} | p \rangle = 0$ because charge and strangeness do not balance). The conditions eq. (50) are also sufficient to force all the relations in Tables 3 and 4 to hold. After imposing eq. (50) we have reduced the initial general tensor with $8^3 = 512$ entries down to a tensor with only 17 independent parameters. From the decomposition of $8 \otimes 8 \otimes 8$ as given in eq. (41) we can work out how many solutions there are of each symmetry. The representations 1, 8, 27 and 64 each have a single state satisfying eq. (50), while the 10, $\overline{10}$, 35 and $\overline{35}$ have no states compatible with eq. (50) because they do not have a $Y = 0, I^2 = 0$ central state, see Fig. 2 and the related discussion. The 17 linearly independent tensors remaining after imposing eq. (50) can now be further classified as eigenstates of the Casimir operator. Finding these tensors is a simple matter of solving simultaneous equations, analogous to determining an eigenvector once the eigenvalue is known.

As in the case of degenerate eigenvalues, there is a degree of choice in choosing which linear combinations of the eigenstates we choose as our basis. Often there are interchange operations which we can choose to be even or odd. In particular we can choose our tensors to be first class or second class depending on the symmetry or antisymmetry when the baryons are switched, as discussed in section 2.

We can see this by introducing a reflection matrix R which inverts each octet,

leaving the central two states unchanged

$$R = \begin{pmatrix} 0 & 0 & 0 & 0 & 0 & 0 & 0 & 1 \\ 0 & 0 & 0 & 0 & 0 & 0 & 1 & 0 \\ 0 & 0 & 0 & 0 & 0 & 1 & 0 & 0 \\ 0 & 0 & 0 & 1 & 0 & 0 & 0 & 0 \\ 0 & 0 & 0 & 0 & 1 & 0 & 0 & 0 \\ 0 & 0 & 1 & 0 & 0 & 0 & 0 & 0 \\ 0 & 1 & 0 & 0 & 0 & 0 & 0 & 0 \\ 1 & 0 & 0 & 0 & 0 & 0 & 0 & 0 \end{pmatrix}. \quad (52)$$

For the mesons this is the charge conjugation operation. We note that $R^2 = I$ (the unit matrix), so R can only have the eigenvalues ± 1 , hence we can classify states according to whether they are even or odd under operations involving R . Tensors can be divided into first or second class depending on the symmetry

$$\begin{aligned} \text{first class} & \quad T_{ijk} = +T_{kai}R_{aj}, \\ \text{second class} & \quad T_{ijk} = -T_{kai}R_{aj}, \end{aligned} \quad (53)$$

in which the baryon order is reversed, and R applied to the current (meson) index. Furthermore the definition of first/second class tensors in eq. (53) agrees with the previous discussion: in eqs. (8, 9) we interchanged B and B' and took the transpose of the flavour matrix, F . This latter operation is easily seen to be equivalent to the reflection, R in eq. (53).

We can further classify tensors by the symmetry when R is applied to all three indices

$$\begin{aligned} d\text{-like} & \quad T_{ijk} = +R_{ia}T_{abc}R_{bj}R_{ck}, \\ f\text{-like} & \quad T_{ijk} = -R_{ia}T_{abc}R_{bj}R_{ck}. \end{aligned} \quad (54)$$

As can be seen from eq. (41) there must be two singlet eigenstates, eight octets, six 27-plets and one 64-plet, 17 in total. All tensors, T , are classified by their symmetry properties, according to whether first or second class, eq. (53), and whether they are f -like or d -like, eq. (54), and are given by

$SU(3)$	T , 1 st class		T , 2 nd class		
	d -like	f -like	d -like	f -like	
1	d	f			
8	r_1, r_2, r_3	s_1, s_2	t_1, t_2	u_1	
27	q_1, q_2	w_1, w_2	x_1	y_1	
64	z				

(55)

Furthermore in Appendix A we list all non-zero elements for all 17 tensors, together with their values. For example in eq. (56) we give the non-zero elements

of the tensors $T = r_1$ and t_1 ,

T	T_{ijk}	ijk								
r_1	1	151	252	353	454	555	656	757	858	(56)
t_1	1	115	225	335	445	665	775	885		
	-1	518	527	536	544	563	572	581		

The values of the non-zero T_{ijk} elements are given in the second column, while their position is given in the third block. In particular we see that the r_1 tensor only has 8 non-zero entries, all identical in value, in the positions T_{i5i} , where i can take any value from 1 to 8. It can easily be checked, for example, that the tensors r_1 and t_1 with non-zero elements as given in eq. (56) are first and second class tensors, respectively.

The r_i tensors are d -like and can be regarded as responsible for the quark-mass dependence of the d coupling (see the d -fan in section 8), while the s_i tensors are f -like and act as quark-mass-dependent additions to the f coupling (as seen in the f -fan – see section 8).

We are now finally in a position to present the $SU(3)$ flavour-symmetry-breaking expansions. As we are considering only the isospin limit, eq. (16), then Table 2 reduces to Table 5. For example, let us consider $\langle p | J^{\pi^+} | n \rangle \equiv \langle B_2 | J^{F_6} | B_1 \rangle$,

Polynomial	$SU(3)$		
1	1		
δm_l	8		
δm_l^2	1	27	
δm_l^2	8	27	
δm_l^3	1	27	64
δm_l^3	8	27	64

Table 5: All the quark-mass polynomials in the isospin limit up to $O(\delta m_l^3)$, classified by symmetry properties.

eq. (28). From Table 3, this is $\sqrt{2}A_{\bar{N}\pi N}$. Hence from eq. (19), and using Table 5 and Appendix A (for the non-zero 261 component of the appropriate tensor) and using the same notation for the expansion coefficients as for the tensor gives the LO expansion

$$\sqrt{2}A_{\bar{N}\pi N} = 1 \times (\sqrt{2}f + \sqrt{6}d) + \delta m_l \times (-2\sqrt{2}r_3 + 2\sqrt{2}s_1). \quad (57)$$

At higher orders, we also need in addition the non-zero elements of the 27- and 64-plet. Further examples are given in the next section in eqs. (61, 62).

6 Coefficient tables

We use the same notation for the expansion coefficients as for the tensor. For example the r_1 tensor (with components T_{i5i}) has expansion coefficient r_1 .

6.1 Leading-order coefficient tables

The $SU(3)$ singlet and octet coefficients in the mass Taylor expansion of operator amplitudes are tabulated in Table 6. These coefficients are sufficient for the linear

I	$A_{\bar{B}'FB}$	1, 1 st class		8, 1 st class					8, 2 nd class		
		$O(1)$		$O(\delta m_l)$					$O(\delta m_l)$		
		f	d	d	d	d	f	f	d	d	f
		f	d	r_1	r_2	r_3	s_1	s_2	t_1	t_2	u_1
0	$\bar{N}\eta N$	$\sqrt{3}$	-1	1	0	0	0	-1	0	0	0
0	$\bar{\Sigma}\eta\Sigma$	0	2	1	0	$2\sqrt{3}$	0	0	0	0	0
0	$\bar{\Lambda}\eta\Lambda$	0	-2	1	2	0	0	0	0	0	0
0	$\bar{\Xi}\eta\Xi$	$-\sqrt{3}$	-1	1	0	0	0	1	0	0	0
1	$\bar{N}\pi N$	1	$\sqrt{3}$	0	0	-2	2	0	0	0	0
1	$\bar{\Sigma}\pi\Sigma$	2	0	0	0	0	-2	$\sqrt{3}$	0	0	0
1	$\bar{\Xi}\pi\Xi$	1	$-\sqrt{3}$	0	0	2	2	0	0	0	0
1	$\bar{\Sigma}\pi\Lambda$	0	2	0	1	$-\sqrt{3}$	0	0	1	0	0
1	$\bar{\Lambda}\pi\Sigma$	0	2	0	1	$-\sqrt{3}$	0	0	-1	0	0
$\frac{1}{2}$	$\bar{N}K\Sigma$	$-\sqrt{2}$	$\sqrt{6}$	0	0	$\sqrt{2}$	$\sqrt{2}$	0	0	$\sqrt{2}$	$\sqrt{6}$
$\frac{1}{2}$	$\bar{N}K\Lambda$	$-\sqrt{3}$	-1	0	1	0	$-\sqrt{3}$	1	1	$\sqrt{3}$	-1
$\frac{1}{2}$	$\bar{\Lambda}K\Xi$	$\sqrt{3}$	-1	0	1	0	$\sqrt{3}$	-1	-1	$-\sqrt{3}$	-1
$\frac{1}{2}$	$\bar{\Sigma}K\Xi$	$\sqrt{2}$	$\sqrt{6}$	0	0	$\sqrt{2}$	$-\sqrt{2}$	0	0	$-\sqrt{2}$	$\sqrt{6}$
$\frac{1}{2}$	$\bar{\Sigma}\bar{K}N$	$-\sqrt{2}$	$\sqrt{6}$	0	0	$\sqrt{2}$	$\sqrt{2}$	0	0	$-\sqrt{2}$	$-\sqrt{6}$
$\frac{1}{2}$	$\bar{\Lambda}\bar{K}N$	$-\sqrt{3}$	-1	0	1	0	$-\sqrt{3}$	1	-1	$-\sqrt{3}$	1
$\frac{1}{2}$	$\bar{\Xi}\bar{K}\Lambda$	$\sqrt{3}$	-1	0	1	0	$\sqrt{3}$	-1	1	$\sqrt{3}$	1
$\frac{1}{2}$	$\bar{\Xi}\bar{K}\Sigma$	$\sqrt{2}$	$\sqrt{6}$	0	0	$\sqrt{2}$	$-\sqrt{2}$	0	0	$\sqrt{2}$	$-\sqrt{6}$

Table 6: Coefficients in the mass Taylor expansion of $A_{\bar{B}'FB}$ operator amplitudes: $SU(3)$ singlet and octet, for both first-class and second-class currents. The first row gives whether singlet or octet and first or second class, and the second row gives the order in δm_l . The third row gives whether the associated tensor is f -like or d -like according to the definition given in eq. (54). These coefficients are sufficient for the linear expansion of hadronic amplitudes.

expansion of hadronic amplitudes on the constant \bar{m} line. (If \bar{m} were not kept constant there would be two more linear terms.)

The table is to be read: for first-class currents the f and d terms are independent of the quark mass, while the r_1, r_2, r_3 and s_1, s_2 coefficients are the leading order (LO) or δm_l terms. For second-class currents, as discussed previously, there are no leading f and d terms, the expansion starts at $O(\delta m_l)$ for the off-diagonal currents or completely vanishing for the diagonal currents.

Thus for example to first order in δm_l (i.e. LO) we can read off from Tables 3, 4 and 6

$$\begin{aligned}
\langle p|J^n|p\rangle &= A_{\bar{N}\eta N} = \sqrt{3}f - d + (r_1 - s_2)\delta m_l, \\
\langle n|J^{K^+}|\Sigma^-\rangle &= A_{\bar{N}K\Sigma} = -\sqrt{2}f + \sqrt{6}d + (\sqrt{2}r_3 + \sqrt{2}s_1)\delta m_l, \\
\langle \Sigma^+|J^n|\Sigma^+\rangle &= A_{\bar{\Sigma}\eta\Sigma} = 2d + (r_1 + 2\sqrt{3}r_3)\delta m_l,
\end{aligned} \tag{58}$$

for first-class currents (for example for the vector current the form factors F_1 and F_2 from eq. (10)) and

$$\begin{aligned}
\langle n|J^{K^+}|\Sigma^-\rangle &= A_{\bar{N}K\Sigma} = (\sqrt{2}t_2 + \sqrt{6}u_1)\delta m_l, \\
\langle \Sigma^-|J^{K^-}|n\rangle &= A_{\bar{\Sigma}K N} = -(\sqrt{2}t_2 + \sqrt{6}u_1)\delta m_l,
\end{aligned} \tag{59}$$

for second-class currents (for example for the F_3 vector form factor).

A notational comment: we shall usually suppress arguments and indices, but each coefficient in Table 6 is a function of the (momentum transfer)², Q^2 , as well as being renormalised or not. Thus for example for the renormalised vector current, the f coefficient in Table 6 is to be understood as $f \rightarrow f^{\text{vR}}(\bar{m}, Q^2)$.

Note that the clean separation of amplitudes and form factors into first and second class depends on the fact that we have defined our amplitudes in ways that treat the parent and daughter baryons symmetrically. If we had used an unsymmetric definition, for instance always normalising amplitudes in terms of the parent baryon's mass, we would find t_i and u_i coefficients appearing in the expansions of quantities which 'should' only involve the symmetric terms.

6.2 Higher-order coefficient tables

For completeness in Table 7 we detail the additional quadratic and cubic coefficients in the mass Taylor expansion of the operator amplitudes for the 27 and 64-plets.

For first-class currents in Table 5 the singlet terms do not contribute at the linear $O(\delta m_l)$ level, but are present at the quadratic $O(\delta m_l^2)$ and cubic $O(\delta m_l^3)$ levels. Similarly the octet terms are missing at the $O(1)$ level, but are present at higher orders. Hence these terms are also present at the higher orders in the $SU(3)$ flavour-breaking expansion. There are $5 + 7 = 12$ amplitudes, and at the $O(\delta m_l^2)$ level 11 free parameters, so there is one constraint. (Alternatively at the $O(\delta m_l^2)$ level one can have all possibilities which are orthogonal to the 64-plet, so there is again just one constraint.) At the $O(\delta m_l^3)$ level one has 12

		27, 1 st class $O(\delta m_l^2)$				64, 1 st $O(\delta m_l^3)$	27, 2 nd class $O(\delta m_l^2)$	
		d	d	f	f	d	d	f
I	$A_{\bar{B}'FB}$	q_1	q_2	w_1	w_2	z	x_1	y_1
0	$\bar{N}\eta N$	9	3	0	$3\sqrt{3}$	$3\sqrt{3}$	0	0
0	$\bar{\Sigma}\eta\Sigma$	-6	-10	0	0	$-\sqrt{3}$	0	0
0	$\bar{\Lambda}\eta\Lambda$	-18	18	0	0	$-9\sqrt{3}$	0	0
0	$\bar{\Xi}\eta\Xi$	9	3	0	$-3\sqrt{3}$	$3\sqrt{3}$	0	0
1	$\bar{N}\pi N$	$-5\sqrt{3}$	$\sqrt{3}$	4	-1	1	0	0
1	$\bar{\Sigma}\pi\Sigma$	0	0	-4	2	0	0	0
1	$\bar{\Xi}\pi\Xi$	$5\sqrt{3}$	$-\sqrt{3}$	4	-1	-1	0	0
1	$\bar{\Sigma}\pi\Lambda$	14	-6	0	0	$-\sqrt{3}$	4	0
1	$\bar{\Lambda}\pi\Sigma$	14	-6	0	0	$-\sqrt{3}$	-4	0
$\frac{1}{2}$	$\bar{N}K\Sigma$	0	$2\sqrt{6}$	$-3\sqrt{2}$	$2\sqrt{2}$	$\sqrt{2}$	$\sqrt{6}$	$\sqrt{2}$
$\frac{1}{2}$	$\bar{N}K\Lambda$	-6	0	$3\sqrt{3}$	0	$3\sqrt{3}$	-3	$3\sqrt{3}$
$\frac{1}{2}$	$\bar{\Lambda}K\Xi$	-6	0	$-3\sqrt{3}$	0	$3\sqrt{3}$	3	$3\sqrt{3}$
$\frac{1}{2}$	$\bar{\Sigma}K\Xi$	0	$2\sqrt{6}$	$3\sqrt{2}$	$-2\sqrt{2}$	$\sqrt{2}$	$-\sqrt{6}$	$\sqrt{2}$
$\frac{1}{2}$	$\bar{\Sigma}\bar{K}N$	0	$2\sqrt{6}$	$-3\sqrt{2}$	$2\sqrt{2}$	$\sqrt{2}$	$-\sqrt{6}$	$-\sqrt{2}$
$\frac{1}{2}$	$\bar{\Lambda}\bar{K}N$	-6	0	$3\sqrt{3}$	0	$3\sqrt{3}$	3	$-3\sqrt{3}$
$\frac{1}{2}$	$\bar{\Xi}\bar{K}\Lambda$	-6	0	$-3\sqrt{3}$	0	$3\sqrt{3}$	-3	$-3\sqrt{3}$
$\frac{1}{2}$	$\bar{\Xi}K\Sigma$	0	$2\sqrt{6}$	$3\sqrt{2}$	$-2\sqrt{2}$	$\sqrt{2}$	$\sqrt{6}$	$-\sqrt{2}$

Table 7: Additional coefficients in the mass Taylor expansion of operator amplitudes: $SU(3)$ 27-plet and 64-plet. These additional terms first appear at the quadratic and cubic levels respectively. The same notation as for Table 6.

free parameters for the 12 amplitudes (11 previous and one extra one from the 64-plet, the z term). Hence there are now no more constraints available at this and higher orders in δm_l .

For second-class currents, there are constraints at the $O(\delta m_l)$ order as we have 5 amplitudes, but only 3 expansion coefficients. However at the next $O(\delta m_l^2)$ level we have additional 2 parameters, so there are no more constraints available. Hence for second-class operators there is no point in going higher than linear in the quark mass in the $SU(3)$ flavour-breaking expansion.

Thus, for example, from Tables 6 and 7 we would have for the first-class current

$$\begin{aligned}
\langle p|J^n|p\rangle &= A_{N\eta N} \\
&= \sqrt{3}f - d + (r_1 - s_2)\delta m_l \\
&\quad + (\sqrt{3}f^x - d^x + r_1^x - s_2^x + 6q_1 + 3q_2 + 3\sqrt{3}w_2)\delta m_l^2
\end{aligned} \tag{60}$$

$$+(\sqrt{3}f^{xx} - d^{xx} + r_1^{xx} - s_2^{xx} + 6q_1^x + 3q_2^x + 3\sqrt{3}w_2^x + 3\sqrt{3}z)\delta m_l^3,$$

where f , d is the leading coefficients, and f^x , f^{xx} and d^x , d^{xx} are the additional subdominant coefficients of the same form as the LO singlet, see Table 5. (We use x and xx superscripts to distinguish them.) Similarly for r_1 , s_2 , q_1 , q_2 and w_2 and the octet. For the second-class current

$$\begin{aligned} \langle n | J^{K^+} | \Sigma^- \rangle &= A_{\bar{N}K\Sigma} \\ &= (\sqrt{2}t_2 + \sqrt{6}u_1)\delta m_l + (\sqrt{2}t_2^x + \sqrt{6}u_1^x + \sqrt{5}x_1 + \sqrt{2}y_1)\delta m_l^2. \end{aligned} \quad (61)$$

However as just discussed the $O(\delta m_l^3)$ term for the first-class currents and the $O(\delta m_l^2)$ term for the second-class currents have no constraints between the coefficients and hence contain no new information.

From eqs. (40, 41) and as previously discussed we see that there is one 64-plet in the decomposition of $8 \otimes 8 \otimes 8$, but none in $8 \otimes 8$ and therefore 64-plet quantities only show up at $O(\delta m_l^3)$ as shown in Table 5. In [2] we have seen that the 64-plet combination of decuplet baryon masses is extremely small and we should probably expect that the 64-plet combination of amplitudes will also remain very small all the way from the symmetric point to the physical point. By using Mathematica we construct the 64-plet flavour tensor, and find that it corresponds to the combination

$$\begin{aligned} Q_{64} &\equiv 2A_{\bar{N}\eta N} - A_{\Sigma\eta\Sigma} - 3A_{\bar{\Lambda}\eta\Lambda} + 2A_{\Xi\eta\Xi} + \frac{2}{\sqrt{3}}(A_{\bar{N}\pi N} - A_{\Xi\pi\Xi}) \\ &\quad - (A_{\Sigma\pi\Lambda} + A_{\bar{\Lambda}\pi\Sigma}) + 2(A_{\bar{\Lambda}K\Xi} + A_{\bar{N}K\Lambda} + A_{\bar{\Lambda}\bar{K}N} + A_{\Xi\bar{K}\Lambda}) \\ &\quad + \sqrt{\frac{2}{3}}(A_{\bar{N}K\Sigma} + A_{\Xi K\Xi} + A_{\Xi\bar{K}\Sigma} + A_{\Xi\bar{K}N}) \\ &= O(\delta m_l^3), \end{aligned} \quad (62)$$

and as expected the linear and quadratic terms in δm_l vanish. We also note that this quantity should be zero at the 1-loop level in chiral perturbation theory [6].

In the remainder of this article we shall not consider these next-to-leading-order (NLO) and next-to-next-leading-order (NNLO) higher orders further.

7 Amplitudes at the symmetric point

We now further discuss amplitudes at the symmetric point. From eq. (41) there are two octets and one singlet in the decomposition of $8 \otimes 8$, so there will be two singlets in $8 \otimes 8 \otimes 8$. This means that at the symmetric point there are two ways to couple an octet operator between octet baryons. These correspond to the first two columns of Table 6. These two couplings are traditionally given the letters F and D . The F coupling has a pattern related to the $SU(3)$ structure constant f_{ijk} and the D coupling is related to d_{ijk} . In terms of the 3×3 matrices, the F coupling is proportional to $\text{Tr}(M[\bar{B}, B])$, the D coupling to $\text{Tr}(M\{\bar{B}, B\})$.

Let us first look at the pattern of amplitudes at the symmetric point (with no breaking of $SU(3)$ flavour symmetry). We can read off the corresponding hadronic matrix elements from Table 6 and can construct many matrix element combinations which have to be equal at the symmetric point, for example

$$\begin{aligned}
\frac{\sqrt{3}}{2}\langle p|J^n|p\rangle + \frac{1}{2}\langle p|J^{\pi^0}|p\rangle &= \langle \Sigma^+|J^{\pi^0}|\Sigma^+\rangle \\
&= -\frac{\sqrt{3}}{2}\langle \Xi^0|J^n|\Xi^0\rangle + \frac{1}{2}\langle \Xi^0|J^{\pi^0}|\Xi^0\rangle \\
&= 2f, \\
-\frac{1}{2}\langle p|J^n|p\rangle + \frac{\sqrt{3}}{2}\langle p|J^{\pi^0}|p\rangle &= \langle \Sigma^+|J^n|\Sigma^+\rangle \\
&= -\langle \Lambda^0|J^n|\Lambda^0\rangle \\
&= -\frac{1}{2}\langle \Xi^0|J^n|\Xi^0\rangle - \frac{\sqrt{3}}{2}\langle \Xi^0|J^{\pi^0}|\Xi^0\rangle \\
&= 2d.
\end{aligned} \tag{63}$$

These relations become more transparent if we write the operators out in $\bar{q}\gamma q$ form, following Table 1 giving

$$\begin{aligned}
\frac{1}{\sqrt{2}}\langle p|(\bar{u}\gamma u - \bar{s}\gamma s)|p\rangle &= \frac{1}{\sqrt{2}}\langle \Sigma^+|(\bar{u}\gamma u - \bar{d}\gamma d)|\Sigma^+\rangle \\
&= \frac{1}{\sqrt{2}}\langle \Xi^0|(\bar{s}\gamma s - \bar{d}\gamma d)|\Xi^0\rangle \\
&= 2f,
\end{aligned} \tag{64}$$

from the first line of eq. (63). Written out in this form, it is clear why these three matrix elements have to be the same at the symmetric point. The u content of the proton is the same as the u content of the Σ^+ or the s content of the Ξ^0 , because in each case it is the ‘doubly represented’ valence quark. Likewise the s in the proton is the same as the d in the Σ^+ or the d in the Ξ^0 because in each case it is the non-valence flavour. So the relations in eq. (64) are simple consequences of flavour permutation (the S_3 subgroup of $SU(3)$). Similarly, the second line of eq. (63) implies

$$\begin{aligned}
\frac{1}{\sqrt{6}}\langle p|(\bar{u}\gamma u + \bar{s}\gamma s - 2\bar{d}\gamma d)|p\rangle &= \frac{1}{\sqrt{6}}\langle \Sigma^+|(\bar{u}\gamma u + \bar{d}\gamma d - 2\bar{s}\gamma s)|\Sigma^+\rangle \\
&= \frac{1}{\sqrt{6}}\langle \Xi^0|(\bar{s}\gamma s + \bar{d}\gamma d - 2\bar{u}\gamma u)|\Xi^0\rangle \\
&= 2d.
\end{aligned} \tag{65}$$

All these matrix elements have the same pattern, ‘doubly represented + non-valence $-2\times$ singly represented’, so again we can understand why they all have

to be the same at the symmetric point. Note that the operator in the d equation, eq. (65), is always orthogonal to the operator in the f equation, eq. (64). We could also look at the pattern ‘doubly represented – singly represented’, which is just a linear combination of eq. (64) and eq. (65). Thus

$$\begin{aligned}
\frac{1}{\sqrt{2}}\langle p|(\bar{u}\gamma u - \bar{d}\gamma d)|p\rangle &\equiv \frac{1}{\sqrt{2}}\langle \Sigma^+ |(\bar{u}\gamma u - \bar{s}\gamma s)|\Sigma^+\rangle \\
&\equiv \frac{1}{\sqrt{2}}\langle \Xi^0 |(\bar{s}\gamma s - \bar{u}\gamma u)|\Xi^0\rangle \\
&= f + \sqrt{3}d.
\end{aligned} \tag{66}$$

Of course we can not deduce the full structure at the symmetric point from flavour permutations alone, identities such as

$$A_{\bar{\Sigma}\eta\Sigma} = -A_{\bar{\Lambda}\eta\Lambda} = A_{\bar{\Lambda}\pi\Sigma}, \tag{67}$$

connecting diagonal matrix elements to transition amplitudes require more general $SU(3)$ rotations to establish them.

8 Mass dependence: ‘fan’ plots

If we move away from the symmetric point, keeping \bar{m} fixed, non-singlet tensors can contribute to eq. (19). To first order in δm_l we only need consider the octets, so we can then read the mass terms off from Table 6 with an example being given in eq. (58). We can examine the violation of $SU(3)$ symmetry caused by the $m_s - m_l$ mass difference by constructing quantities which must all be equal in the fully symmetric case, but which can differ in the case of $n_f = 2 + 1$ quark masses.

We now discuss two so-called ‘fan’ plots – the d -fan plot and the f -fan plot. In Appendix B we discuss some further fan plots (called there the doubly represented – singly represented fan plots, namely the P -fan plot and the V -fan plot).

8.1 The d -fan

Using Table 6 we can construct seven quantities, D_i , which all have the same value ($2d$) at the symmetric point, but which can differ once $SU(3)$ is broken

$$\begin{aligned}
D_1 &\equiv -(A_{\bar{N}\eta N} + A_{\bar{\Xi}\eta\Xi}) = 2d - 2r_1\delta m_l, \\
D_2 &\equiv A_{\bar{\Sigma}\eta\Sigma} = 2d + (r_1 + 2\sqrt{3}r_3)\delta m_l, \\
D_3 &\equiv -A_{\bar{\Lambda}\eta\Lambda} = 2d - (r_1 + 2r_2)\delta m_l, \\
D_4 &\equiv \frac{1}{\sqrt{3}}(A_{\bar{N}\pi N} - A_{\bar{\Xi}\pi\Xi}) = 2d - \frac{4}{\sqrt{3}}r_3\delta m_l,
\end{aligned} \tag{68}$$

$$\begin{aligned}
D_5 &\equiv A_{\bar{\Sigma}\pi\Lambda} &= 2d + (r_2 - \sqrt{3}r_3)\delta m_l, \\
D_6 &\equiv \frac{1}{\sqrt{6}}(A_{\bar{N}K\Sigma} + A_{\bar{\Sigma}K\Xi}) &= 2d + \frac{2}{\sqrt{3}}r_3\delta m_l, \\
D_7 &\equiv -(A_{\bar{N}K\Lambda} + A_{\bar{\Lambda}K\Xi}) &= 2d - 2r_2\delta m_l.
\end{aligned}$$

Plotting these quantities gives a fan plot with seven lines, but only three slope parameters (r_1, r_2 and r_3), so the splittings between these observables are highly constrained. Of course, these seven quantities are not a unique choice, other linear combinations of them could be chosen. At the next order (quadratic) in δm_l there is one constraint, from eq. (62). In terms of the D_i this reads

$$-2D_1 - D_2 + 3D_3 + 2D_4 - 2D_5 + 4D_6 - 4D_7 = O(\delta m_l^3). \quad (69)$$

In the d -fan we can thus choose six independent quadratic coefficients, and fix the seventh from this constraint.

A useful ‘average D ’ can be constructed from the diagonal amplitudes

$$X_D \equiv \frac{1}{6}(D_1 + 2D_2 + 3D_4) = 2d + O(\delta m_l^2), \quad (70)$$

chosen so that the $O(\delta m_l)$ coefficient vanishes. Other average D quantities are possible if we also incorporate transition matrix elements. These average quantities can be useful for helping to set the lattice scale, [24].

It is useful to construct from this fan plots of D_i/X_D . However for our later example of the vector current, X_D vanishes at $Q^2 = 0$ and is always small, so we consider alternatively here $\tilde{D}_i \equiv D_i/X_F$.

8.2 The f -fan

Again using Table 6 we can construct five quantities F_i , which all have the same value ($2f$) at the symmetric point, but which can differ once $SU(3)$ is broken.

$$\begin{aligned}
F_1 &\equiv \frac{1}{\sqrt{3}}(A_{\bar{N}\eta N} - A_{\bar{\Xi}\eta\Xi}) &= 2f - \frac{2}{\sqrt{3}}s_2\delta m_l, \\
F_2 &\equiv (A_{\bar{N}\pi N} + A_{\bar{\Xi}\pi\Xi}) &= 2f + 4s_1\delta m_l, \\
F_3 &\equiv A_{\bar{\Sigma}\pi\Sigma} &= 2f + (-2s_1 + \sqrt{3}s_2)\delta m_l, \\
F_4 &\equiv \frac{1}{\sqrt{2}}(A_{\bar{\Sigma}K\Xi} - A_{\bar{N}K\Sigma}) &= 2f - 2s_1\delta m_l, \\
F_5 &\equiv \frac{1}{\sqrt{3}}(A_{\bar{\Lambda}K\Xi} - A_{\bar{N}K\Lambda}) &= 2f + \frac{2}{\sqrt{3}}(\sqrt{3}s_1 - s_2)\delta m_l.
\end{aligned} \quad (71)$$

Plotting these quantities gives a fan plot with 5 lines, but only two slope parameters (s_1 and s_2), so the splittings between these observables are again highly constrained. At quadratic and higher level there are no constraints between the coefficients for the f -fan.

Again a useful ‘average F ’ can be constructed from the diagonal amplitudes

$$X_F \equiv \frac{1}{6}(3F_1 + F_2 + 2F_3) = 2f + O(\delta m_l^2), \quad (72)$$

and again we can we can construct fan plots of $\tilde{F}_i \equiv F_i/X_F$.

The f -fan has the nice property that, to linear order, there is no error from dropping quark-line-disconnected contributions. This is because r_1 is the only parameter with a quark-line-disconnected piece, and none of the r_i parameters appear in the f -fan. We shall prove and expand on this point in the following sections by considering the connected and disconnected expansions separately.

9 Quark-line-connected and -disconnected diagrams

In lattice QCD for the three point function and its associated matrix element (see section 12.1 for some further details) we have two classes of diagrams to compute: quark-line connected (left panel of Fig. 3) and quark-line disconnected (the right

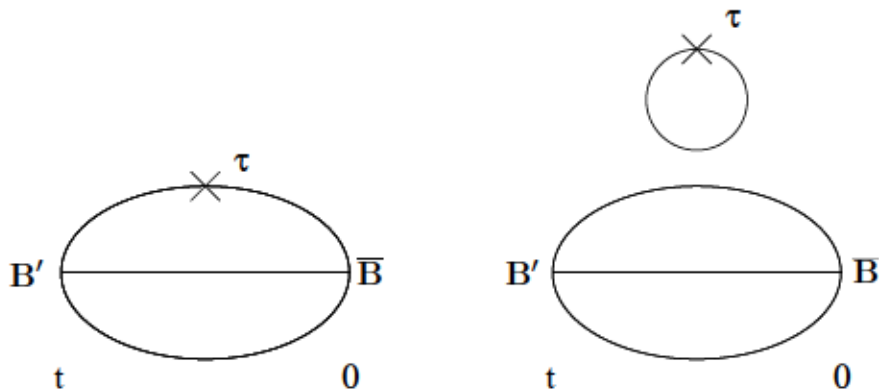


Figure 3: The three point quark correlation function for a baryon. The cross represents the current insertion. Left panel: the quark-line-connected piece; right panel: the quark-line-disconnected piece.

panel of Fig. 3). We first write

$$\langle B'|J^F|B \rangle = \langle B'|J^F|B \rangle^{\text{con}} + \langle B'|J^F|B \rangle^{\text{dis}}, \quad (73)$$

corresponding to the left and right panels of Fig. 3 respectively. Note that an alternative notation for the quark-line-connected piece is the valence matrix element $\langle B'|J^F|B \rangle^{\text{con}} \equiv \langle B'|J^F|B \rangle^{\text{val}}$. However we shall usually just say connected matrix element.

The quark-line-disconnected diagrams cannot occur for transition matrix elements, $B' \neq B$, but can for diagonal matrix elements $B' = B$. From Table 1

we see that disconnected diagonal matrix elements can only happen for the currents J^{π^0} , J^η and J^η' (indices 4, 5 and 0 respectively). As we are only considering mass degenerate u and d quarks then for the J^{π^0} operators, the u -loop and d -loop quark-line-disconnected pieces always cancel. Thus apart from the singlet operator J^η' , this leaves only the J^η operator to consider. At the symmetric point, the disconnected contribution to J^η will cancel. If one moves to $m_s \neq m_l$, then disconnected η contributions will become non-zero, as twice the strange loop will not be equal to the u loop + d loop. However, at leading order, this effect is going to be the same for all baryons, so it has the pattern only of r_1 in Table 6. Hence r_1 must have a disconnected piece.

More explicitly first consider the flavour diagonal amplitudes. In each baryon the disconnected u and d terms are equal (as $m_u = m_d$), so

$$\langle p|J^{\pi^0}|p\rangle^{\text{dis}}, \quad \langle \Sigma^+|J^{\pi^0}|\Sigma^+\rangle^{\text{dis}}, \quad \langle \Xi^0|J^{\pi^0}|\Xi^0\rangle^{\text{dis}}, \quad (74)$$

all vanish. Hence

$$f^{\text{dis}} + \sqrt{3}d^{\text{dis}} = 0, \quad f^{\text{dis}} = 0, \quad f^{\text{dis}} - \sqrt{3}d^{\text{dis}} = 0 \quad (75)$$

and

$$-r_3^{\text{dis}} + s_1^{\text{dis}} = 0, \quad -2s_1^{\text{dis}} + \sqrt{3}s_2^{\text{dis}} = 0, \quad r_3^{\text{dis}} + s_1^{\text{dis}} = 0 \quad (76)$$

giving

$$f^{\text{dis}}, d^{\text{dis}}, r_3^{\text{dis}}, s_1^{\text{dis}}, s_2^{\text{dis}} = 0. \quad (77)$$

This was briefly considered for the axial current in [25] but the results here are more general than given there.

Consider now the transition amplitudes. As stated previously disconnected terms cannot cause a transition that changes flavour. In particular considering K current transitions they must all be connected, so from Table 6 this again shows that all the above coefficients in eq. (77) have no disconnected piece, together with the additional result

$$r_2^{\text{dis}} = 0, \quad (78)$$

which means that indeed only r_1^{dis} contributes. Thus in future we need only distinguish between connected and disconnected contributions for the r_1 coefficient. Differences between the disconnected pieces in different baryons will therefore first contribute at quadratic order in the $SU(3)$ flavour-symmetry-breaking expansion.

We shall now develop and make these considerations more explicit in the following section.

10 Mass dependence: flavour-diagonal matrix elements

In the previous sections we have developed $SU(3)$ flavour-breaking expansions for $\langle B'|J^F|B\rangle$, which are sufficient for transition matrix elements. However for diagonal matrix elements we need the additional expansion $\langle B|J^{\eta'}|B\rangle$ as discussed in section 5.1. This will now enable all diagonal matrix elements to be given for each individual quark flavour.

From Table 1 we see that the diagonal flavour states are given by π^0 (index 4) and η (index 5), together with the singlet flavour state, η' (index 0). These can be inverted to give $\bar{u}\gamma u$, $\bar{d}\gamma d$ and $\bar{s}\gamma s$ in terms of $J^{\eta'}$, J^{π^0} and J^η as

$$\begin{aligned}\bar{u}\gamma u &= \frac{1}{\sqrt{3}}J^{\eta'} + \frac{1}{\sqrt{2}}J^{\pi^0} + \frac{1}{\sqrt{6}}J^\eta, \\ \bar{d}\gamma d &= \frac{1}{\sqrt{3}}J^{\eta'} - \frac{1}{\sqrt{2}}J^{\pi^0} + \frac{1}{\sqrt{6}}J^\eta, \\ \bar{s}\gamma s &= \frac{1}{\sqrt{3}}J^{\eta'} - \sqrt{\frac{2}{3}}J^\eta.\end{aligned}\tag{79}$$

As discussed previously in section 5.1, the additional expansion for the singlet current $J^{\eta'}$ is the same as the mass expansion presented in [2]. We shall only consider LO here (higher orders are also given in [2]). We take the expansion as already given in eq. (39).

Using eq. (79), together with eq. (39) and Tables 3 and 6 allows us to give the $SU(3)$ flavour-breaking expansion for flavour diagonal matrix elements. In Appendix C we give this expansion to LO for the representative octet baryons p , Σ^+ , Λ^0 and Ξ^0 (the others n , Σ^- , Σ^0 and Ξ^- can be similarly determined).

While it appears from eq. (39) that we now have extra coefficients a_0 , a_1 and a_2 that have to be determined, this can be somewhat ameliorated when the quark-line-connected and -disconnected matrix elements are considered. There was a general discussion in section 9. We now consider this in more detail by considering separate expansions for both the connected and disconnected pieces. So the previous equations are doubled, as given in eq. (73). For example

$$\langle p|\bar{u}\gamma u|p\rangle = \langle p|\bar{u}\gamma u|p\rangle^{\text{con}} + \langle p|\bar{u}\gamma u|p\rangle^{\text{dis}},\tag{80}$$

corresponding to the left and right panels of Fig. 3 respectively. There are now some additional constraints.

For completeness we list the disconnected matrix element results in Appendix D, using a_0^{dis} , a_1^{dis} , a_2^{dis} and eqs. (77, 78).

10.1 Connected terms

For $p(uud)$, $\Sigma^+(u us)$ and $\Xi^0(s s u)$ there are no connected pieces for $\langle p|\bar{s}\gamma s|p\rangle$, $\langle \Sigma^+|\bar{d}\gamma d|\Sigma^+\rangle$ and $\langle \Xi^0|\bar{d}\gamma d|\Xi^0\rangle$. Thus there are now conditions on a_0^{con} , a_1^{con} and

a_2^{con} from the previous expansion parameters. We find

$$\begin{aligned}
a_0^{\text{con}} &= \sqrt{6}f - \sqrt{2}d, \\
3a_1^{\text{con}} &= \sqrt{2}r_1^{\text{con}} - \sqrt{2}s_2, \\
3a_2^{\text{con}} &= \frac{1}{\sqrt{2}}r_1^{\text{con}} + \sqrt{6}r_3 + \sqrt{6}s_1 - \frac{3}{\sqrt{2}}s_2.
\end{aligned} \tag{81}$$

(These consistently satisfy all the previous equations.) Using these expressions for a_0^{con} , a_1^{con} and a_2^{con} gives for the octet baryons p , Σ^+ , Λ^0 and Ξ^0

$$\langle p|\bar{u}\gamma u|p\rangle^{\text{con}} = 2\sqrt{2}f + \left(\sqrt{\frac{3}{2}}r_1^{\text{con}} - \sqrt{2}r_3 + \sqrt{2}s_1 - \sqrt{\frac{3}{2}}s_2 \right) \delta m_l, \tag{82}$$

$$\langle p|\bar{d}\gamma d|p\rangle^{\text{con}} = \sqrt{2}(f - \sqrt{3}d) + \left(\sqrt{\frac{3}{2}}r_1^{\text{con}} + \sqrt{2}r_3 - \sqrt{2}s_1 - \sqrt{\frac{3}{2}}s_2 \right) \delta m_l,$$

$$\langle \Sigma^+|\bar{u}\gamma u|\Sigma^+\rangle^{\text{con}} = 2\sqrt{2}f + (-2\sqrt{2}s_1 + \sqrt{6}s_2) \delta m_l,$$

$$\begin{aligned}
\langle \Sigma^+|\bar{s}\gamma s|\Sigma^+\rangle^{\text{con}} &= \sqrt{2}(f - \sqrt{3}d) \\
&+ \left(-\sqrt{\frac{3}{2}}r_1^{\text{con}} - 3\sqrt{2}r_3 - \sqrt{2}s_1 + \sqrt{\frac{3}{2}}s_2 \right) \delta m_l,
\end{aligned} \tag{83}$$

$$\begin{aligned}
\langle \Lambda^0|\bar{u}\gamma u|\Lambda^0\rangle^{\text{con}} &= \langle \Lambda^0|\bar{d}\gamma d|\Lambda^0\rangle^{\text{con}} \\
&= \sqrt{2}\left(f - \frac{2}{\sqrt{3}}d \right) \\
&+ \left(\sqrt{\frac{2}{3}}r_1^{\text{con}} + \sqrt{\frac{2}{3}}r_2 + \sqrt{2}r_3 + \sqrt{2}s_1 - \sqrt{\frac{3}{2}}s_2 \right) \delta m_l,
\end{aligned} \tag{84}$$

$$\begin{aligned}
\langle \Lambda^0|\bar{s}\gamma s|\Lambda^0\rangle^{\text{con}} &= \sqrt{2}\left(f + \frac{1}{\sqrt{3}}d \right) \\
&+ \left(-\frac{1}{\sqrt{6}}r_1^{\text{con}} - \frac{4}{\sqrt{6}}r_2 + \sqrt{2}r_3 + \sqrt{2}s_1 - \sqrt{\frac{3}{2}}s_2 \right) \delta m_l,
\end{aligned}$$

and

$$\langle \Xi^0|\bar{u}\gamma u|\Xi^0\rangle^{\text{con}} = \sqrt{2}(f - \sqrt{3}d) + (2\sqrt{2}r_3 + 2\sqrt{2}s_1) \delta m_l,$$

$$\langle \Xi^0|\bar{s}\gamma s|\Xi^0\rangle^{\text{con}} = 2\sqrt{2}f + \left(-\sqrt{\frac{3}{2}}r_1^{\text{con}} + \sqrt{2}r_3 + \sqrt{2}s_1 - \sqrt{\frac{3}{2}}s_2 \right) \delta m_l. \tag{85}$$

Without Λ^0 there are six equations, together with six parameters, so no constraint. Adding the Λ^0 gives two more equations and one extra parameter, so this is now constrained. In addition off-diagonal matrix elements would also give more constraints.

10.2 The electromagnetic current

Using the previous results of this section, we can also give the results for the electromagnetic current, eq. (12). Using this equation we find, for example, that for the octet baryons p , Σ^+ , Λ^0 and Ξ^0

$$\begin{aligned}
\langle p|J_{\text{em}}|p\rangle^{\text{con}} &= \sqrt{2}f + \sqrt{\frac{2}{3}}d + \left(\frac{1}{\sqrt{6}}r_1^{\text{con}} - \sqrt{2}r_3 + \sqrt{2}s_1 - \frac{1}{\sqrt{6}}s_2 \right) \delta m_l, \\
\langle \Sigma^+|J_{\text{em}}|\Sigma^+\rangle^{\text{con}} &= \sqrt{2}f + \sqrt{\frac{2}{3}}d + \left(\frac{1}{\sqrt{6}}r_1^{\text{con}} + \sqrt{2}r_3 - \sqrt{2}s_1 - \sqrt{\frac{3}{2}}s_2 \right) \delta m_l, \\
\langle \Lambda^0|J_{\text{em}}|\Lambda^0\rangle^{\text{con}} &= -\sqrt{\frac{2}{3}}d + \left(\frac{1}{\sqrt{6}}r_1^{\text{con}} + \sqrt{\frac{2}{3}}r_3 \right) \delta m_l, \\
\langle \Xi^0|J_{\text{em}}|\Xi^0\rangle^{\text{con}} &= -2\sqrt{\frac{2}{3}}d + \left(\frac{1}{\sqrt{6}}r_1^{\text{con}} + \sqrt{2}r_3 + \sqrt{2}s_1 + \frac{1}{\sqrt{6}}s_2 \right) \delta m_l,
\end{aligned} \tag{86}$$

for the quark-line-connected terms, and for the quark-line-disconnected terms

$$\langle p|J_{\text{em}}|p\rangle^{\text{dis}} = \langle \Lambda^0|J_{\text{em}}|\Lambda^0\rangle^{\text{dis}} = \langle \Sigma^+|J_{\text{em}}|\Sigma^+\rangle^{\text{dis}} = \langle \Xi^0|J_{\text{em}}|\Xi^0\rangle^{\text{dis}} = \frac{1}{\sqrt{6}}r_1^{\text{dis}}\delta m_l. \tag{87}$$

Similar expansions hold for the n , Σ^0 , Σ^- and Ξ^- electromagnetic matrix elements.

11 Renormalisation and $O(a)$ improvement for the vector current

11.1 General comments

The computed matrix elements are bare (or lattice) quantities and must be renormalised and $O(a)$ improved. We would expect that the effect of the $O(a)$ improvement terms is simply to modify the $SU(3)$ flavour-breaking expansion coefficients. In this section we shall show that this expectation is indeed correct. Again, for illustration, we shall only consider the diagonal sector ($B' = B$) of the vector current here. By using the results and notation in [12] (see also [26]) we have for on-shell improvement

$$\begin{aligned}
V_\mu^{\pi^0\text{R}} &= Z_V [1 + (b_V + 3\bar{b}_V)\bar{m} + b_V\delta m_l] \mathcal{V}_\mu^{\pi^0}, \\
V_\mu^{\eta\text{R}} &= Z_V \left[(1 + (b_V + 3\bar{b}_V)\bar{m} - b_V\delta m_l) \mathcal{V}_\mu^\eta + \sqrt{2}(b_V + 3f_V)\delta m_l \mathcal{V}_\mu^{\eta'} \right], \\
V_\mu^{\eta'\text{R}} &= Z_V r_V \left[(1 + (d_V + 3\bar{d}_V)\bar{m}) \mathcal{V}_\mu^{\eta'} + 2\sqrt{2}d_V\delta m_l \mathcal{V}_\mu^\eta \right].
\end{aligned} \tag{88}$$

where \mathcal{V} for the local vector current denotes

$$\mathcal{V}_\mu^F = V_\mu^F + ic_V \partial_\nu T_{\mu\nu}^F, \quad (89)$$

with $T_{\mu\nu}^F = \bar{q}F\sigma_{\mu\nu}q$ and $\partial_\mu\phi(x) = [\phi(x + \hat{\mu}) - \phi(x - \hat{\mu})]/2$. This additional term only plays a role in non-forward matrix elements. Note that all the improvement coefficients b_V , d_V , \bar{b}_V , \bar{d}_V and c_V are just functions of the coupling constant, g_0^5 . Thus we do not have to be precisely at the correct (physical) \bar{m} to determine the coefficients. The r_V parameter accounts for the fact that the singlet renormalisation is different to the non-singlet renormalisation, $Z_V(g_0)$. r_V also depends on the chosen scheme and scale. Tree level gives for the relevant coefficients

$$b_V(g_0) = 1 + O(g_0^2), \quad f_V(g_0) = O(g_0^2), \quad c_V(g_0) = O(g_0^2), \quad (90)$$

(together with $Z_V(g_0) = 1 + O(g_0^2)$ and $d_V(g_0) = O(g_0^2)$) where $\bar{b}_V(g_0)$, $\bar{d}_V(g_0)$, being connected with the sea contributions are $\sim O(g_0^4)$, and are usually taken as negligible. Furthermore we can write

$$\begin{aligned} V_\mu^{\pi^0\text{R}} &= \hat{Z}_V \left[1 + \hat{b}_V \delta m_l \right] \mathcal{V}_\mu^{\pi^0}, \\ V_\mu^{\eta\text{R}} &= \hat{Z}_V \left[(1 - \hat{b}_V \delta m_l) \mathcal{V}_\mu^\eta + \sqrt{2}(\hat{b}_V + 3\hat{f}_V) \delta m_l \mathcal{V}_\mu^{\eta'} \right], \\ V_\mu^{\eta'\text{R}} &= \hat{Z}_V \hat{r}_V \left[\mathcal{V}_\mu^{\eta'} + 2\sqrt{2}\hat{d}_V \delta m_l \mathcal{V}_\mu^\eta \right], \end{aligned} \quad (91)$$

where for constant \bar{m} we have absorbed these \bar{m} terms into the renormalisation constant and improvement coefficients. For example we have⁶

$$\begin{aligned} \hat{Z}_V &= Z_V(1 + (b_V + 3\bar{b}_V)\bar{m}), \\ \hat{b}_V &= b_V(1 + (b_V + 3\bar{b}_V)\bar{m})^{-1}, \\ \hat{f}_V &= f_V(1 + (b_V + 3\bar{b}_V)\bar{m})^{-1}. \end{aligned} \quad (92)$$

We take eq. (91) as our definition of the improvement coefficients, as the $SU(3)$ flavour-breaking expansion coefficients are already functions of \bar{m} . To avoid confusion with the previous $SU(3)$ flavour-breaking expansion coefficients we have denoted them with a caret. Note that in any case we have also numerically that $|\bar{m}\delta m_l| \ll 1$ and $\bar{m}^2 \ll 1$ so the improvement coefficients are effectively unchanged.

⁵There is a further improvement coefficient, $g_0^2 \rightarrow \hat{g}_0^2 = g_0^2(1 + b_g\bar{m})$, where b_g is a function of g_0^2 . Little is known about the value of b_g , however perturbatively it is very small, so we shall ignore it here. Note that as we always consider $\bar{m} = \text{const.}$, then the value of g_0^2 is only slightly shifted by a constant.

⁶Similarly $\hat{r}_V = r_V(1 + (d_V + 3\bar{d}_V)\bar{m})(1 + (b_V + 3\bar{b}_V)\bar{m})^{-1}$ and $\hat{d}_V = d_V(1 + (d_V + 3\bar{d}_V)\bar{m})^{-1}$.

11.1.1 $V_\mu^{\pi^0 R}$

Let us first consider $V_\mu^{\pi^0 R}$ in eq. (91), together with (for example) $\langle p|V_4^{\pi^0}|p\rangle^R$, $\langle \Sigma^+|V_4^{\pi^0}|\Sigma^+\rangle^R$, $\langle \Xi^0|V_4^{\pi^0}|\Xi^0\rangle^R$. From the expansion for $F = \pi^0$ given in Table 6 for $A_{\bar{N}\pi N}$, $A_{\bar{\Sigma}\pi\Sigma}$ and $A_{\bar{\Xi}\pi\Xi}$ we see that as expected the effects of the expansion coefficients simply change their value slightly

$$\begin{aligned} s_1 &\rightarrow s'_1 = s_1 + \frac{1}{2}f\hat{b}_V, \\ s_2 &\rightarrow s'_2 = s_2 + \sqrt{3}f\hat{b}_V, \\ r_3 &\rightarrow r'_3 = r_3 - \frac{\sqrt{3}}{2}d\hat{b}_V. \end{aligned} \quad (93)$$

Furthermore, as a reminder, from eq. (77) the disconnected pieces for f , d , r_2 , r_3 , s_1 , s_2 all vanish, which implies that \hat{b}_V also has no disconnected piece. In particular this means that the results for $V_\mu^{\pi^0 R}$ remain valid when just considering the connected matrix elements.

11.1.2 $V_\mu^{\eta R}$

We can repeat the process for $V_\mu^{\eta R}$, which gives in addition to the results of eq. (93), the further results

$$\begin{aligned} r_1 \rightarrow r'_1 &= r_1 + d\hat{b}_V + \sqrt{2}a_0(\hat{b}_V + 3\hat{f}_V), \\ r_2 \rightarrow r'_2 &= r_2 + d\hat{b}_V. \end{aligned} \quad (94)$$

In addition splitting r_1 into r_1^{con} and r_1^{dis} pieces gives upon using a_0^{con} from eq. (81)

$$\begin{aligned} r_1^{\text{con}} &\rightarrow r_1^{\text{con}'} = r_1^{\text{con}} + 2\sqrt{3}f(\hat{b}_V + 3\hat{f}_V^{\text{con}}) - d(\hat{b}_V + 6\hat{f}_V^{\text{con}}), \\ r_1^{\text{dis}} &\rightarrow r_1^{\text{dis}'} = r_1^{\text{dis}} + 3\sqrt{2}a_0^{\text{dis}}\hat{f}_V^{\text{dis}}. \end{aligned} \quad (95)$$

11.1.3 $V_\mu^{\eta' R}$

Lastly, considering $V_\mu^{\eta' R}$, we find

$$\begin{aligned} a_1 \rightarrow a'_1 &= a_1 + 2\sqrt{\frac{2}{3}}\left(f - \frac{1}{\sqrt{3}}d\right)\hat{d}_V, \\ a_2 \rightarrow a'_2 &= a_2 - \frac{4}{3}\sqrt{2}d\hat{d}_V. \end{aligned} \quad (96)$$

11.1.4 Concluding remarks

As expected, all improvement coefficients are terms in the $SU(3)$ symmetry flavour-breaking expansion, and indeed upon inclusion leads to slightly modified expansion coefficients, as given in eqs. (93, 94, 96). We anticipate that the additional improvement term, \hat{c}_V , is also of this form.

11.2 Determination of \hat{Z}_V and $\hat{b}_V, \hat{f}_V^{\text{con}}$

There is an exact global symmetry of the lattice action, $q \rightarrow e^{-i\alpha_q}q$, valid for each quark separately. Using Noether's theorem this leads to an exactly conserved vector current, CVC. Practically the operator counts the number of u quarks and the number of d quarks in the baryon. The local current considered here is not exactly conserved, so that $V_{\text{CVC}} = V + O(a)$. We can use this to define the renormalisation constant and several improvement terms. (A similar method was used for two flavours and quenched QCD in, e.g., [27].) Thus we shall see that imposing CVC is equivalent to determining some improvement coefficients.

Practically here we restrict our considerations to the forward matrix elements for V_4 at $Q^2 = 0$ (no momentum transfer, so there is no additional \hat{c}_V term).

11.2.1 $V_4^{\pi^0 \text{R}}$

First for the CVC, we consider the representative matrix elements

$$\begin{aligned} \langle p | V_4^{\pi^0} | p \rangle^{\text{R}} &= A_{N\pi N}^{\text{R}} = \frac{1}{\sqrt{2}}(2 - 1), \\ \langle \Sigma^+ | V_4^{\pi^0} | \Sigma^+ \rangle^{\text{R}} &= A_{\Sigma\pi\Sigma}^{\text{R}} = \frac{1}{\sqrt{2}}(2 - 0), \\ \langle \Xi^0 | V_4^{\pi^0} | \Xi^0 \rangle^{\text{R}} &= A_{\Xi\pi\Xi}^{\text{R}} = \frac{1}{\sqrt{6}}(1 - 0). \end{aligned} \quad (97)$$

Using this together with $V_4^{\pi^0}$ in eq. (91) gives

$$f = \frac{1}{\sqrt{2}\hat{Z}_V}, \quad d = 0. \quad (98)$$

One possibility is thus to determine f from X_F at $Q^2 = 0$, see eq. (72) as

$$\hat{Z}_V = \frac{\sqrt{2}}{X_F}. \quad (99)$$

Also from eq. (93) and due to the lack of $O(\delta m_l)$ terms in eq. (97) we have $s'_1 = 0$, $s'_2 = 0$ and $r'_3 = 0$ or

$$s_1 = -\frac{1}{2}f\hat{b}_V, \quad s_2 = -\sqrt{3}f\hat{b}_V, \quad r_3 = 0. \quad (100)$$

Using $\tilde{s}_i = s_i/X_F$, which to leading order is $s_i/(2f)$, gives directly the \hat{b}_V improvement coefficient.

11.2.2 $V_4^{\eta R}$

Additionally using the equivalent results from eq. (97) but now for $V_4^{\eta R}$ namely

$$\begin{aligned}\langle p|V_4^\eta|p\rangle^R &= A_{N\eta N}^R = \frac{1}{\sqrt{6}}(2+1-0), \\ \langle \Sigma^+|V_4^\eta|\Sigma^+\rangle^R &= A_{\Sigma\eta\Sigma}^R = \frac{1}{\sqrt{6}}(2+0-2), \\ \langle \Xi^0|V_4^\eta|\Xi^0\rangle^R &= A_{\Xi\eta\Xi}^R = \frac{1}{\sqrt{2}}(1+0-4),\end{aligned}\tag{101}$$

not only gives consistency with the previous results eqs. (98, 99), but in addition we have $r_1^{\text{con}'} = 0$, $r_2' = 0$ or from eqs. (94, 95)

$$r_1^{\text{con}} = -2\sqrt{3}f \left(\hat{b}_V + 3\hat{f}_V^{\text{con}} \right), \quad r_2 = 0.\tag{102}$$

Again using $\tilde{r}_1^{\text{con}} = r_1^{\text{con}}/X_F = r_1^{\text{con}}/(2f)$ automatically eliminates f . We observe that once \hat{Z}_V , \hat{b}_V (and \hat{f}_V^{con}) have been determined then by using eq. (92) and varying \hat{m} , then it is in principle possible to determine \hat{b}_V .

11.2.3 The Ademollo–Gatto theorem

The Ademollo–Gatto theorem [28] (see also [29, 13]) in the context of our flavour-breaking expansions states that the $O(\delta m_l)$ terms vanish for the $F_1^{\bar{B}'FB}$ form factor at $Q^2 = 0$ and $B' \neq B$. This means that r_2 , r_3 , s_1 , s_2 vanish at $Q^2 = 0$ (or the primed versions if we include the improvement coefficients). This agrees with the results of this section.

12 Lattice computations of form factors

12.1 General discussion

We now need to determine the matrix elements from a lattice simulation which computes two- and three-point correlation functions. For completeness as well as form factors with $B = B'$, we are developing a formalism for semileptonic decays, $B \neq B'$ so we first consider the general method here.

The baryon two-point correlation function is given by

$$C_\Gamma^B(t; \vec{p}) = \sum_{\alpha\beta} \Gamma_{\beta\alpha} \langle B_\alpha(t; \vec{p}) \bar{B}_\beta(0; \vec{p}) \rangle ,\tag{103}$$

while the three-point correlation function generalises this and is given by

$$C_\Gamma^{B'B}(t, \tau; \vec{p}, \vec{p}'; J) = \sum_{\alpha\beta} \Gamma_{\beta\alpha} \langle B'_\alpha(t; \vec{p}') J(\tau; \vec{q}) \bar{B}_\beta(0; \vec{p}) \rangle ,\tag{104}$$

with J at time τ either the vector, axial or tensor current, and where the source is at time 0, the sink operator is at time t and

$$\Gamma \equiv \Gamma^{\text{unpol}} = \frac{1}{2}(1 + \gamma_4), \quad \text{or} \quad \Gamma \equiv \Gamma^{\text{pol}} = \frac{1}{2}(1 + \gamma_4)i\gamma_5\vec{\gamma} \cdot \vec{n}, \quad (105)$$

where \vec{n} is the polarisation axis.

To eliminate overlaps of the source and sink operators with the vacuum, we build ratios of 3-point to 2-point correlation functions. More explicitly let us set

$$\begin{aligned} R_\Gamma(t, \tau; \vec{p}, \vec{p}'; J) &= \frac{C_\Gamma^{B'B}(t, \tau; \vec{p}, \vec{p}'; J)}{C_{\Gamma^{\text{unpol}}}^{B'}(t; \vec{p}')} \sqrt{\frac{C_{\Gamma^{\text{unpol}}}^{B'}(\tau; \vec{p}')C_{\Gamma^{\text{unpol}}}^{B'}(t; \vec{p}')C_{\Gamma^{\text{unpol}}}^B(t - \tau; \vec{p})}{C_{\Gamma^{\text{unpol}}}^B(\tau; \vec{p})C_{\Gamma^{\text{unpol}}}^B(t; \vec{p})C_{\Gamma^{\text{unpol}}}^{B'}(t - \tau; \vec{p}')}}. \end{aligned} \quad (106)$$

This is designed so that any smearing for the source and sink operators is cancelled in the ratios, e.g. [30, 31]; of course smearing the baryon operators improves the overlap with the lowest-lying state, so the relevant overlaps for the two- and three-point correlation functions must match.

Inserting complete sets of unit-normalised states in eq. (106) and for $0 \ll \tau \ll t \ll \frac{1}{2}T$ gives

$$R_\Gamma(t, \tau; \vec{p}, \vec{p}'; J) = \sqrt{\frac{E_B(\vec{p})E_{B'}(\vec{p}')}{(E_B(\vec{p}) + M_B)(E_{B'}(\vec{p}') + M_{B'})}} F(\Gamma, \mathcal{J}), \quad (107)$$

with

$$F(\Gamma, \mathcal{J}) = \frac{1}{4} \text{tr} \Gamma \left(\gamma_4 - i \frac{\vec{p}' \cdot \vec{\gamma}}{E_{B'}(\vec{p}')} + \frac{M_{B'}}{E_{B'}(\vec{p}')} \right) \mathcal{J} \left(\gamma_4 - i \frac{\vec{p} \cdot \vec{\gamma}}{E_B(\vec{p})} + \frac{M_B}{E_B(\vec{p})} \right) \quad (108)$$

(with \mathcal{J} being given from the Euclideanised version of eq. (5)). The transferred (Euclidean) momentum from the initial, B , to final, B' state is given by $Q = (i(E_{B'}(\vec{p}') - E_B(\vec{p})), \vec{p}' - \vec{p})$ so

$$Q^2 = -(M_{B'} - M_B)^2 + 2(E_{B'}(\vec{p}')E_B(\vec{p}) - M_{B'}M_B - \vec{p} \cdot \vec{p}'). \quad (109)$$

To illustrate the previous $SU(3)$ flavour symmetry-breaking results, we shall now consider here only the vector current. Furthermore in general for arbitrary momenta geometry, the kinematic factors can be complicated; in this article we shall only be considering the simpler case $\vec{p}' = \vec{0}$. The technical reason is that in the lattice evaluation, it requires less numerical inversions and is hence computationally cheaper. (Physically, of course it is more natural to start with a stationary baryon, but computationally of course it does not matter.) Evaluating Q^2 in this frame, eq. (109), shows that for flavour diagonal matrix elements form factors Q^2 is always positive, while for semileptonic decays for small momentum it can also

be negative. For the vector current with $\vec{p}' = \vec{0}$ this gives⁷.

$$\begin{aligned}
R_{\Gamma^{\text{unpol}}}(t, \tau; \vec{p}, 0; V_4) &= \sqrt{\frac{E_{\vec{p}}^B + M_B}{2E_{\vec{p}}^B}} \left[F_1^{\bar{B}'FB} - \frac{E_{\vec{p}}^B - M_B}{M_B + M_{B'}} F_2^{\bar{B}'FB} \right. \\
&\quad \left. - \frac{E_{\vec{p}}^B - M_{B'}}{M_B + M_{B'}} F_3^{\bar{B}'FB} \right], \\
R_{\Gamma^{\text{unpol}}}(t, \tau; \vec{p}, 0; V_i) &= -\frac{i p_i}{\sqrt{2E_{\vec{p}}^B(E_{\vec{p}}^B + M_B)}} \left[F_1^{\bar{B}'FB} - \frac{E_{\vec{p}}^B - M_{B'}}{M_B + M_{B'}} F_2^{\bar{B}'FB} \right. \\
&\quad \left. - \frac{E_{\vec{p}}^B + M_B}{M_B + M_{B'}} F_3^{\bar{B}'FB} \right], \quad (110) \\
R_{\Gamma^{\text{pol}}}(t, \tau; \vec{p}, 0; V_i) &= \frac{(\vec{p} \times \vec{n})_i}{\sqrt{2E_{\vec{p}}^B(E_{\vec{p}}^B + M_B)}} \left[F_1^{\bar{B}'FB} + F_2^{\bar{B}'FB} \right], \\
R_{\Gamma^{\text{pol}}}(t, \tau; \vec{p}, 0; V_4) &= 0.
\end{aligned}$$

In particular for $\vec{p} = 0$ then the only non-zero ratio is

$$R_{\Gamma^{\text{unpol}}}(t, \tau; 0, 0; V_4) = F_1^{\bar{B}'FB} - \frac{M_B - M_{B'}}{M_B + M_{B'}} F_3^{\bar{B}'FB}, \quad (111)$$

so we see that in this case for $B' \neq B$ then we cannot disentangle $F_1^{\bar{B}'FB}$ from $F_3^{\bar{B}'FB}$. However to LO (i.e. $O(\delta m_l)$ effects in the matrix elements) and as $M_B - M_{B'} \propto \delta m_l$ then from eq. (111) we can write

$$R_{\Gamma^{\text{unpol}}}(t, \tau; 0, 0; V_4) = F_1^{\bar{B}'FB} + O(\delta m_l^2), \quad (112)$$

for all B and B' , where the $O(\delta m_l^2)$ term is not present when $B' = B$.

12.2 Lattice details

As a demonstration of the method we apply the formalism outlined in the previous sections to the form factors published in [33, 34]. Further details of the numerical simulations can be found there. The simulations have been performed using $n_f = 2+1$, $O(a)$ improved clover fermions [35] at $\beta \equiv 10/g_0^2$ of 5.50 and on $32^3 \times 64$ lattice sizes, [2]. Errors given here are primarily statistical (using $\sim O(1500)$ configurations).

As discussed previously and particularly in section 3.1 our strategy is to keep the bare quark-mass constant. Thus once the $SU(3)$ flavour degenerate sea quark mass, m_0 , is chosen, subsequent sea quark-mass points m_l, m_s are then arranged

⁷We use the Euclideanisation conventions given in [32]. In particular $V_4 = V^{(\mathcal{M})0}$, $V_i = -iV^{(\mathcal{M})i}$ with $\gamma_4 = \gamma^{(\mathcal{M})0}$, $\gamma_i = -i\gamma^{(\mathcal{M})i}$, $\gamma_5 = -\gamma_5^{(\mathcal{M})}$, $\sigma_{\mu\nu} = i/2[\gamma_\mu, \gamma_\nu]$.

in the various simulations to keep \bar{m} ($= m_0$) constant. This then ensures that all the expansion coefficients given previously do not change. In [2], masses were investigated and it was seen that a linear fit provides a good description of the numerical data on the unitary line over the relatively short distance from the $SU(3)$ flavour symmetric point down to the physical pion mass. This proved useful in helping us in choosing the initial point on the $SU(3)$ flavour symmetric line to give a path that reaches (or is very close to) the physical point.

The bare unitary quark masses in lattice units are given by

$$m_q = \frac{1}{2} \left(\frac{1}{\kappa_q} - \frac{1}{\kappa_{0c}} \right) \quad \text{with } q = l, s, \quad (113)$$

and where vanishing of the quark mass along the $SU(3)$ flavour symmetric line determines κ_{0c} . We denote the $SU(3)$ flavour symmetric kappa value, κ_0 , as being the initial point on the path that leads to the physical point. m_0 is given in eq. (113) by replacing κ_q by κ_0 . Keeping $\bar{m} = \text{constant} = m_0$ then gives

$$\delta m_q = \frac{1}{2} \left(\frac{1}{\kappa_q} - \frac{1}{\kappa_0} \right). \quad (114)$$

We see that κ_{0c} has dropped out of eq. (114), so we do not need its explicit value here. Along the unitary line the quark masses are restricted and we have

$$\kappa_s = \frac{1}{\frac{3}{\kappa_0} - \frac{2}{\kappa_l}}. \quad (115)$$

So a given κ_l determines κ_s here. This approach is much cleaner than the more conventional approach of keeping (the renormalised) strange quark mass constant, as this necessitates numerically determining the bare strange quark mass. In addition the $O(a)$ improvement of the coupling constant is much simpler, in our approach as it only depends on \bar{m} , [2]. Thus here, the coupling constant remains constant and hence the lattice spacing does not change as the quark mass is changed. In the more conventional approach this can be problematical as you must in principle monitor the changing of the coupling constant as the quark masses vary.

An appropriate $SU(3)$ flavour symmetric κ_0 value chosen here for this action was found to be $\kappa_0 = 0.120900$, [2]. The constancy of flavour-singlet quantities along the unitary line to the physical point [2], leads directly from X_π to an estimate for the pion mass of ~ 465 MeV at our chosen $SU(3)$ flavour symmetric point and from X_N an estimation of the lattice spacing of $a_N(\kappa_0 = 0.120900) = 0.074$ fm.

Specifically as indicated in Table 8 we have generated configurations, [33, 34], at the (κ_l, κ_s) values listed, all with $\kappa_0 = 0.120900$.

Eqs. (110, 112) are used to determine from the ratio, R , the appropriate form factor. As described in [33, 34], we bin Q^2 to directly compare each configuration

κ_l	κ_s	M_π MeV
0.120900	0.120900	465
0.121040	0.120620	360
0.121095	0.120512	310

Table 8: Outline of the ensembles used here on the $32^3 \times 64$ lattices together with the corresponding pion masses.

and using the bootstrapped lattice configurations, we set up a weighted least squares to extract the linear fit parameters and weighted errors at each Q^2 value. The lattice momenta used here in this study in units of $2\pi/32$ are given by $a\vec{q} = (0, 0, 0)$, $(1, 0, 0)$, $(1, 1, 0)$, $(1, 1, 1)$, $(2, 0, 0)$, $(2, 1, 0)$, $(2, 1, 1)$, $(2, 2, 0)$ together with all permutations (where different) and all possible \pm values.

13 Results

We now illustrate some of the features that we have described in previous sections, using our lattice calculations and the ensembles in Table 8.

13.1 X plots

We first consider the lattice quantities $X_D^{F_1 \text{ con}}$, $X_F^{F_1}$ and $X_D^{F_2 \text{ con}}$, $X_F^{F_2}$. As discussed previously we only consider diagonal form factors to construct the X s, i.e. the equations: D_1^{con} , D_2^{con} and D_4 in eq. (68) and F_1 , F_2 and F_3 in eq. (71)⁸. Using the method of section 12.2 allows us to create the appropriate D_1^{con} , D_2^{con} and D_4 defined in eq. (68) and hence $X_D^{F_1 \text{ con}}$, $X_D^{F_2 \text{ con}}$ in eq. (70) or F_1 , F_2 and F_3 in eq. (71) and thus again $X_F^{F_1}$, $X_F^{F_2}$ in eq. (72). In Fig. 4 we consider $X_D^{F_1 \text{ con}}$ and $X_F^{F_1}$ for the F_1 form factor for $Q^2 = 0$ and 0.49 GeV^2 ⁹. First, as we expect they are constant and show little sign of $O(\delta m_l^2)$ or curvature effects. Although not so relevant on this plot, as an indication of how far we must extrapolate in the quark mass from the symmetric point to the physical point, we also give this, using the previous determination, [21], of $\delta m_l^* = -0.01103$. Note also as shown in eq. (98) for $Q^2 = 0$, $X_D^{F_1 \text{ con}}$ vanishes as $d = 0$, which we also see on the plot.

This constancy of X does not depend on the form factor used. In Fig. 5 we show similar plots, but now for the F_2 form factors: $X_D^{F_2 \text{ con}}$ and $X_F^{F_2}$, for $Q^2 = 0.25$ ¹⁰ and 0.49 GeV^2 . Again these are all constant, within our statistics.

⁸We note that care needs to be taken to distinguish the F_i corresponding to a form factor and the F_i defined in eq. (71).

⁹This corresponds to a lattice momentum of $a\vec{q} = (2\pi)/32(1, 1, 0)$.

¹⁰This corresponds to a lattice momentum of $a\vec{q} = (2\pi)/32(1, 0, 0)$.

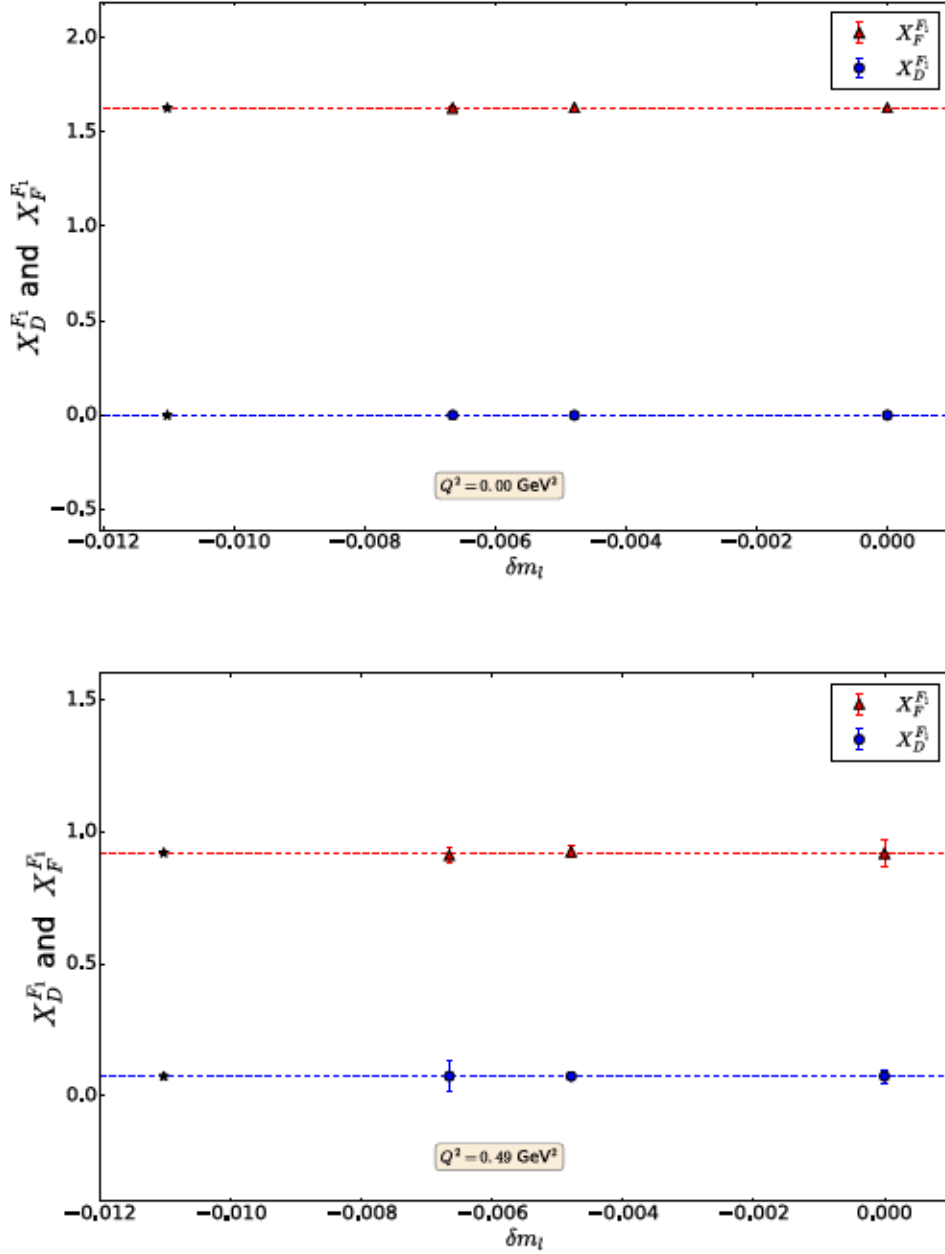


Figure 4: $X_D^{F_1 \text{ con}}$ and $X_F^{F_1}$ for F_1 at $Q^2 = 0$, top panel and for $Q^2 = 0.49 \text{ GeV}^2$, lower panel. The lower filled circles in each plot are $X_D^{F_1 \text{ con}}$, the upper filled triangles are $X_F^{F_1}$. The dashed lines are constant fits and the stars represent the physical point.

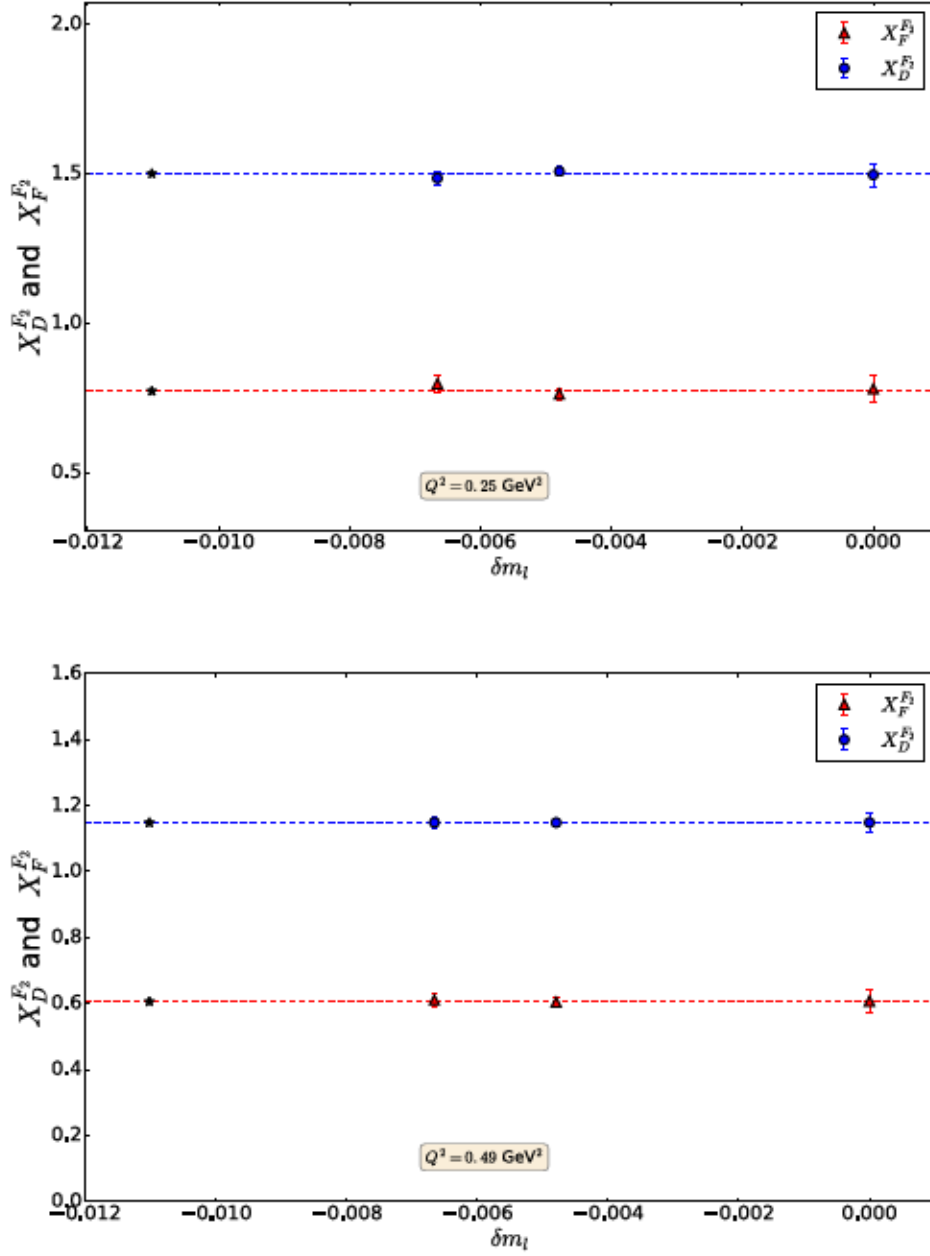


Figure 5: $X_D^{F_2^{con}}$ and $X_F^{F_2}$ for F_2 at $Q^2 = 0.25 \text{ GeV}^2$, top panel and for $Q^2 = 0.49 \text{ GeV}^2$, lower panel. The same notation as for Fig. 4.

(We can only determine $X_D^{F_2^{\text{con}}}$ at $Q^2 = 0$ via an extrapolation, so we show $Q^2 = 0.25 \text{ GeV}^2$ instead.)

Finally we can plot the dependence of X on Q^2 . In Fig. 6 we show $X_D^{F_1^{\text{con}}}$ and $X_F^{F_1}$ and similarly for X^{F_2} versus Q^2 (using the previously determined fitted values). This gives the Q^2 dependence of d and f respectively. For $X_F^{F_1}$, d is initially zero and remains small for larger Q^2 , while f drops monotonically. We expect d and f to drop like $\sim 1/Q^2$ for large Q^2 for all the form factors.

13.2 Fan plots

We now turn to ‘fan’ plots, as defined by eqs. (68) and (71). Note that again we only consider lattice quantities, the improved operator would have small changes to the $SU(3)$ flavour-breaking expansion, as discussed in section 11.1. Again we only consider diagonal form factors in these equations: D_1^{con} , D_2^{con} and D_4 in eq. (68) and F_1 , F_2 and F_4 in eq. (71). We construct the system of linear equations in eq. (68) with parameters r_1^{con} , r_3 and d for the d -fan and eq. (71) with parameters s_1 , s_2 and f for the f -fan. In Fig. 7 we show $\tilde{D}_i^{F_1} = D_i^{F_1}/X_F$ for $i = 1, 2$ and 4 and $\tilde{F}_i^{F_1} = F_i^{F_1}/X_F$ for $i = 1, 2$ and 3 . Note that as d vanishes for the F_1 form factor at $Q^2 = 0$, and even away from $Q^2 = 0$ it remains small, see the lower panel of Fig. 4, then dividing by $X_D^{F_1}$ is not possible or very noisy, so we use $X_F^{F_1}$. Although for $X_D^{F_2}$ this is not the case (as seen in Fig. 5) however for consistency we still use $X_F^{F_2}$. The only change in these cases is that the value at the symmetric point is no longer one.

The lines shown in Fig. 8 correspond to linear fits to the $D_i^{F_1^{\text{con}}}$ using eq. (68) (upper plot) and $F_i^{F_1^{\text{con}}}$ using eq. (71) (lower plot). The fits to $D_i^{F_1^{\text{con}}}$ determine r_1^{con} , r_3 using three fits and are hence constrained. Furthermore determining these two parameters also allows us to plot the off-diagonal hyperon decays for $i = 6$, which is also shown. Similarly for $F_i^{F_1}$, we first determine the constrained fit parameters $\tilde{s}_1 = s_1/X_F$, $\tilde{s}_2 = s_2/X_F$ and then plot the off-diagonal hyperon decays for $i = 4, 5$.

Similarly in Fig. 8 we show the equivalent results for F_2 . As previously we have normalised the parameters, $\tilde{r}_1^{\text{con}} = r_1^{\text{con}}/X_F$, $\tilde{r}_3 = r_3/X_F$ and $\tilde{s}_1 = s_1/X_F$, $\tilde{s}_2 = s_2/X_F$. Again we have some constraints. In addition off-diagonal hyperon decays for $i = 6$, d -fan plot and $i = 4, 5$, f -fan plot are also shown.

From these fan plots at various Q^2 we can determine the dependence of the expansion coefficients as a function of Q^2 . In Fig. 9 we show the expansion coefficients r_1^{con} , r_3 , s_1 , s_2 for the F_1^{con} and F_2 form factors as function of Q^2 . As discussed previously in section 11.1, at $Q^2 = 0$ the expansion coefficients for F_1^{con} vanish, which determines the improvement coefficients b_V , f_V^{con} . Thus in the top panel of Fig. 9 the negative values of the r_1^{con} , s_1 , s_2 are a clear indication of the nature of the improvement coefficients. For rather small Q^2 , these all change sign rather quickly and also their order inverts. We have (approximately) $|r_3|$, $|s_1| \approx 0$ and $|r_1^{\text{con}}|$ is a factor of 2–4 larger than $|s_2|$. For F_2 the expansion coefficients tend

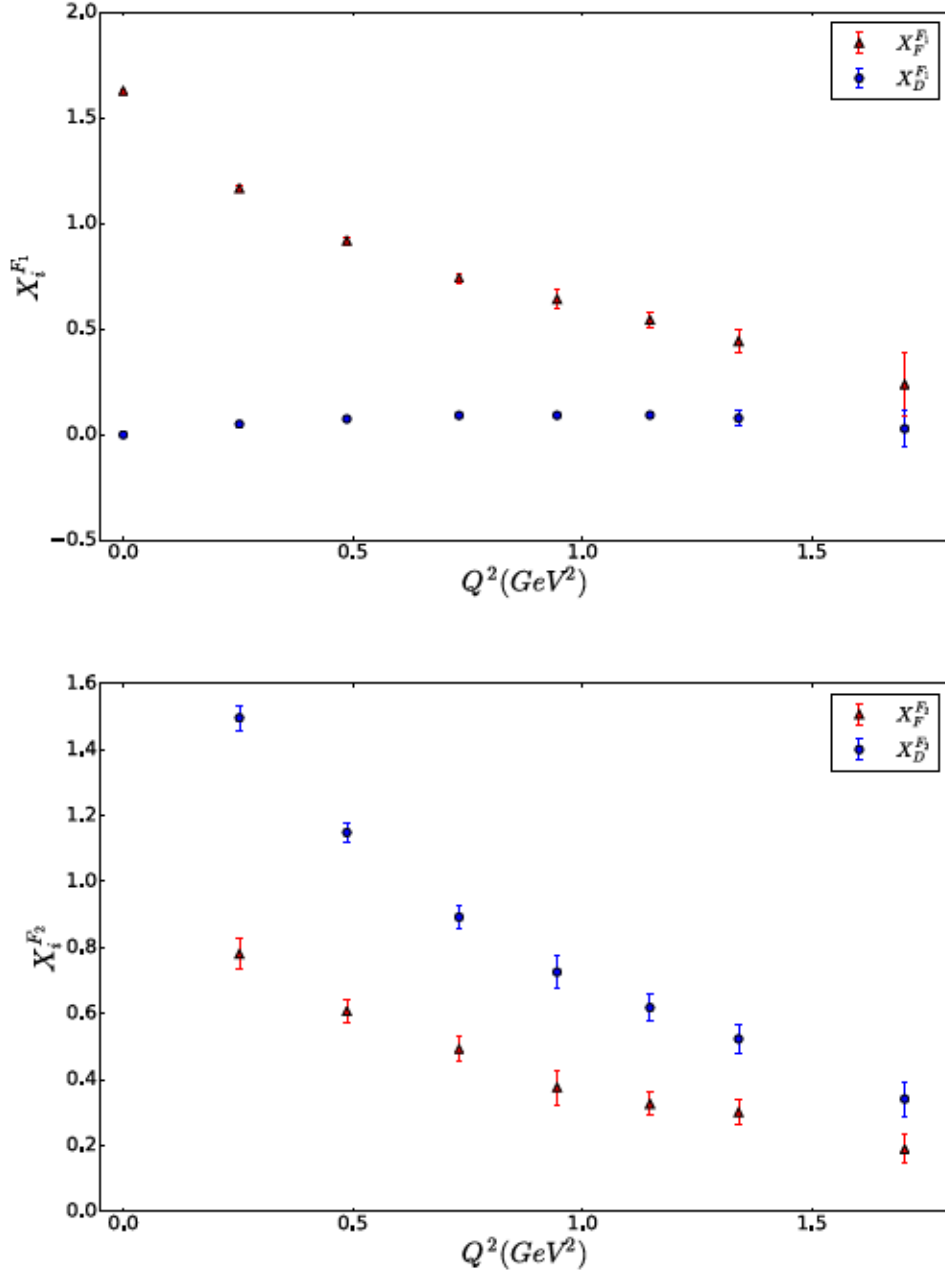


Figure 6: Top panel: $X_F^{F_1}$ (filled circles) and $X_D^{F_1 \text{ con}}$ (filled triangles) versus Q^2 . Lower panel: Similarly for F_2 .

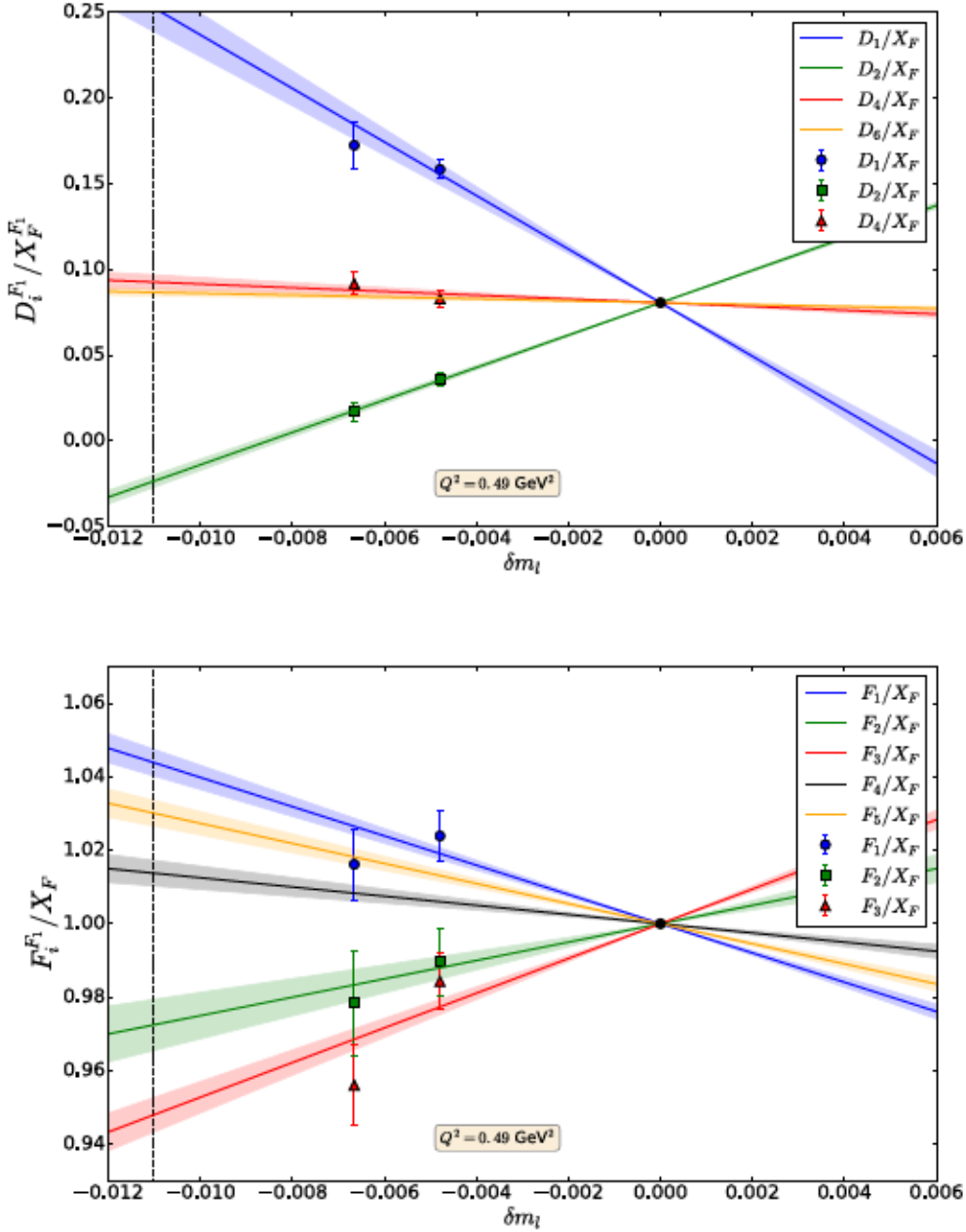


Figure 7: Top panel: $\tilde{D}_i^{F_1} \equiv D_i^{F_1}/X_F^{F_1}$ for $i = 1$ (filled circles), 2 (filled squares) and 4 (filled triangles) for $Q^2 = 0.49 \text{ GeV}^2$. The three fits are from eq. (68), the line for $i = 6$ is also shown. The vertical dotted line represents the physical point. Lower panel: $\tilde{F}_i^{F_1} \equiv F_i^{F_1}/X_F^{F_1}$ again at $Q^2 = 0.49 \text{ GeV}^2$ for $i = 1$ (filled circles), 2 (filled squares) and 3 (filled triangles), together with fits from eq. (71) normalised by $X_F^{F_1}$. The line for $i = 5$ is also shown.

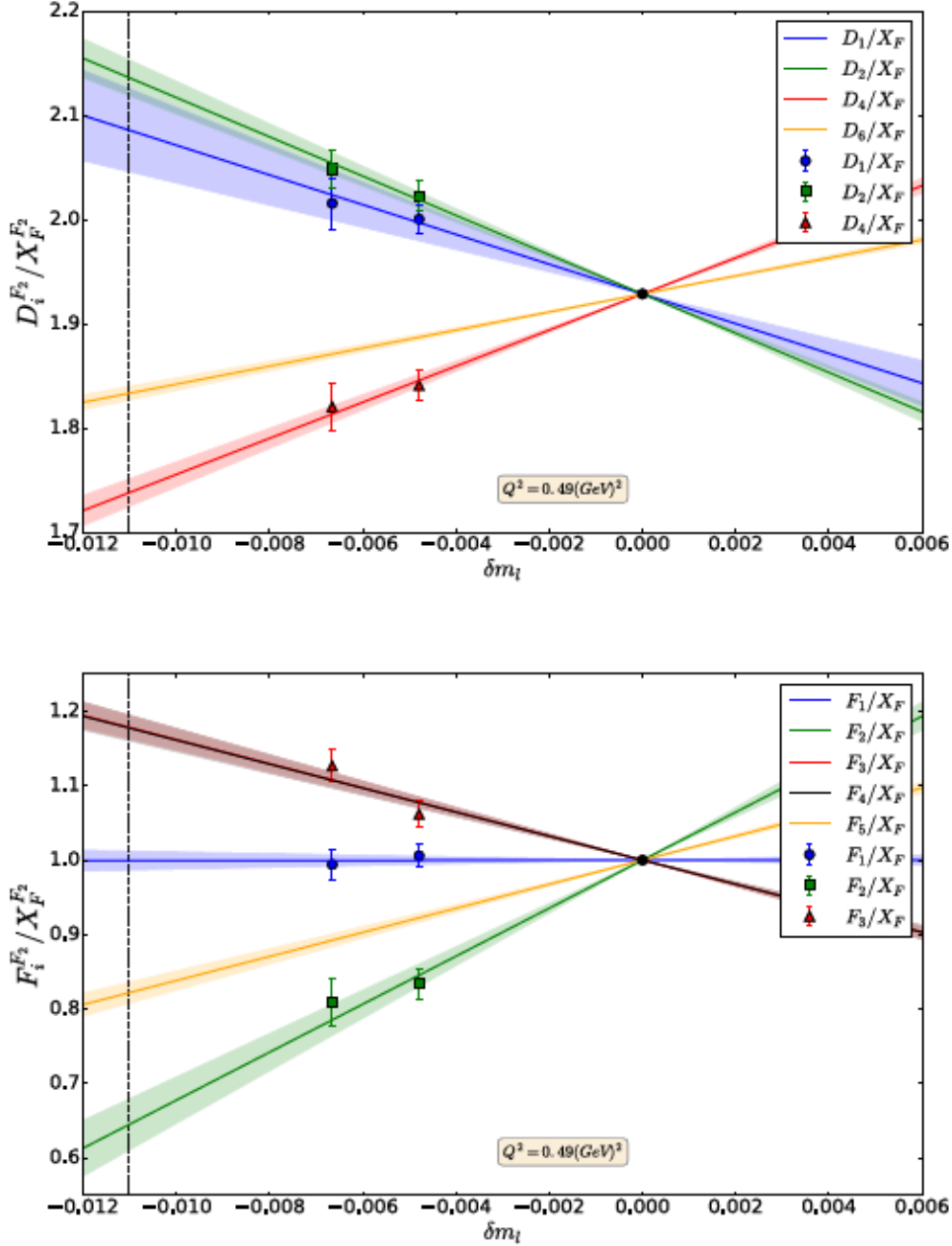


Figure 8: Top panel: $\bar{D}_i^{F_2}$ for $i = 1$ (filled circles), 2 (filled squares) and 4 (filled triangles) for $Q^2 = 0.49 \text{ GeV}^2$. The three fits are from eq. (68) normalised by $X_D^{F_2}$, also shown is the $i = 6$ line. The vertical dotted line represents the physical point. Lower panel: $\bar{F}_i^{F_2}$ for $i = 1$ (filled circles), 2 (filled squares) and 3 (filled triangles), also for $Q^2 = 0.49 \text{ GeV}^2$, together with fits from eq. (71) normalised by $X_F^{F_2}$. Also shown are the lines $i = 4$ (upper line), 5 (lower line).

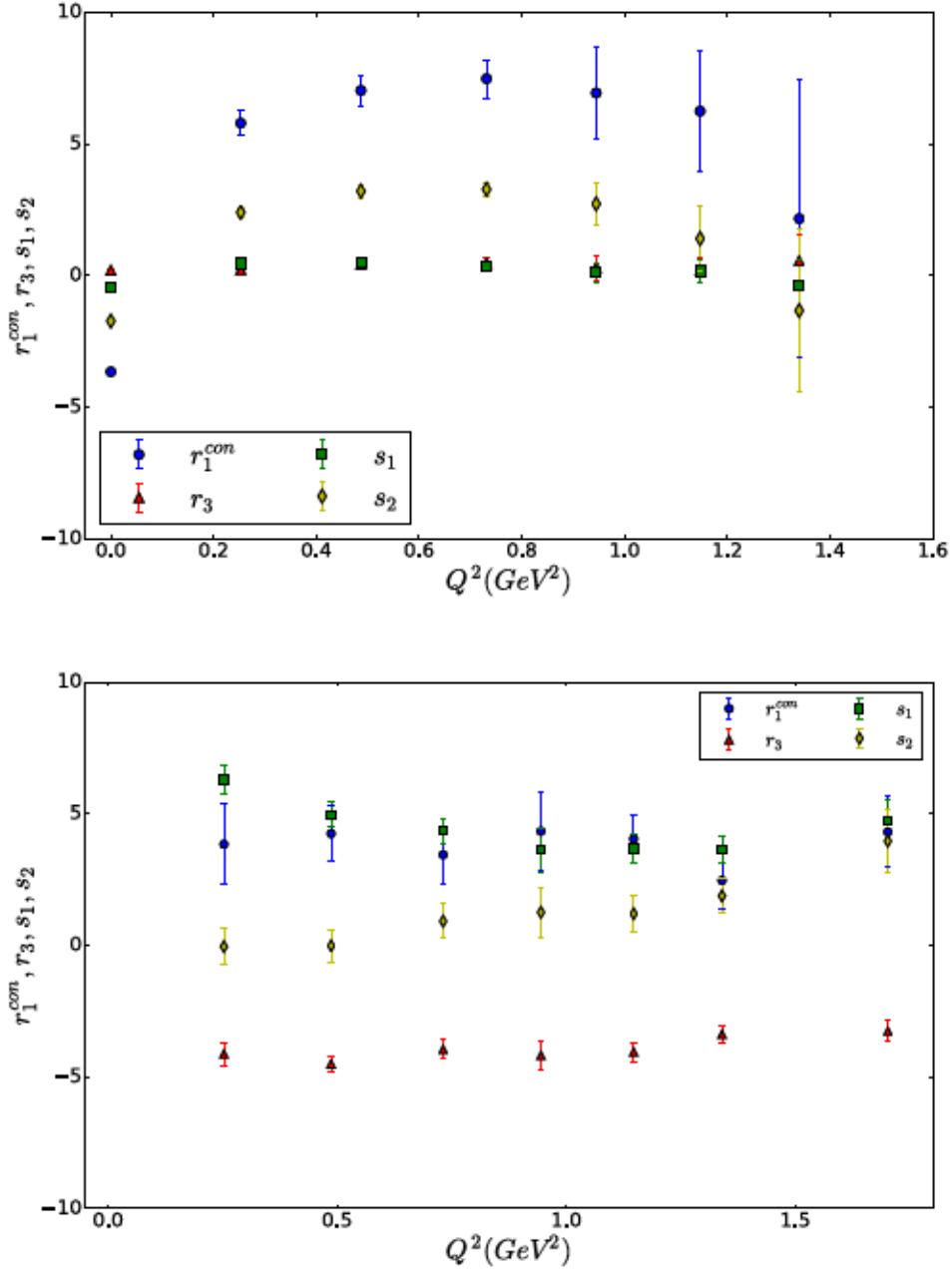


Figure 9: Top panel: r_1^{con} (filled circles), r_3 (filled triangles), s_1 (filled squares) and s_2 (filled diamonds) expansion coefficients for the vector F_1^{con} form factor as a function of Q^2 . Lower panel: Similarly for the F_2 form factor.

to be flatter. Also $s_2 \approx 0$, indicated in Fig. (8) by the small difference between $\tilde{F}_3^{F_2}$ and $\tilde{F}_4^{F_2}$.

13.3 Estimating \hat{Z}_V and \hat{b}_V , \hat{f}_V^{con}

$X_F^{F_1}$ at $Q^2 = 0$ determines the renormalisation constant \hat{Z}_V via eq. (99). The constant fit described in eq. (72) and shown in Fig. 4, see also Fig. 6, leads to $f = 0.814(1)$ or

$$\hat{Z}_V = 0.869(1). \quad (116)$$

Our previous non-perturbative estimates of Z_V at $\beta = 5.50$ are given in [36, 37] of 0.863(4), 0.857(1) respectively, and are quite close to \hat{Z}_V in eq. (116). Note that the different determinations can have $O(a)$ differences. Also \hat{Z}_V has been measured rather than Z_V . The difference is $\sim 1 + b_V \bar{m}$. Here we have $b_V \sim O(1)$ and $\bar{m} \sim 0.01$ (using the κ_{0c} found in [2]), so there a further possible difference (and reduction from the \hat{Z}_V value) of $\sim 1\%$.

From Fig. 9, the $Q^2 = 0$ value for r_3 is 0.06(2), which compared to other values is compatible with zero. The $Q^2 = 0$ values for s_1, s_2 are $s_1 = -0.479(22)$ and $s_2 = -1.643(44)$, respectively. The ratio is $s_2/s_1 = 3.42$, which is in good agreement with the theoretical value for the ratio from eq. (100) of $2\sqrt{3} \sim 3.46$. Similarly, using eq. (100), we find a weighted average of

$$\hat{b}_V = 1.174(21), \quad (117)$$

which is about a 15% increase from the tree-level value. Although a strict comparison with other determinations of this improvement coefficient is not possible, it is interesting to note that compared to other computations, e.g. [26] and for $n_f = 0, 2$, [27] the value determined here is much closer to its tree-level value eq. (90). This suggests that improvement coefficients are small, including possibly \hat{c}_V .

Using the value of \hat{b}_V from s_1, s_2 and using eq. (102) together with $r_1^{\text{con}} = -3.65(8)$ gives a weighted average of

$$\hat{f}_V^{\text{con}} = 0.041(4). \quad (118)$$

As expected this is quite small.

13.4 Electromagnetic form factor results

With a knowledge of f, d and $r_1^{\text{con}}, r_3, d, s_1, s_2$ we can find the electromagnetic Dirac form factor $F_1^{\text{con}}(Q^2)$ and Pauli form factor $F_2^{\text{con}}(Q^2)$ using the electromagnetic current $J_{\text{em}\mu}^{\text{con}}$ (see section 10.2) and results of eq. (86). Also we shall use \hat{Z}_V, \hat{b}_V and \hat{f}_V^{con} (i.e. equivalent to CVC) from section 13.3.

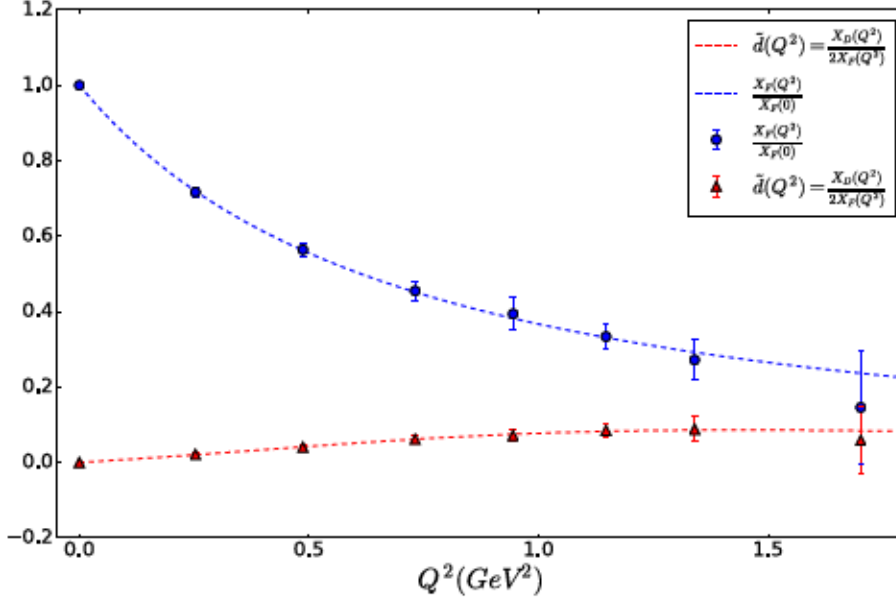


Figure 10: $X_F(Q^2)/X_F(0)$ (filled circles) and $\tilde{d}(Q^2)$ (filled triangles) for F_1^{con} against Q^2 . The interpolation formulae used are given in eq. (121).

It is interesting to determine the various contributions to the form factors from the expansion coefficients. For illustrative purposes, we shall just consider F_1^{con} here and for p and Ξ^0 . From eq. (86) we can write

$$\begin{aligned} \langle p | J_{\text{em}} | p \rangle^{\text{con R}} &= \frac{X_F(Q^2, \bar{m})}{X_F(0, \bar{m})} \left[1 + \frac{2}{\sqrt{3}} \tilde{d}(Q^2, \bar{m}) + \tilde{\epsilon}'_p(Q^2, \bar{m}) \delta m_l \right], \\ \langle \Xi^0 | J_{\text{em}} | \Xi^0 \rangle^{\text{con R}} &= -\frac{X_F(Q^2, \bar{m})}{X_F(0, \bar{m})} \left[\frac{4}{\sqrt{3}} \tilde{d}(Q^2, \bar{m}) - \tilde{\epsilon}'_{\Xi^0}(Q^2, \bar{m}) \delta m_l \right], \end{aligned} \quad (119)$$

with

$$\begin{aligned} \tilde{\epsilon}'_p &= \frac{1}{\sqrt{3}} (\tilde{r}_1^{\text{con}'} - \tilde{s}'_2) + 2(\tilde{s}'_1 - \tilde{r}'_3), \\ \tilde{\epsilon}'_{\Xi^0} &= \frac{1}{\sqrt{3}} (\tilde{r}_1^{\text{con}'} + \tilde{s}'_2) + 2(\tilde{s}'_1 + \tilde{r}'_3), \end{aligned} \quad (120)$$

where, for example, $\tilde{r}_1^{\text{con}'} = r_1^{\text{con}'}(Q^2, \bar{m})/X_F(Q^2, \bar{m})$ and similarly for the other expansion coefficients. The prime includes the improvement terms, see eqs. (93, 94). In this form, we can investigate the contributions to the form factors. In Fig. 10 we show the results for the terms of eq. (119): $X_F(Q^2)/X_F(0)$ and \tilde{d} . In Fig. 11 we show $\tilde{r}_1^{\text{con}'}$, \tilde{s}'_2 , \tilde{r}'_3 and \tilde{s}'_1 . All the interpolation formulae (fits) are of

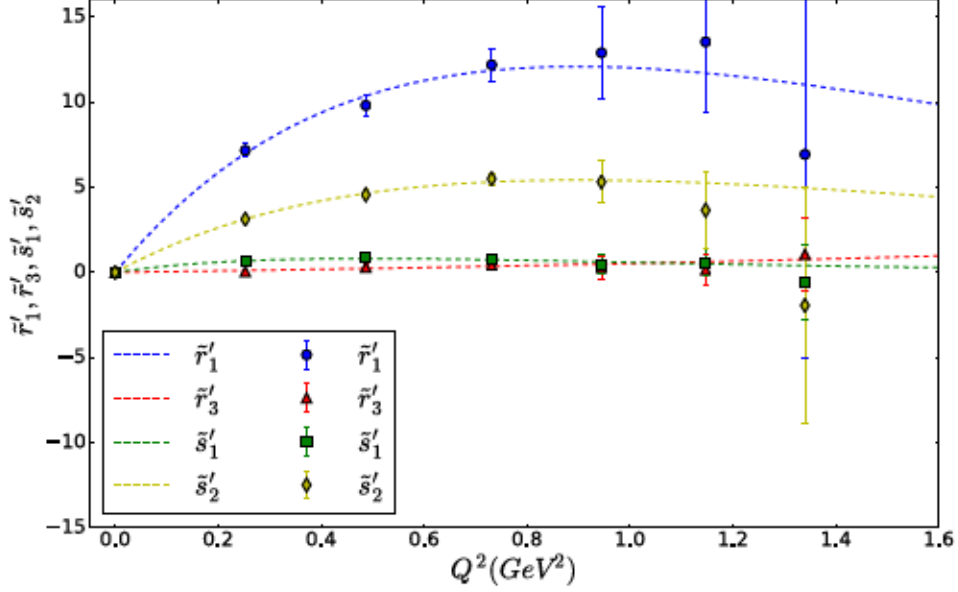


Figure 11: \tilde{r}'_1 (filled circles), \tilde{s}'_2 (filled diamonds), \tilde{s}'_1 (filled squares) and \tilde{r}'_3 (filled triangles) against Q^2 together with interpolation formulae also given by eq. (121).

the form

$$\frac{AQ^2}{1 + BQ^2 + C(Q^2)^2}. \quad (121)$$

From Fig. 10 and the leading term in eq. (119) for the proton form factor, the dominant contribution comes from $X_F(Q^2)/X_F(0)$ – the f term, while there is a small contribution from the d term (as d). Furthermore from Fig. 11 we see that for the $\tilde{\epsilon}$ coefficients, \tilde{r}'_3 and \tilde{s}'_1 are essentially negligible and most of the contribution comes from \tilde{r}'_1 and \tilde{s}'_2 .

We illustrate this for the F_1 form factor for the p and Ξ^0 . In Fig. 12 we show F_1^{conR} for these baryons at the physical point $\delta m_l^* = -0.01103$. i.e. a small and negative value. The dashed line is $X_F(Q^2)/X_F(0)$, The dashed-dotted lines are the complete leading terms: $X_F(Q^2, \bar{m})/X_F(0, \bar{m})(1 + 2/\sqrt{3}\tilde{d}(Q^2, \bar{m}))$ for p and $X_F(Q^2, \bar{m})/X_F(0, \bar{m}) \times 4/\sqrt{3}\tilde{d}(Q^2, \bar{m})$ for the Ξ^0 , while the full lines are the complete expressions in eq. (119).

We see that for the proton the f term (represented by $X_F(Q^2, \bar{m})/X_F(0, \bar{m})$) gives a result very close to the numerical result; the addition of the \tilde{d} term pulls it slightly away in the +ve direction. The inclusion of the $O(\delta m_l)$ term, being –ve pushes it back. However the additional terms to the f term contributes very little (only a few percent) to the final result. For the Ξ^0 the $O(\delta m_l)$ term improves the agreement.

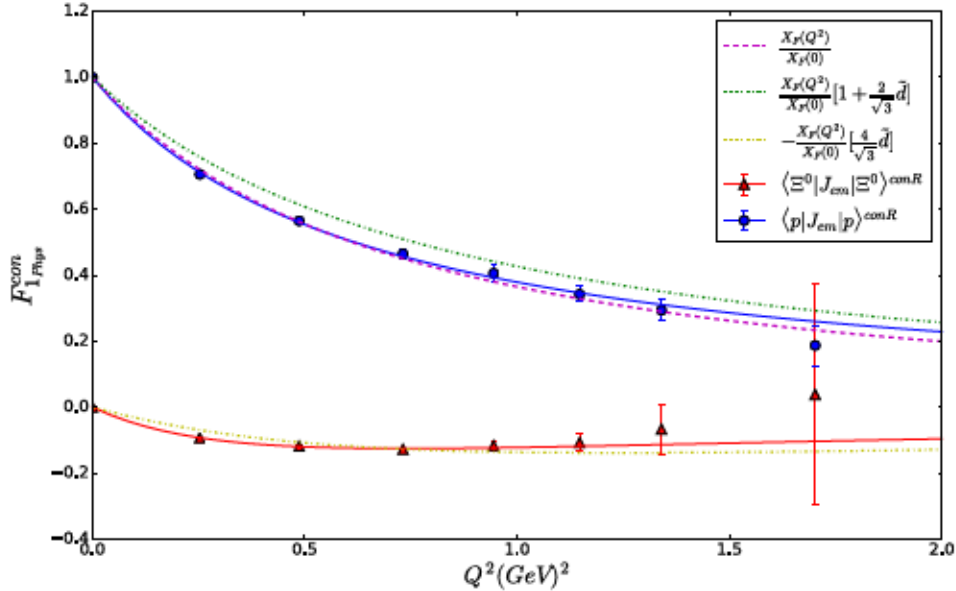


Figure 12: F_1^{con} for the proton (filled circles) and Ξ^0 (filled triangles) at the physical point. The dashed line is $X_F(Q^2)/X_F(0)$. The dashed-dotted lines are the complete leading terms, for the proton: $X_F(Q^2, \bar{m})/X_F(0, \bar{m})(1 + 2/\sqrt{3}\bar{d}(Q^2, \bar{m}))$ and for Ξ^0 : $X_F(Q^2, \bar{m})/X_F(0, \bar{m}) \times 4/\sqrt{3}\bar{d}(Q^2, \bar{m})$, while the full lines are the complete expressions in eq. (119).

14 Conclusions and outlook

In this article we have outlined a programme for investigating the quark-mass behaviour of matrix elements, for $n_f = 2 + 1$ quark flavours starting from a point on the $SU(3)$ flavour symmetric line when the u , d and s quarks have the same mass and then following a path keeping the singlet quark-mass constant. This is an extension of our original programme for masses, [1, 2], using a generalisation of the techniques developed there.

When flavour $SU(3)$ is unbroken all baryon matrix elements of a given operator octet can be expressed in terms of just two couplings (f and d), as is well known. We find that when $SU(3)$ flavour symmetry is broken, at LO and NLO, the expansions are constrained (but not at further higher orders). By this we mean that there are a large number of relations between the expansion coefficients. Our main results for the expansions are contained in sections 6.1 and 6.2. Although we concentrated on the $n_f = 2 + 1$ case, in which symmetry breaking is due to mass differences between the strange and light quarks our methods are also applicable to isospin-breaking effects coming from a non-zero $m_d - m_u$ along the lines of [38, 21].

The results here parallel those for the mass case. Firstly, for example we have

constructed ‘singlet-like’ matrix elements – collectively called X here – where the LO term vanishes. As noted in [2] these can be extrapolated to the physical point, using a one-parameter constant fit. In this article we constructed several of these X functions, and indeed can isolate the constant as either the f or d coupling. Secondly again in analogy to the mass expansions we constructed ‘fan’ plots, each element of which is a linear combination of matrix elements, where at the $SU(3)$ flavour symmetric point all the elements have a common value, and then radiate away from this point as the quark masses change. This is slightly more complicated than for the mass case as we now have two couplings, f and d . Indeed the ‘fan’ plot expansions can be constructed involving either f or d alone at the $SU(3)$ flavour symmetric point (more generally we have some combination of them).

Technically important for lattice determinations of matrix elements is the difference between quark-line-connected and quark-line-disconnected terms in the calculation of the three-point correlation functions. (The quark-line-disconnected terms are small, but difficult to compute using lattice methods, due to large gluon fluctuations.) Applying the $SU(3)$ flavour breaking expansion to these cases separately, we have identified which expansion coefficient(s) have contributions coming from the quark-line-disconnected terms. We found that at LO there is just one expansion coefficient which has a quark-line-disconnected piece.

As numerically we are using Wilson clover improved fermions, then for $O(a^2)$ continuum expansions, improvement coefficients need to be determined. The general structure for $n_f = 2 + 1$ flavours of fermions has been determined, see e.g. [12]. We showed here these coefficients are equivalent to modifications to the expansion parameters. Using the subsidiary condition that the relation between the local and conserved vector current is $O(a)$ allowed us to determine two improvement terms (together with the renormalisation constant).

To demonstrate how the expansions work, we discussed numerical results using the vector current and diagonal matrix elements. However these can be extended to include transition hyperon decays (a phenomenological review is given in [13]). These would allow an alternative method to the standard $K_{\ell 3}$ decays of determining $|V_{us}|$, e.g. [39, 13, 40]. Earlier quenched and $n_f = 2$ results for $\Sigma^- \rightarrow n\ell\nu$ and $\Xi^0 \rightarrow \Sigma^+\ell\nu$ can be found in [41, 42], and $n_f = 2 + 1$ results have been obtained in [43, 44]. The latter reference also investigates the possibility of non-linear effects in the quark-mass, which in the $SU(3)$ symmetry flavour-breaking expansion means including terms from Table 7.

Future theoretical developments include extending the formalism to partially quenched quark masses, when the valence quark mass, $\delta\mu_q$, does not have to be the same as the sea or unitary quark mass. Then eq. (14) is replaced by $\delta\mu_q = \mu_q - \bar{m}$. In this case the generalisation of eq. (17) does not hold. This allows the determination of the expansion coefficients over a larger quark mass range than is possible using the unitary quark masses (and allows, for example, the charm quark to be included, [45]). Furthermore expansions for ‘fake’ hadrons

would be useful. Possible are a ‘nucleon’ with three mass degenerate strange quarks and a ‘Lambda’ with two mass degenerate strange quarks. Although they are not physical states, they can be measured on the lattice, and do not introduce any more $SU(3)$ mass flavour-breaking expansion coefficients, so simply add more constraints to the coefficient determination. An example of this for the baryon octet masses is given in [21].

Another extension of the $SU(3)$ mass flavour breaking method is to the baryon decuplet with $10 \otimes 8 \otimes 10$ tensors, and also to the meson octet. While the latter extension is straightforward, there are some extra constraints, as due to charge conjugation, the particles in the meson octet are related to each other.

Furthermore generalised currents can be evaluated between quark states. This leads to a $SU(3)$ mass flavour-breaking expansion involving $3 \otimes 8 \otimes 3$ tensors. This will help when considering the non-perturbative $RI' - MOM$ scheme which defines the renormalisation constants (and improvement constants) by considering the generalised currents between quark states. Useful would also be to consider the axial current improvement coefficients using a partially conserved axial-vector current (PCAC) along the lines of [12].

Finally, a more distant prospect is to include QED corrections to the matrix elements, [10], along the lines of our previous studies of the $SU(3)$ flavour-breaking expansion for masses, [3, 4, 5].

Acknowledgements

The numerical configuration generation (using the BQCD lattice QCD program [46]) and data analysis (using the Chroma software library [47]) was carried out on the IBM BlueGene/Q and HP Tesseract using DIRAC 2 resources (EPCC, Edinburgh, UK), the IBM BlueGene/Q (NIC, Jülich, Germany) and the Cray XC40 at HLRN (The North-German Supercomputer Alliance), the NCI National Facility in Canberra, Australia (supported by the Australian Commonwealth Government) and Phoenix (University of Adelaide). We would like to thank Ashley Cooke for useful discussions at an early stage in this project. RH was supported by STFC through grant ST/P000630/1. HP was supported by DFG Grant No. PE 2792/2-1. PELR was supported in part by the STFC under contract ST/G00062X/1. GS was supported by DFG Grant No. SCHI 179/8-1. RDY and JMZ were supported by the Australian Research Council Grants FT120100821, FT100100005, DP140103067 and DP190100297. We thank all funding agencies.

Appendix

A Non-zero tensor elements

The non-zero elements of the tensors T_{ijk} are listed in Tables 9 – 13.

tensor	value	position								
f	2	334	463	646						
	-2	343	436	664						
	$\sqrt{3}$	151	252	518	527	775	885			
	$-\sqrt{3}$	115	225	572	581	757	858			
	$\sqrt{2}$	132	261	317	628	783	876			
	$-\sqrt{2}$	123	216	371	682	738	867			
	1	114	242	427	481	774	848			
	-1	141	224	418	472	747	884			
d	$\sqrt{6}$	123	132	216	261	317	371			
		628	682	738	783	867	876			
	2	335	353	445	454	536	544	563	656	665
	-2	555								
	$\sqrt{3}$	224	242	427	472	747	774			
	$-\sqrt{3}$	114	141	418	481	848	884			
	-1	115	151	225	252	518	527			
		572	581	757	775	858	885			

Table 9: Flavour-singlet first-class non-zero elements of the f and d tensors.

B Alternative fan plots

B.1 The doubly represented – singly represented fan, the P -fan

The traditional way of expressing the two ways of coupling octet operators to octet hadrons are the f and d couplings. In terms of hadron structure, this choice is perhaps more natural for octet mesons than it is for octet baryons. Consider the eqs. (64, 65). In the K^+ , with quark content $u\bar{s}$ the f combination $\langle K^+ | (\bar{u}\gamma u - \bar{s}\gamma s) | K^+ \rangle$ is very natural (the difference between the two valence quarks), and the d combination $\langle K^+ | (\bar{u}\gamma u + \bar{s}\gamma s - 2\bar{d}\gamma d) | K^+ \rangle$ is also a natural-looking symmetric combination. For the Λ , the d combination is also the natural non-singlet operator to consider, $d \propto \langle \Lambda | (2\bar{s}\gamma s - \bar{u}\gamma u - \bar{d}\gamma d) | \Lambda \rangle$ because the u and d in the Λ have the same structure functions, while the s structure is different (even before breaking $SU(3)$).

tensor	value	position								
r_1	1	151	252	353	454	555	656	757	858	
r_2	2	555								
	1	115	225	335	445	518	527	536		
		544	563	572	581	665	775	885		
r_3	$2\sqrt{3}$	353	454	656						
	$-2\sqrt{2}$	132	261	738	867					
	2	141	848							
	-2	242	747							
	$-\sqrt{3}$	335	445	536	544	563	665			
	$\sqrt{2}$	123	216	317	371	628	682	783	876	
	1	224	427	472	774					
	-1	114	418	481	884					
s_1	$2\sqrt{2}$	132	261							
	$-2\sqrt{2}$	738	867							
	2	242	343	436	664	848				
	-2	141	334	463	646	747				
	$\sqrt{3}$	518	527	775	885					
	$-\sqrt{3}$	115	225	572	581					
	$\sqrt{2}$	123	216	371	682					
	$-\sqrt{2}$	317	628	783	876					
	1	224	418	472	884					
	-1	114	427	481	774					
s_2	$\sqrt{3}$	334	463	646						
	$-\sqrt{3}$	343	436	664						
	1	115	225	572	581	757	858			
	-1	151	252	518	527	775	885			

Table 10: First-class octet non-zero elements of the r_1 , r_2 , r_3 and s_1 , s_2 tensors.

But in the proton, it might be a bit more natural to choose the combinations $(\bar{u}\gamma u - \bar{d}\gamma d)$ and $(\bar{u}\gamma u + \bar{d}\gamma d - 2\bar{s}\gamma s)$ instead. The first combination is the non-singlet combination normally considered in discussions of proton structure, the second is almost (but not exactly) a measure of the total valence contribution, because the quark-line-disconnected (sea) contribution to $(\bar{u}\gamma u + \bar{d}\gamma d - 2\bar{s}\gamma s)$ is zero at the symmetric point, and will probably stay small if the nucleon's sea is approximately $SU(3)$ symmetric.

We can therefore construct a fan plot for the doubly represented – singly represented quark.

$$P_1 = \sqrt{2}A_{\bar{N}\pi N} = \left(\sqrt{2}f + \sqrt{6}d\right) - 2\sqrt{2}(r_3 - s_1)\delta m_l,$$

tensor	value	position						
t_1	1	115	225	335	445	665	775	885
	-1	518	527	536	544	563	572	581
t_2	$\sqrt{3}$	115	225	775	885			
	$-\sqrt{3}$	518	527	572	581			
	$\sqrt{2}$	123	216	783	876			
	$-\sqrt{2}$	317	371	628	682			
	1	224	418	481	774			
	-1	114	427	472	884			
u_1	$\sqrt{6}$	123	216	317	628			
	$-\sqrt{6}$	371	682	783	876			
	$\sqrt{3}$	224	427	481	884			
	$-\sqrt{3}$	114	418	472	774			
	1	572	581	775	885			
	-1	115	225	518	527			

Table 11: Second-class octet non-zero elements of the t_1 , t_2 and u_1 tensors.

$$\begin{aligned}
P_2 &= \frac{1}{\sqrt{2}}(A_{\bar{\Sigma}\pi\Sigma} + \sqrt{3}A_{\bar{\Sigma}\eta\Sigma}) = (\sqrt{2}f + \sqrt{6}d) \\
&\quad + \frac{1}{\sqrt{2}}(\sqrt{3}r_1 + 6r_3 - 2s_1 + \sqrt{3}s_2)\delta m_l, \\
P_3 &= -\frac{1}{\sqrt{2}}(A_{\bar{\Xi}\pi\Xi} + \sqrt{3}A_{\bar{\Xi}\eta\Xi}) = (\sqrt{2}f + \sqrt{6}d) \\
&\quad - \frac{1}{\sqrt{2}}(\sqrt{3}r_1 + 2r_3 + 2s_1 + \sqrt{3}s_2)\delta m_l, \\
P_4 &= A_{\bar{\Sigma}K\Xi} = (\sqrt{2}f + \sqrt{6}d) + \sqrt{2}(r_3 - s_1)\delta m_l.
\end{aligned} \tag{122}$$

We have based this fan plot on the doubly – singly represented structure, so several of the observables have very simple quark structures.

$$\begin{aligned}
P_1 &= \langle p | (\bar{u}\gamma u - \bar{d}\gamma d) | p \rangle, \\
P_2 &= \langle \Sigma^+ | (\bar{u}\gamma u - \bar{s}\gamma s) | \Sigma^+ \rangle, \\
P_3 &= \langle \Xi^0 | (\bar{s}\gamma s - \bar{u}\gamma u) | \Xi^0 \rangle, \\
P_4 &= \langle \Sigma^+ | \bar{u}\gamma s | \Xi^0 \rangle.
\end{aligned} \tag{123}$$

This P fan only includes the ‘outer’ octet baryons. The natural plot for the Λ structure is the d -fan. There are two linear constraints on the P -fan,

$$\begin{aligned}
\frac{1}{3}(P_1 + P_2 + P_3) &= (\sqrt{2}f + \sqrt{6}d) + O(\delta m_l^2), \\
\frac{1}{3}(P_1 + 2P_4) &= (\sqrt{2}f + \sqrt{6}d) + O(\delta m_l^2).
\end{aligned} \tag{124}$$

tensor	value	position							
q_1	-18	555							
	14	335	445	536	544	563	665		
	$-5\sqrt{6}$	132	261	738	867				
	9	151	252	757	858				
	$5\sqrt{3}$	141	848						
	$-5\sqrt{3}$	242	747						
	-6	115	225	353	454	518	527		
		572	581	656	775	885			
q_2	18	555							
	-10	353	454	656					
	-6	335	445	536	544	563	665		
	$2\sqrt{6}$	123	216	317	371	628	682	783	876
	$2\sqrt{3}$	224	427	472	774				
	$-2\sqrt{3}$	114	418	481	884				
	3	151	252	757	858				
	$\sqrt{6}$	132	261	738	867				
	$\sqrt{3}$	242	747						
	$-\sqrt{3}$	141	848						
w_1	$4\sqrt{2}$	132	261						
	$-4\sqrt{2}$	738	867						
	$3\sqrt{3}$	115	225	572	581				
	$-3\sqrt{3}$	518	527	775	885				
	$3\sqrt{2}$	317	628	783	876				
	$-3\sqrt{2}$	123	216	371	682				
	4	242	343	436	664	848			
	-4	141	334	463	646	747			
	3	114	427	481	774				
-3	224	418	472	884					
w_2	$3\sqrt{3}$	151	252						
	$-3\sqrt{3}$	757	858						
	$2\sqrt{2}$	123	216	371	682				
	$-2\sqrt{2}$	317	628	783	876				
	2	224	334	418	463	472	646	884	
	-2	114	343	427	436	481	664	774	
	$\sqrt{2}$	738	867						
	$-\sqrt{2}$	132	261						
	1	141	747						
-1	242	848							

Table 12: First-class 27-plet non-zero elements of the q_1 , q_2 and w_1 , w_2 tensors.

tensor	value	position									
z	$-9\sqrt{3}$	555									
	$3\sqrt{3}$	115	151	225	252	518	527				
		572	581	757	775	858	885				
	$-\sqrt{3}$	335	353	445	454	536	544	563	656	665	
	$\sqrt{2}$	123	132	216	261	317	371				
		628	682	738	783	867	876				
	1	224	242	427	472	747	774				
	-1	114	141	418	481	848	884				
	x_1	4	335	445	665						
		-4	536	544	563						
3		518	527	572	581						
-3		115	225	775	885						
$\sqrt{6}$		123	216	783	876						
$-\sqrt{6}$		317	371	628	682						
$\sqrt{3}$		224	418	481	774						
$-\sqrt{3}$		114	427	472	884						
y_1		$3\sqrt{3}$	115	225	518	527					
	$-3\sqrt{3}$	572	581	775	885						
	$\sqrt{2}$	123	216	317	628						
	$-\sqrt{2}$	371	682	783	876						
	1	224	427	481	884						
	-1	114	418	472	774						

Table 13: First-class 64-plet and second-class 27-plet non-zero elements of the z and x_1, y_1 tensors.

A fan with just the four lines from eq. (123), P_1, P_2, P_3, P_4 , is a four-line plot with just two independent slope parameters, $(r_3 - s_1)$ and $(\sqrt{3}r_1 + 4r_3 + \sqrt{3}s_2)$.

The advantage of this fan plot is that some of the quantities are of immediate physical interest, for example in the weak decay case P_1 gives the neutron decay constant, while P_4 gives the semileptonic decays $\Xi^0 \rightarrow \Sigma^+ l^- \bar{\nu}_l$, $\Xi^- \rightarrow \Sigma^0 l^- \bar{\nu}_l$. The disadvantages are that there are fewer constraints than the d -fan. Also, the d -fan and f -fan are independent – they involve different parameters, and there are no constraints that mix F_i and D_i quantities. A first attempt to show this fan plot for the fraction of the baryon’s momentum carried by a quark, i.e. $\langle x \rangle$, is given in [48].

Finally it is again often useful to note from eq. (124) that for example

$$X_P = \frac{1}{3}(P_1 + P_2 + P_3) = (\sqrt{2}f + \sqrt{6}d) + O(\delta m_l^2), \quad (125)$$

and to consider the quantities P_i/X_P .

B.2 The V -fan

The other natural non-singlet to look at in the proton is $\langle p | (\bar{u}\gamma u + \bar{d}\gamma d - 2\bar{s}\gamma s) | p \rangle$. This is approximately the total valence distribution, the quark-line-disconnected (sea) contribution to $(\bar{u}\gamma u + \bar{d}\gamma d - 2\bar{s}\gamma s)$ is zero at the symmetric point, and will probably stay small if the nucleon's sea is approximately $SU(3)$ symmetric.

$$\begin{aligned}
V_1 &= \sqrt{6}A_{\bar{N}\eta N} = \sqrt{6}(\sqrt{3}f - d) + \sqrt{6}(r_1 - s_2)\delta m_l, \\
V_2 &= \frac{3}{\sqrt{2}}A_{\Sigma\pi\Sigma} - \sqrt{\frac{3}{2}}A_{\Sigma\eta\Sigma}, = \sqrt{6}(\sqrt{3}f - d) \\
&\quad - \frac{1}{\sqrt{2}}\left(\sqrt{3}r_1 + 6r_3 + 6s_1 - 3\sqrt{3}s_2\right)\delta m_l, \\
V_3 &= \frac{3}{\sqrt{2}}A_{\Xi\pi\Xi} - \sqrt{\frac{3}{2}}A_{\Xi\eta\Xi} = \sqrt{6}(\sqrt{3}f - d), \\
&\quad - \frac{1}{\sqrt{2}}\left(\sqrt{3}r_1 - 6r_3 - 6s_1 + \sqrt{3}s_2\right)\delta m_l, \\
V_4 &= \sqrt{2}(A_{\bar{N}\pi N} + 2A_{\Xi\pi\Xi}) = \sqrt{6}(\sqrt{3}f - d) + 2\sqrt{2}(r_3 + 3s_1)\delta m_l, \\
V_5 &= (A_{\Xi K\Xi} - 2A_{\bar{N}K\Sigma}) = \sqrt{6}(\sqrt{3}f - d) - \sqrt{2}(r_3 + 3s_1)\delta m_l.
\end{aligned} \tag{126}$$

We have the two constraints

$$\begin{aligned}
\frac{1}{3}(V_1 + V_2 + V_3) &= \sqrt{6}(\sqrt{3}f - d) + O(\delta m_l^2), \\
\frac{1}{3}(V_4 + 2V_5) &= \sqrt{6}(\sqrt{3}f - d) + O(\delta m_l^2),
\end{aligned} \tag{127}$$

and can again construct an X_V from either combination, for example set

$$X_V = \frac{1}{3}(V_1 + V_2 + V_3), \tag{128}$$

and again consider ratios such as V_i/X_V .

C LO flavour diagonal matrix elements

To leading order we have for the representative octet baryons p , Σ^+ , Λ^0 and Ξ^0

$$\begin{aligned}
&\langle p | \bar{u}\gamma u | p \rangle \\
&= \frac{1}{\sqrt{3}}\left(a_0 + \sqrt{6}f + \sqrt{2}d\right) + \frac{1}{\sqrt{3}}\left(3a_1 + \frac{1}{\sqrt{2}}r_1 - \sqrt{6}r_3 + \sqrt{6}s_1 - \frac{1}{\sqrt{2}}s_2\right)\delta m_l, \\
&\langle p | \bar{d}\gamma d | p \rangle \\
&= \frac{1}{\sqrt{3}}\left(a_0 - 2\sqrt{2}d\right) + \frac{1}{\sqrt{3}}\left(3a_1 + \frac{1}{\sqrt{2}}r_1 + \sqrt{6}r_3 - \sqrt{6}s_1 - \frac{1}{\sqrt{2}}s_2\right)\delta m_l, \\
&\langle p | \bar{s}\gamma s | p \rangle \\
&= \frac{1}{\sqrt{3}}\left(a_0 - \sqrt{6}f + \sqrt{2}d\right) + \frac{1}{\sqrt{3}}\left(3a_1 - \sqrt{2}r_1 + \sqrt{2}s_2\right)\delta m_l,
\end{aligned} \tag{129}$$

$$\begin{aligned}
& \langle \Sigma^+ | \bar{u} \gamma u | \Sigma^+ \rangle \\
&= \frac{1}{\sqrt{3}} \left(a_0 + \sqrt{6}f + \sqrt{2}d \right) + \frac{1}{\sqrt{3}} \left(-3a_2 + \frac{1}{\sqrt{2}}r_1 + \sqrt{6}r_3 - \sqrt{6}s_1 + \frac{3}{\sqrt{2}}s_2 \right) \delta m_l, \\
& \langle \Sigma^+ | \bar{d} \gamma d | \Sigma^+ \rangle \\
&= \frac{1}{\sqrt{3}} \left(a_0 - \sqrt{6}f + \sqrt{2}d \right) + \frac{1}{\sqrt{3}} \left(-3a_2 + \frac{1}{\sqrt{2}}r_1 + \sqrt{6}r_3 + \sqrt{6}s_1 - \frac{3}{\sqrt{2}}s_2 \right) \delta m_l, \\
& \langle \Sigma^+ | \bar{s} \gamma s | \Sigma^+ \rangle \\
&= \frac{1}{\sqrt{3}} \left(a_0 - 2\sqrt{2}d \right) + \frac{1}{\sqrt{3}} \left(-3a_2 - \sqrt{2}r_1 - 2\sqrt{6}r_3 \right) \delta m_l, \\
& \langle \Lambda | \bar{u} \gamma u | \Lambda \rangle = \langle \Lambda | \bar{d} \gamma d | \Lambda \rangle, \\
&= \frac{1}{\sqrt{3}} \left(a_0 - \sqrt{2}d \right) + \frac{1}{\sqrt{3}} \left(3a_2 + \frac{1}{\sqrt{2}}r_1 + \sqrt{2}r_2 \right) \delta m_l, \\
& \langle \Lambda | \bar{s} \gamma s | \Lambda \rangle = \frac{1}{\sqrt{3}} \left(a_0 + 2\sqrt{2}d \right) + \frac{1}{\sqrt{3}} \left(3a_2 - \sqrt{2}r_1 - 2\sqrt{2}r_2 \right) \delta m_l, \quad (131)
\end{aligned}$$

and

$$\begin{aligned}
& \langle \Xi^0 | \bar{u} \gamma u | \Xi^0 \rangle \\
&= \frac{1}{\sqrt{3}} \left(a_0 - 2\sqrt{2}d \right) + \frac{1}{\sqrt{3}} \left(-3(a_1 - a_2) + \frac{1}{\sqrt{2}}r_1 + \sqrt{6}r_3 + \sqrt{6}s_1 + \frac{1}{\sqrt{2}}s_2 \right) \delta m_l, \\
& \langle \Xi^0 | \bar{d} \gamma d | \Xi^0 \rangle \\
&= \frac{1}{\sqrt{3}} \left(a_0 - \sqrt{6}f + \sqrt{2}d \right) \\
&\quad + \frac{1}{\sqrt{3}} \left(-3(a_1 - a_2) + \frac{1}{\sqrt{2}}r_1 - \sqrt{6}r_3 - \sqrt{6}s_1 + \frac{1}{\sqrt{2}}s_2 \right) \delta m_l, \\
& \langle \Xi^0 | \bar{s} \gamma s | \Xi^0 \rangle \\
&= \frac{1}{\sqrt{3}} \left(a_0 + \sqrt{6}f + \sqrt{2}d \right) + \frac{1}{\sqrt{3}} \left(-3(a_1 - a_2) - \sqrt{2}r_1 - \sqrt{2}s_2 \right) \delta m_l. \quad (132)
\end{aligned}$$

D LO disconnected flavour diagonal matrix elements

From eqs. (77, 78) we have f^{dis} , d^{dis} , r_2^{dis} , r_3^{dis} , s_1^{dis} and s_2^{dis} all vanishing at LO and only r_1^{dis} contributing. Thus we have

$$\begin{aligned}
\langle N | \bar{u} \gamma u | N \rangle^{\text{dis}} &= \langle N | \bar{d} \gamma d | N \rangle^{\text{dis}} \\
&= \frac{1}{\sqrt{3}} a_0^{\text{dis}} + \left(\sqrt{3} a_1^{\text{dis}} + \frac{1}{\sqrt{6}} r_1^{\text{dis}} \right) \delta m_l, \\
\langle N | \bar{s} \gamma s | N \rangle^{\text{dis}} &= \frac{1}{\sqrt{3}} a_0^{\text{dis}} + \left(\sqrt{3} a_1^{\text{dis}} - \sqrt{\frac{2}{3}} r_1^{\text{dis}} \right) \delta m_l, \quad (133)
\end{aligned}$$

(for n, p),

$$\begin{aligned}
\langle \Sigma | \bar{u} \gamma u | \Sigma \rangle^{\text{dis}} &= \langle \Sigma | \bar{d} \gamma d | \Sigma \rangle^{\text{dis}} \\
&= \frac{1}{\sqrt{3}} a_0^{\text{dis}} + \left(-\sqrt{3} a_2^{\text{dis}} + \frac{1}{\sqrt{6}} r_1^{\text{dis}} \right) \delta m_l, \\
\langle \Sigma | \bar{s} \gamma s | \Sigma \rangle^{\text{dis}} &= \frac{1}{\sqrt{3}} a_0^{\text{dis}} + \left(-\sqrt{3} a_2^{\text{dis}} - \sqrt{\frac{2}{3}} r_1^{\text{dis}} \right) \delta m_l,
\end{aligned} \tag{134}$$

(for $\Sigma^+, \Sigma^0, \Sigma^-$),

$$\begin{aligned}
\langle \Lambda | \bar{u} \gamma u | \Lambda \rangle^{\text{dis}} &= \langle \Lambda | \bar{d} \gamma d | \Lambda \rangle^{\text{dis}} \\
&= \frac{1}{\sqrt{3}} a_0^{\text{dis}} + \left(\sqrt{3} a_2^{\text{dis}} + \frac{1}{\sqrt{6}} r_1^{\text{dis}} \right) \delta m_l, \\
\langle \Lambda | \bar{s} \gamma s | \Lambda \rangle^{\text{dis}} &= \frac{1}{\sqrt{3}} a_0^{\text{dis}} + \left(\sqrt{3} a_2^{\text{dis}} - \sqrt{\frac{2}{3}} r_1^{\text{dis}} \right) \delta m_l,
\end{aligned} \tag{135}$$

(for Λ^0) and

$$\begin{aligned}
\langle \Xi | \bar{u} \gamma u | \Xi \rangle^{\text{dis}} &= \langle \Xi | \bar{d} \gamma d | \Xi \rangle^{\text{dis}} \\
&= \frac{1}{\sqrt{3}} a_0^{\text{dis}} + \left(-\sqrt{3} (a_1^{\text{dis}} - a_2^{\text{dis}}) + \frac{1}{\sqrt{6}} r_1^{\text{dis}} \right) \delta m_l, \\
\langle \Xi | \bar{s} \gamma s | \Xi \rangle^{\text{dis}} &= \frac{1}{\sqrt{3}} a_0^{\text{dis}} + \left(-\sqrt{3} (a_1^{\text{dis}} - a_2^{\text{dis}}) - \sqrt{\frac{2}{3}} r_1^{\text{dis}} \right) \delta m_l,
\end{aligned} \tag{136}$$

(for Ξ^0, Ξ^-).

References

- [1] W. Bietenholz, V. Bornyakov, N. Cundy, M. Göckeler, R. Horsley, A. D. Kennedy, W. G. Lockhart, Y. Nakamura, H. Perlt, D. Pleiter, P. E. L. Rakow, A. Schäfer, G. Schierholz, A. Schiller, H. Stüben and J. M. Zanotti [QCDSF–UKQCD Collaboration], *Phys. Lett.* **B690** (2010) 436, [arXiv:1003.1114 [hep-lat]].
- [2] W. Bietenholz, V. Bornyakov, M. Göckeler, R. Horsley, W. G. Lockhart, Y. Nakamura, H. Perlt, D. Pleiter, P. E. L. Rakow, G. Schierholz, A. Schiller, T. Streuer, H. Stüben, F. Winter and J. M. Zanotti [QCDSF–UKQCD Collaboration], *Phys. Rev.* **D84** (2011) 054509, [arXiv:1102.5300 [hep-lat]].
- [3] R. Horsley, Y. Nakamura, H. Perlt, D. Pleiter, P. E. L. Rakow, G. Schierholz, A. Schiller, R. Stokes, H. Stüben, R. D. Young and J. M. Zanotti *J. Phys.* **G43** (2016) 10LT02, [arXiv:1508.06401 [hep-lat]].

- [4] R. Horsley, Y. Nakamura, H. Perlt, D. Pleiter, P. E. L. Rakow, G. Schierholz, A. Schiller, R. Stokes, H. Stüben, R. D. Young and J. M. Zanotti [QCDSF-UKQCD Collaboration], *JHEP* **1604** (2016) 093, [arXiv:1509.00799 [hep-lat]].
- [5] R. Horsley, Z. Koumi, Y. Nakamura, H. Perlt, D. Pleiter, P. E. L. Rakow, G. Schierholz, A. Schiller, H. Stüben, R. D. Young and J. M. Zanotti [CSSM and QCDSF and UKQCD Collaborations], *J. Phys.* **G46** (2019) 115004, [arXiv:1904.02304 [hep-lat]].
- [6] E. E. Jenkins, A. V. Manohar, J. W. Negele and A. Walker-Loud, *Phys. Rev.* **D81** (2010) 014502, [arXiv:0907.0529 [hep-lat]].
- [7] M. Gell-Mann, *Phys. Rev.* **125** (1962) 1067.
- [8] S. Okubo, *Prog. Theor. Phys.* **27** (1962) 949.
- [9] A. N. Cooke, R. Horsley, Y. Nakamura, D. Pleiter, P. E. L. Rakow, G. Schierholz and J. M. Zanotti *PoS LATTICE 2012* (2012) 116, arXiv:1212.2564 [hep-lat].
- [10] QCDSF Collaboration, in preparation.
- [11] A. Accardi *et al.*, *Eur. Phys. J.* **A52** (2016) 268, [arXiv:1212.1701 [nucl-ex]].
- [12] T. Bhattacharya, R. Gupta, W. Lee, S. R. Sharpe and J. M. S. Wu *Phys. Rev.* **D73** (2006) 034504 [arXiv:hep-lat/0511014].
- [13] N. Cabibbo, E. C. Swallow and R. Winston, *Ann. Rev. Nucl. Part. Sci.* **53** (2003) 39, [arXiv:hep-ph/0307298].
- [14] S. Weinberg, *Phys. Rev.* **112** (1958) 1375.
- [15] H. Georgi, *Weak Interactions and Modern Particle Theory*, Benjamin/Cummings (1984).
- [16] V. G. Bornyakov, R. Horsley, Y. Nakamura, H. Perlt, D. Pleiter, P. E. L. Rakow, G. Schierholz, A. Schiller, H. Stüben, and J. M. Zanotti [QCDSF-UKQCD Collaboration], *Phys. Lett.* **B767** (2017) 366, [arXiv:1612.04798 [hep-lat]].
- [17] S. Gasiorowicz, *Elementary Particle Physics*, John Wiley & Sons, New York, 1966.
- [18] M. J. Savage and J. Walden, *Phys. Rev.* **D55** (1997) 5376, [arXiv:hep-ph/9611210].

- [19] A. Walker-Loud, *Nucl. Phys. A* **747** (2005) 476, [arXiv:hep-lat/0405007].
- [20] W. Pfeifer, *The Lie Algebras $su(N)$, An Introduction*, Birkhäuser, Basel, 2003.
- [21] R. Horsley, J. Najjar, Y. Nakamura, H. Perlt, D. Pleiter, P. E. L. Rakow, G. Schierholz, A. Schiller, H. Stüben and J. M. Zanotti [QCDSF–UKQCD Collaborations], *Phys. Rev. D* **91** (2015) 074512, [arXiv:1411.7665 [hep-lat]].
- [22] W. Greiner and B. Müller, *Quantum Mechanics: Symmetries*, Springer, Heidelberg, 1994.
- [23] Wolfram Research, Inc., *Mathematica*, Version 12.0, Champaign, IL (2019).
- [24] V. G. Bornyakov, R. Horsley, R. Hudspith, Y. Nakamura, H. Perlt, D. Pleiter, P. E. L. Rakow, G. Schierholz, A. Schiller, H. Stüben and J. M. Zanotti [QCDSF-UKQCD Collaboration], arXiv:1508.05916 [hep-lat].
- [25] R. Horsley, Y. Nakamura, H. Perlt, D. Pleiter, P. E. L. Rakow, G. Schierholz, A. Schiller, H. Stüben, R. D. Young and J. M. Zanotti [QCDSF-UKQCD Collaborations], *PoS(LATTICE2018)* (2018) 119, arXiv:1901.04792 [hep-lat].
- [26] A. Gerardin, T. Harris and H. B. Meyer, *Phys. Rev. D* **99** (2019) 014519, [arXiv:1811.08209 [hep-lat]].
- [27] T. Bakeyev, M. Göckeler, R. Horsley, D. Pleiter, P. E. L. Rakow, G. Schierholz and H. Stüben [QCDSF-UKQCD Collaboration], *Phys. Lett. B* **580** (2004) 197, [arXiv:hep-lat/0305014].
- [28] M. Ademollo and R. Gatto, *Phys. Rev. Lett.* **13** (1964) 264.
- [29] J. Anderson and M. A. Luty, *Phys. Rev. D* **47** (1993) 4975, [arXiv:hep-ph/9301219].
- [30] S. Capitani, M. Göckeler, R. Horsley, B. Klaus, H. Oelrich, H. Perlt, D. Petters, D. Pleiter, P. E. L. Rakow, G. Schierholz, A. Schiller and P. Stephenson, *Nucl. Phys. Proc. Suppl.* **73** (1999) 294, arXiv:hep-lat/9809172.
- [31] M. Göckeler, T. R. Hemmert, R. Horsley, D. Pleiter, P. E. L. Rakow, A. Schäfer and G. Schierholz [QCDSF Collaboration], *Phys. Rev. D* **71** (2005) 034508, [arXiv:hep-lat/0303019].
- [32] C. Best, M. Göckeler, R. Horsley, E.-M. Ilgenfritz, H. Perlt, P. Rakow, A. Schäfer, G. Schierholz, A. Schiller and S. Schramm, *Phys. Rev. D* **56** (1997) 2743, [arXiv:hep-lat/9703014].

- [33] P. E. Shanahan, A. W. Thomas, R. D. Young, J. M. Zanotti, R. Horsley, Y. Nakamura, D. Pleiter, P. E. L. Rakow, G. Schierholz and H. Stüben [CSSM and QCDSF/UKQCD Collaborations], *Phys. Rev.* **D89** (2014) 074511, [arXiv:1401.5862 [hep-lat]].
- [34] P. E. Shanahan, A. W. Thomas, R. D. Young, J. M. Zanotti, R. Horsley, Y. Nakamura, D. Pleiter, P. E. L. Rakow, G. Schierholz and H. Stüben [CSSM and QCDSF/UKQCD Collaborations], *Phys. Rev.* **D90** (2014) 034502, [arXiv:1403.1965 [hep-lat]].
- [35] N. Cundy, M. Göckeler, R. Horsley, T. Kaltenbrunner, A. D. Kennedy, Y. Nakamura, H. Perlt, D. Pleiter, P. E. L. Rakow, A. Schäfer, G. Schierholz, A. Schiller, H. Stüben, and J. M. Zanotti [QCDSF–UKQCD Collaboration], *Phys. Rev. D* **79** (2009) 094507, [arXiv:0901.3302 [hep-lat]].
- [36] N. Cundy, M. Göckeler, R. Horsley, T. Kaltenbrunner, A. D. Kennedy, Y. Nakamura, H. Perlt, D. Pleiter, P. E. L. Rakow, A. Schäfer, G. Schierholz, A. Schiller, H. Stüben and J. M. Zanotti [QCDSF–UKQCD Collaboration], *PoS LATTICE 2008* (2008) 132, arXiv:0811.2355 [hep-lat].
- [37] M. Constantinou, R. Horsley, H. Panagopoulos, H. Perlt, P. E. L. Rakow, G. Schierholz, A. Schiller and J. M. Zanotti, *Phys. Rev.* **D91** (2015) 014502, [arXiv:1408.6047 [hep-lat]].
- [38] R. Horsley, J. Najjar, Y. Nakamura, D. Pleiter, P. E. L. Rakow, G. Schierholz and J. M. Zanotti [QCDSF–UKQCD Collaborations], *Phys. Rev.* **D86** (2012) 114511, [arXiv:1206.3156 [hep-lat]].
- [39] N. Cabibbo, E. C. Swallow and R. Winston, *Phys. Rev. Lett.* **92** (2004) 251803, [arXiv:hep-ph/0307214].
- [40] V. Mateu and A. Pich, *JHEP* **0510** (2005) 041, [arXiv:hep-ph/0509045].
- [41] D. Guadagnoli, V. Lubicz and M. Papinutto *Nucl. Phys.* **B761** (2007) 63, [arXiv:hep-ph/0606181 [hep-lat]].
- [42] S. Sasaki and T. Yamazaki, *Phys. Rev.* **D79** (2009) 074508, [arXiv:0811.1406 [hep-lat]].
- [43] S. Sasaki, *Phys. Rev.* **D86** (2012) 114502, [arXiv:1209.6115 [hep-lat]].
- [44] S. Sasaki, *Phys. Rev.* **D96** (2017) 074509, [arXiv:1708.04008 [hep-lat]].
- [45] R. Horsley, Z. Koumi, Y. Nakamura, H. Perlt, P. E. L. Rakow, G. Schierholz, A. Schiller, H. Stüben, R. D. Young and J. M. Zanotti [QCDSF–UKQCD Collaborations], *EPJ Web Conf.* **175** (2018) 06017, arXiv:1711.02485 [hep-lat].

- [46] T. R. Haar, Y. Nakamura and H. Stüben, *EPJ Web Conf.* **175** (2018) 14011, [arXiv:1711.03836 \[hep-lat\]](#).
- [47] R. G. Edwards and B. Joó, *Nucl. Phys. Proc. Suppl.* **140** (2005) 832, [arXiv:hep-lat/0409003](#).
- [48] M. Göckeler, Ph. Hägler, R. Horsley, Y. Nakamura, D. Pleiter, P. E. L. Rakow, A. Schäfer, G. Schierholz, H. Stüben and J. M. Zanotti [QCDSF/UKQCD Collaboration], *PoS LATTICE 2010* (2010) 163, [arXiv:1102.3407 \[hep-lat\]](#).